Supplement of Geosci. Model Dev., 14, 2867–2897, 2021
https://doi.org/10.5194/gmd-14-2867-2021-supplement

Geoscientific Model Development
Open Access

Supplement of

The Community Multiscale Air Quality (CMAQ) model versions 5.3 and 5.3.1: system updates and evaluation

K. Wyat Appel et al.

Correspondence to: K. Wyat Appel (appel.wyat@epa.gov)

Table S1. New species introduced in AERO7 compared to AERO6. Species 1-21 are new to AERO7i. Other species in AERO7i (including species 22-24) previously existed in AERO6i. All gas-phase semi-volatiles use species-specific wet and dry deposition surrogates. Note that underscores are no longer used in species names in any aerosol or non-reactives namelist. For example, SV_ISO1 is now SVISO1 in the non-reactives namelist (i.e. NR*.nml) in CMAQ.

	Species	**Phase**	**Description**	**Scientific Basis**	**Model Implementation**
1	AMT1J	particle	low volatility particulate matter from monoterpene photoxidation (OH and O_3 reaction), C*=0.01 μg m^{-3}	dark α-pinene ozonolysis (Saha and Grieshop, 2016, *ES&T*)	Xu et al., 2018, *ACP*
2	AMT2J	particle	low volatility particulate matter from monoterpene photoxidation (OH and O_3 reaction), C*=0.1 μg m^{-3}	dark α-pinene ozonolysis (Saha and Grieshop, 2016, *ES&T*)	Xu et al., 2018, *ACP*
3	AMT3J	particle	semivolatile particulate matter from monoterpene photoxidation (OH and O_3 reaction), C*=1 μg m^{-3}	dark α-pinene ozonolysis (Saha and Grieshop, 2016, *ES&T*)	Xu et al., 2018, *ACP*
4	AMT4J	particle	semivolatile particulate matter from monoterpene photoxidation (OH and O_3 reaction), C*=10 μg m^{-3}	dark α-pinene ozonolysis (Saha and Grieshop, 2016, *ES&T*)	Xu et al., 2018, *ACP*
5	AMT5J	particle	semivolatile particulate matter from monoterpene photoxidation (OH and O_3 reaction), C*=100 μg m^{-3}	dark α-pinene ozonolysis (Saha and Grieshop, 2016, *ES&T*)	Xu et al., 2018, *ACP*
6	AMT6J	particle	semivolatile particulate matter from monoterpene photoxidation (OH and O_3 reaction), C*=1000 μg m^{-3}	dark α-pinene ozonolysis (Saha and Grieshop, 2016, *ES&T*)	Xu et al., 2018, *ACP*
7	SVMT1	gas	low volatility gas from monoterpene photoxidation (OH and O_3 reaction), C*=0.01 μg m^{-3}	dark α-pinene ozonolysis (Saha and Grieshop, 2016, *ES&T*)	Xu et al., 2018, *ACP*
8	SVMT2	gas	low volatility gas from monoterpene photoxidation (OH and O_3 reaction), C*=0.1 μg m^{-3}	dark α-pinene ozonolysis (Saha and Grieshop, 2016, *ES&T*)	Xu et al., 2018, *ACP*
9	SVMT3	gas	semivolatile gas from monoterpene photoxidation (OH and O_3 reaction), C*=1 μg m^{-3}	dark α-pinene ozonolysis (Saha and Grieshop, 2016, *ES&T*)	Xu et al., 2018, *ACP*

	Species	Phase	Description	Scientific Basis	Model Implementation
10	SVMT4	gas	semivolatile gas from monoterpene photoxidation (OH and O_3 reaction), C*=10 µg m^{-3}	dark α-pinene ozonolysis (Saha and Grieshop, 2016, *ES&T*)	Xu et al., 2018, *ACP*
11	SVMT5	gas	semivolatile gas from monoterpene photoxidation (OH and O_3 reaction), C*=100 µg m^{-3}	dark α-pinene ozonolysis (Saha and Grieshop, 2016, *ES&T*)	Xu et al., 2018, *ACP*
12	SVMT6	gas	semivolatile gas from monoterpene photoxidation (OH and O_3 reaction), C*=1000 µg m^{-3}	dark α-pinene ozonolysis (Saha and Grieshop, 2016, *ES&T*)	Xu et al., 2018, *ACP*
13	AORGH2OJ	particle	water associated with organic species of particulate matter	hygroscopicity parameters (Petters and Kreidenweis, 2007, *ACP*) as a function of degree of oxygenation (Lambe et al., 2011, *ACP*)	Pye et al., 2017, *ACP*
14	AAVB1J	particle	low volatility organic particulate matter from oxidation of anthropogenic VOCs (benzene, toluene, xylene, PAHs, alkanes)	GEOS-Chem VBS parameterization (Pye et al., 2010, *ACP*) for aromatics and PAHs with long-chain alkanes following Pye and Pouliot (2012, *ES&T*) but with Presto et al. (2010, *ES&T*) VBS fits; all underlying experimental datasets are the same as in *aero6*	Qin et al., *in prep.*
15	AAVB2J	particle	semivolatile organic particulate matter from oxidation of anthropogenic VOCs (benzene, toluene, xylene, PAHs, alkanes)	see AAVB1J	Qin et al., *in prep.*
16	AAVB3J	particle	semivolatile organic particulate matter from oxidation of anthropogenic VOCs (benzene, toluene, xylene, PAHs, alkanes)	see AAVB1J	Qin et al., *in prep.*
17	AAVB4J	particle	semivolatile organic particulate matter from oxidation of anthropogenic VOCs (benzene, toluene, xylene, PAHs, alkanes)	see AAVB1J	Qin et al., *in prep.*

	Species	Phase	Description	Scientific Basis	Model Implementation
18	SVAVB1	gas	low volatility organic gas from oxidation of anthropogenic VOCs (benzene, toluene, xylene, PAHs, alkanes)	see AAVB1J	Qin et al., *in prep.*
19	SVAVB2	gas	semivolatile organic gas from oxidation of anthropogenic VOCs (benzene, toluene, xylene, PAHs, alkanes)	see AAVB1J	Qin et al., *in prep.*
20	SVAVB3	gas	semivolatile organic gas from oxidation of anthropogenic VOCs (benzene, toluene, xylene, PAHs, alkanes)	see AAVB1J	Qin et al., *in prep.*
21	SVAVB4	gas	semivolatile organic gas from oxidation of anthropogenic VOCs (benzene, toluene, xylene, PAHs, alkanes)	see AAVB1J	Qin et al., *in prep.*
22	MTNO3	gas	organic nitrates from monoterpene oxidation	gas-phase SAPRC yields (should not be counted as gas-phase organic nitrate for evaluation purposes in CB6r3 mechanisms)	Pye et al., 2015, *ES&T*
23	AMTNO3J	particle	semivolatile organic nitrates from monoterpene oxidation	Fry et al. (2009, *ACP*) for vapor pressure of monoterpene organic nitrates	Pye et al., 2015, *ES&T*
24	AMTHYDJ	particle	organic pseudo-hydrolysis accretion product from monoterpene organic nitrates (AMTNO3J)	Boyd et al. (2015, *ACP*) for hydrolysis timescale for tertiary nitrates, but applied to all MTNO3 following Pye et al. (2015, *ES&T*)	Pye et al., 2015, *ES&T*

*Species in AERO6/6i that are deprecated in AERO7/7i (these species should NOT appear in an AERO7/7i namelist): ATRP1J, ATRP2J, SV_TRP1, SV_TRP2, ABNZ1J, ABNZ2J, ABNZ3J, SV_BNZ1, SV_BNZ2, AXYL1J, AXYL2J, AXYL3J, SV_XYL1, SV_XYL2, ATOL1J, ATOL2J, ATOL3J, SV_TOL1, SV_TOL2, APAH1J, APAH2J, APAH3J, SV_PAH1, SV_PAH2, AALK1J, AALK2J, SV_ALK1, SV_ALK2

Table S2. Namelist options used for WRF version 3.8 simulation.

```
&time_control
 start_year                        = 2015,
 start_month                       = 12,
 start_day                         = 21,
 start_hour                        = 00,
 start_minute                      = 00,
 start_second                      = 00,
 end_year                          = 2015,
 end_month                         = 12,
 end_day                           = 27,
 end_hour                          = 00,
 end_minute                        = 01,
 end_second                        = 00,
 interval_seconds                  = 10800,
 input_from_file                   = .true.,
 history_interval                  = 60,
 frames_per_outfile                = 24,
 restart                           = .FALSE.,
 restart_interval                  = 1440,
 io_form_history                   = 2
 io_form_restart                   = 2
 io_form_input                     = 2
 io_form_boundary                  = 2
 debug_level                       = 0
 io_form_auxinput2                 = 2
 io_form_auxinput4                 = 2
 auxinput1_inname                  = "metoa_em.d01.<date>"
 auxinput4_inname                  = "wrflowinp_d01"
 auxinput4_interval                = 180
 auxinput4_end_h                   = 9025
 write_hist_at_0h_rst              = .true.,
 io_form_auxinput8                 = 2,
 auxinput8_inname                  = 'LTNG_<year>_<month>.nc',
 frames_per_auxinput8              = 1600,
 auxinput8_interval_m              = 30,
 auxinput8_end_h                   = 9999,
 /

 &domains
 time_step                         = 60,
 time_step_fract_num               = 0,
 time_step_fract_den               = 1,
 use_adaptive_time_step            = .false.
 max_dom                           = 1,
 s_we                              = 1,
 e_we                              = 472,
 s_sn                              = 1,
 e_sn                              = 312,
 s_vert                            = 1,
 e_vert                            = 36,
 p_top_requested                   = 5000,
 eta_levels                        = 1.000, 0.9975, 0.995, 0.990, 0.985,
                                     0.980, 0.970, 0.960, 0.950,
                                     0.940, 0.930, 0.920, 0.910,
```

```
                         0.900, 0.880, 0.860, 0.840,
                         0.820, 0.800, 0.770, 0.740,
                         0.700, 0.650, 0.600, 0.550,
                         0.500, 0.450, 0.400, 0.350,
                         0.300, 0.250, 0.200, 0.150,
                         0.100, 0.050, 0.000
num_metgrid_levels       = 40,
dx                       = 12000,
dy                       = 12000,
grid_id                  = 1,
parent_id                = 0,
i_parent_start           = 0,
j_parent_start           = 0,
parent_grid_ratio        = 1,
parent_time_step_ratio   = 1,
feedback                 = 1,
smooth_option            = 0,
/

&physics
mp_physics               = 10,
ra_lw_physics            = 4,
ra_sw_physics            = 4,
radt                     = 20,
sf_sfclay_physics        = 7,
sf_surface_physics       = 7,
bl_pbl_physics           = 7,
bldt                     = 0,
cu_physics               = 1,
kfeta_trigger            = 1,
cudt                     = 10,
ltg_assim                = .true.,
suppress_opt             = 2,
isfflx                   = 1,
ifsnow                   = 1,
icloud                   = 1,
cu_rad_feedback          = .true.,
surface_input_source     = 1,
num_soil_layers          = 2,
sst_update               = 1,
pxlsm_smois_init         = 1,
slope_rad                = 1,
topo_shading             = 1,
shadlen                  = 25000.,
num_land_cat             = 40,
prec_acc_dt              = 60,
mp_zero_out              = 2,
fractional_seaice        = 1,
seaice_threshold         = 0.0,
/

&fdda
grid_fdda                = 1,
grid_sfdda               = 1,
pxlsm_soil_nudge         = 1,
sgfdda_inname            = "wrfsfdda_d01",
```

```
sgfdda_end_h                    = 9025,
sgfdda_interval_m               = 180,
sgfdda_interval                 = 10800,
gfdda_inname                    = "wrffdda_d<domain>",
gfdda_end_h                     = 9025,
gfdda_interval_m                = 180,
fgdt                            = 0,
if_no_pbl_nudging_uv            = 1,
if_no_pbl_nudging_t             = 1,
if_no_pbl_nudging_q             = 1,
if_zfac_uv                      = 0,
 k_zfac_uv                      = 13,
if_zfac_t                       = 0,
 k_zfac_t                       = 13,
if_zfac_q                       = 0,
 k_zfac_q                       = 13,
guv                             = 0.0001,
gt                              = 0.0001,
gq                              = 0.00001,
guv_sfc                         = 0.0000,
gt_sfc                          = 0.0000,
gq_sfc                          = 0.0000,
if_ramping                      = 0,
dtramp_min                      = 60.0,
io_form_gfdda                   = 2,
rinblw                          = 250.0
/

&dynamics
w_damping                       = 1,
diff_opt                        = 1,
km_opt                          = 4,
diff_6th_opt                    = 2,
diff_6th_factor                 = 0.12,
damp_opt                        = 3,
base_temp                       = 290.
zdamp                           = 5000.,
dampcoef                        = 0.05,
khdif                           = 0,
kvdif                           = 0,
non_hydrostatic                 = .true.,
moist_adv_opt                   = 2,
tke_adv_opt                     = 2,
scalar_adv_opt                  = 2,
/

&dfi_control
dfi_opt                         = 0
dfi_nfilter                     = 7
dfi_write_filtered_input        = .true.
dfi_write_dfi_history           = .false.
dfi_cutoff_seconds              = 60
dfi_time_dim                    = 1000
dfi_bckstop_year                = 2006
dfi_bckstop_month               = 08
dfi_bckstop_day                 = 04
```

```
dfi_bckstop_hour                    = 12
dfi_bckstop_minute                    = 00
dfi_bckstop_second                    = 00
dfi_fwdstop_year                    = 2006
dfi_fwdstop_month                    = 08
dfi_fwdstop_day                    = 04
dfi_fwdstop_hour                    = 13
dfi_fwdstop_minute                    = 00
dfi_fwdstop_second                    = 00
/

&bdy_control
spec_bdy_width                      = 5,
spec_zone                           = 1,
relax_zone                          = 4,
specified                           = .true.,
nested                              = .false.,
/

&grib2
/

&namelist_quilt
nio_tasks_per_group = 0,
nio_groups = 1,
/
```

Table S3. Namelist options used in WRF version 4.1.1 simulation.

```
&time_control
 start_year                        = $YS
 start_month                       = $MS
 start_day                         = $DS
 start_hour                        = 00
 start_minute                      = 00,
 start_second                      = 00,
 end_year                          = $YE
 end_month                         = $ME
 end_day                           = $DE
 end_hour                          = 00
 end_minute                        = 00,
 end_second                        = 00,
 interval_seconds                  = 10800
 input_from_file                   = .true.,
 history_interval                  = 60,
 frames_per_outfile                = 24,
 restart                           = .true.
 restart_interval                  = 1440,
 write_hist_at_0h_rst              = .true.,
 io_form_history                   = 2
 io_form_restart                   = 2
 io_form_input                     = 2
 io_form_boundary                  = 2
 io_form_auxinput2                 = 2
 io_form_auxinput4                 = 2
 io_form_auxinput8                 = 2,
 debug_level                       = 0
 auxinput1_inname                  = "met_em.d01.<date>"
 auxinput4_inname                  = "wrflowinp_d01"
 auxinput4_interval                = 180
 auxinput4_end_h                   = 999999999
 auxinput8_inname                  = "LIGHTNING"
 auxinput8_interval                = 30
 auxinput8_end_h                   = 999999999
 frames_per_auxinput8              = 7344,
 reset_simulation_start            = .false.,
 iofields_filename                 = "output.var.txt"
 force_use_old_data                = .true.
/

 &domains
 time_step                         = 60,
 time_step_fract_num               = 0,
 time_step_fract_den               = 1,
 max_dom                           = 1,
 s_we                              = 1,
 e_we                              = 472,
 s_sn                              = 1,
 e_sn                              = 312,
 s_vert                            = 1,
 e_vert                            = 36,
 p_top_requested                   = 5000,
 eta_levels                        = 1.000, 0.9975, 0.995, 0.990, 0.985,
```

```
                              0.980, 0.970, 0.960, 0.950,
                              0.940, 0.930, 0.920, 0.910,
                              0.900, 0.880, 0.860, 0.840,
                              0.820, 0.800, 0.770, 0.740,
                              0.700, 0.650, 0.600, 0.550,
                              0.500, 0.450, 0.400, 0.350,
                              0.300, 0.250, 0.200, 0.150,
                              0.100, 0.050, 0.000
num_metgrid_levels                  = 40,
dx                            = 12000,
dy                            = 12000,
grid_id                        = 1,
parent_id                       = 0,
i_parent_start                   = 0,
j_parent_start                   = 0,
parent_grid_ratio                  = 1,
parent_time_step_ratio                = 1,
feedback                        = 1,
smooth_option                      = 0,
/

&physics
mp_physics                        = 10,
mp_zero_out                       = 2,
mp_zero_out_thresh                  = 1.0e-8,
ra_lw_physics                      = 4,
ra_sw_physics                      = 4,
radt                          = 20,
co2tf                          = 1,
sf_sfclay_physics                  = 7,
num_soil_layers                    = 2,
pxlsm_smois_init                    = 0,
pxlsm_modis_veg                     = 1,
sf_surface_physics                  = 7,
sf_urban_physics                    = 0,
bl_pbl_physics                     = 7,
bldt                          = 0,
cu_physics                       = 1,
kfeta_trigger                    = 1,
cudt                           = 0,
prec_acc_dt                       = 60,
isfflx                         = 1,
ifsnow                          = 1,
icloud                         = 1,
cu_rad_feedback                     = .true.,
surface_input_source                 = 1,
num_land_cat                       = 40,
num_soil_cat                      = 16,
sst_update                       = 1,
seaice_threshold                   = 100,
slope_rad                        = 1,
topo_shading                      = 1,
shadlen                         = 25000.,
do_radar_ref                      = 1,
grav_settling                     = 0,
ltg_assim                        = .true.,
```

```
suppress_opt                        = 2,
/

&fdda
grid_fdda                           = 1,
grid_sfdda                          = 1,
pxlsm_soil_nudge                    = 1,
sgfdda_inname                       = "wrfsfdda_d01",
sgfdda_end_h                        = 999999999,
sgfdda_interval_m                   = 180,
gfdda_inname                        = "wrffdda_d<domain>",
gfdda_end_h                         = 999999999,
gfdda_interval_m                    = 180,
fgdt                                = 0,
if_no_pbl_nudging_uv                = 1,
if_no_pbl_nudging_t                 = 1,
if_no_pbl_nudging_q                 = 1,
if_zfac_uv                          = 0,
 k_zfac_uv                          = 13,
if_zfac_t                           = 0,
 k_zfac_t                           = 13,
if_zfac_q                           = 0,
 k_zfac_q                           = 13,
guv                                 = 0.0001,
gt                                  = 0.0001,
gq                                  = 0.00001,
guv_sfc                             = 0.0000,
gt_sfc                              = 0.0000,
gq_sfc                              = 0.0000,
if_ramping                          = 1,
dtramp_min                          = 60.0,
io_form_gfdda                       = 2,
rinblw                              = 250.0
/

&dynamics
hybrid_opt                          = 2,
w_damping                           = 1,
diff_opt                            = 1,
km_opt                              = 4,
diff_6th_opt                        = 2,
diff_6th_factor                     = 0.12,
damp_opt                            = 3,
base_temp                           = 290.
zdamp                               = 5000.,
dampcoef                            = 0.05,
khdif                               = 0,
kvdif                               = 0,
non_hydrostatic                     = .true.,
moist_adv_opt                       = 2,
tke_adv_opt                         = 2,
scalar_adv_opt                      = 2,
/

&bdy_control
spec_bdy_width                      = 5,
```

```
spec_zone                 = 1,
relax_zone                = 4,
specified                 = .true.,
spec_exp                  = 0.0,
nested                    = .false.,
/

&grib2
/

&namelist_quilt
nio_tasks_per_group = 0,
nio_groups = 1,
```

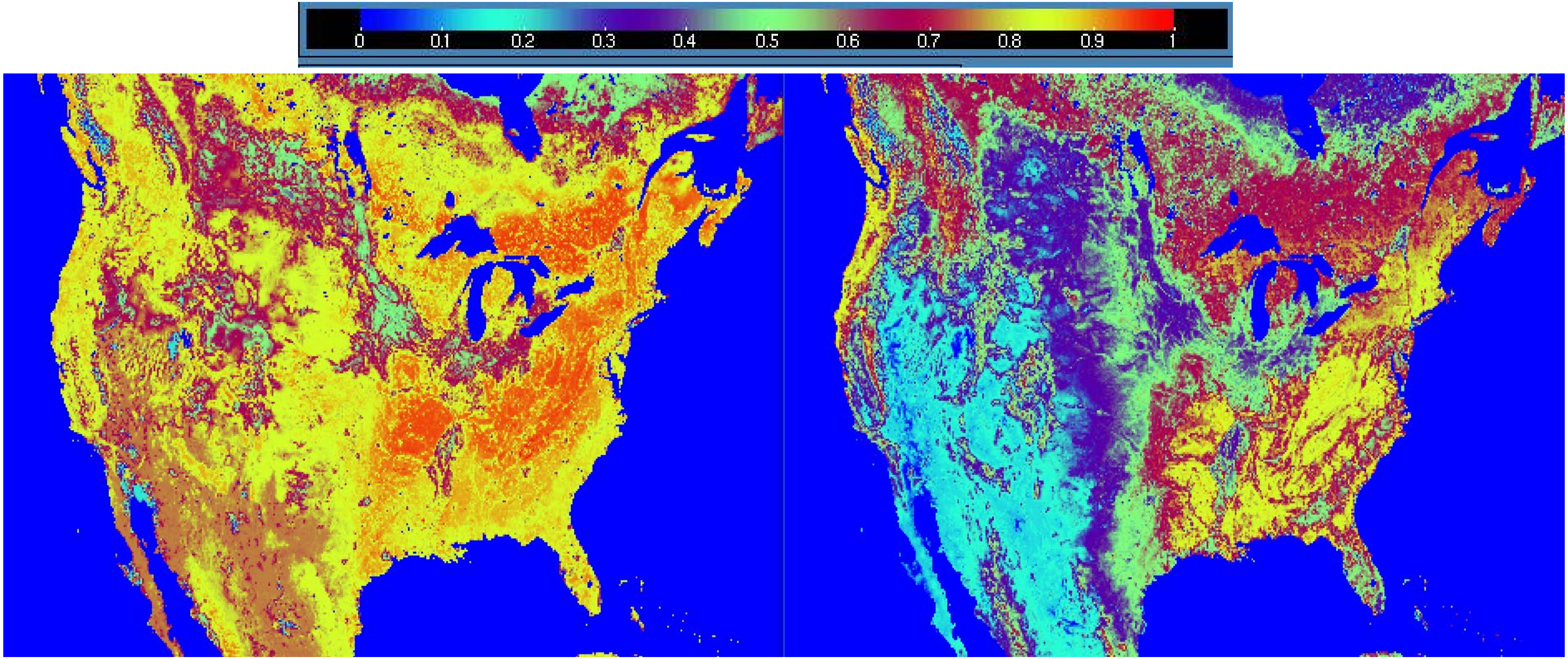

Figure S1. Vegetation Fraction (VF) on June 1, 2016 from WRF38 (left) and WRF411 (right).

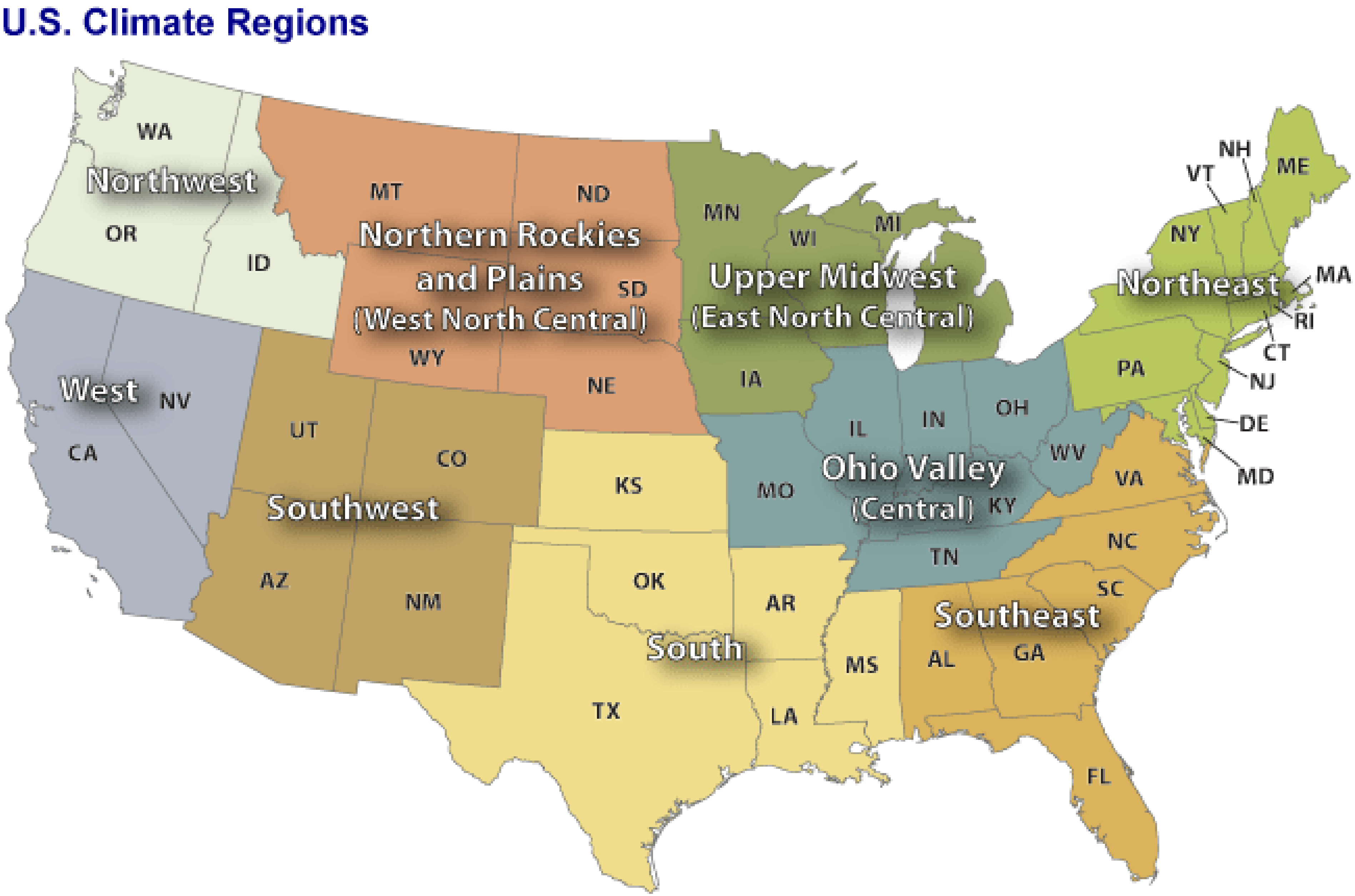

Figure S2. Map of the NOAA U.S. climate regions. Image source: https://www.ncdc.noaa.gov/monitoring-references/maps/us-climate-regions.php.

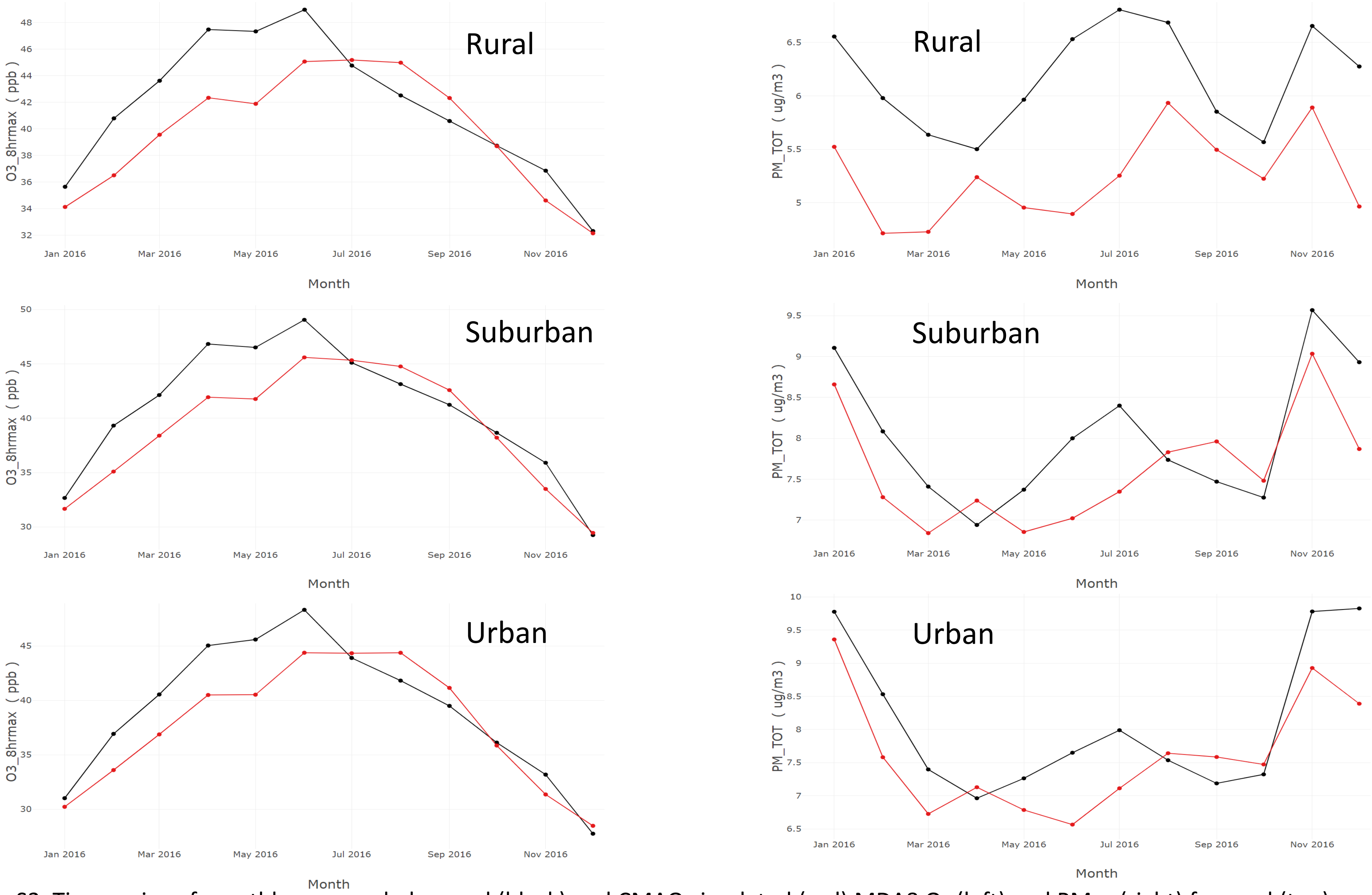

Figure S3. Time series of monthly averaged observed (black) and CMAQ simulated (red) MDA8 O_3 (left) and $PM_{2.5}$ (right) for rural (top), suburban (middle), and urban (bottom) AQS sites. Similar trends in observed and simulated monthly average values are seen for all three land-use classifications.

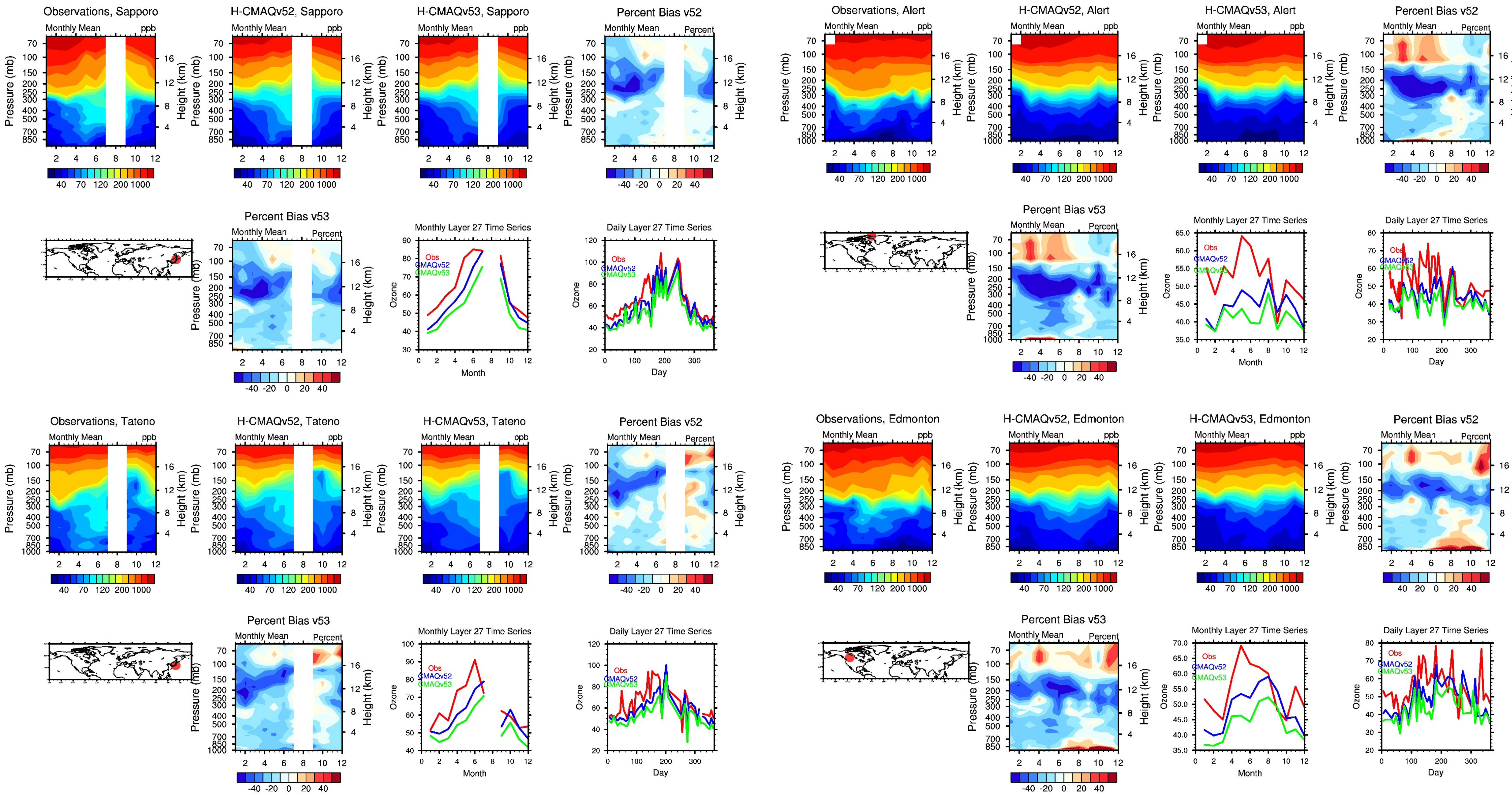

Figure S4. Comparison of ozonesonde data for the Sapporo, JP (upper left), Alert, GRL (upper right), Tateno, JP (lower left), and Edmonton, CA (lower right) WOUDC sites. Each panel consists of eight plots: observed O_3 (ppbv; top far left); HCMAQ52 modeled O_3 (ppbv; top middle left); HCMAQ53 modeled O_3 (ppbv; top middle right); HCMAQ52 bias (%; top far right); approximate site location (bottom far left); HCMAQ53 bias (%; bottom middle left); layer 27 monthly average O_3 time series (ppbv; bottom middle right); layer 27 daily average O_3 time series (ppbv; bottom far right).

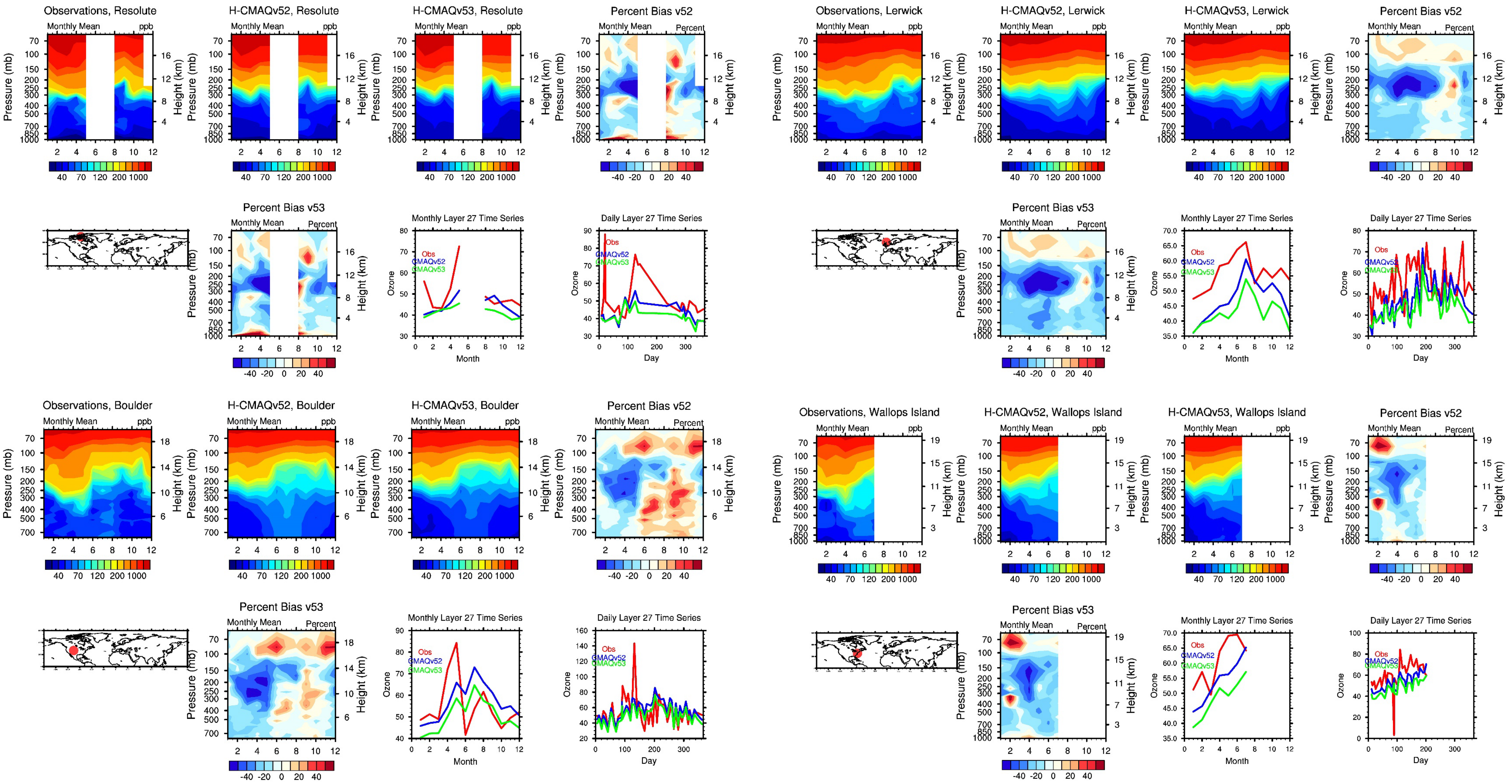

Figure S5. Comparison of ozonesonde data for the Resolute, CA (upper left), Lerwick, SCT (upper right), Boulder, US (lower left), and Wallops Island, US (lower right) WOUDC sites. Each panel consists of eight plots: observed O_3 (ppbv; top far left); HCMAQ52 modeled O_3 (ppbv; top middle left); HCMAQ53 modeled O_3 (ppbv; top middle right); HCMAQ52 bias (%; top far right); approximate site location (bottom far left); HCMAQ53 bias (%; bottom middle left); layer 27 monthly average O_3 time series (ppbv; bottom middle right); layer 27 daily average O_3 time series (ppbv; bottom far right).

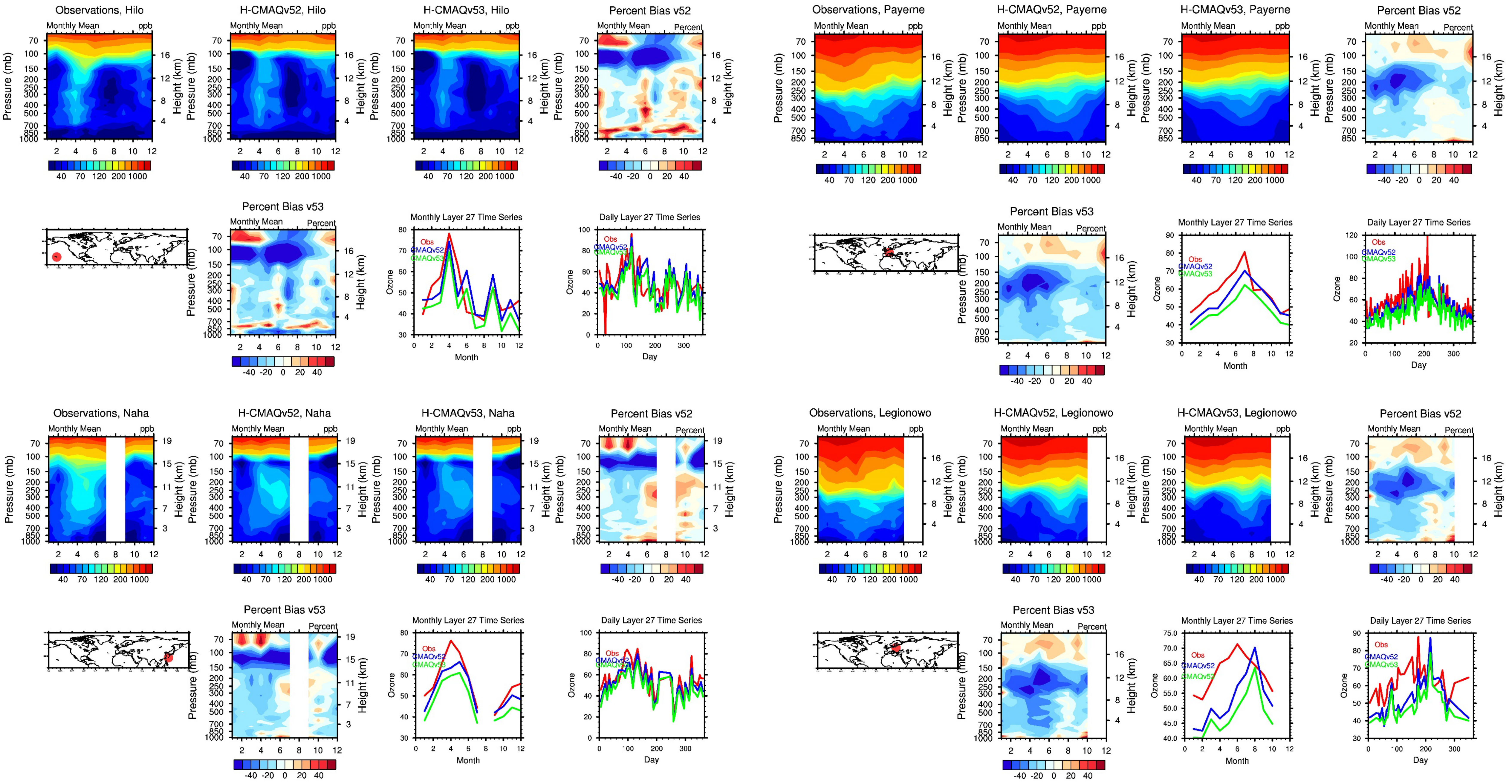

Figure S6. Comparison of ozonesonde data for the Hilo, US (upper left), Payerne, CH (upper right), Naha, JP (lower left), and Legionwo, PL (lower right) WOUDC sites. Each panel consists of eight plots: observed O_3 (ppbv; top far left); HCMAQ52 modeled O_3 (ppbv; top middle left); HCMAQ53 modeled O_3 (ppbv; top middle right); HCMAQ52 bias (%; top far right); approximate site location (bottom far left); HCMAQ53 bias (%; bottom middle left); layer 27 monthly average O_3 time series (ppbv; bottom middle right); layer 27 daily average O_3 time series (ppbv; bottom far right).

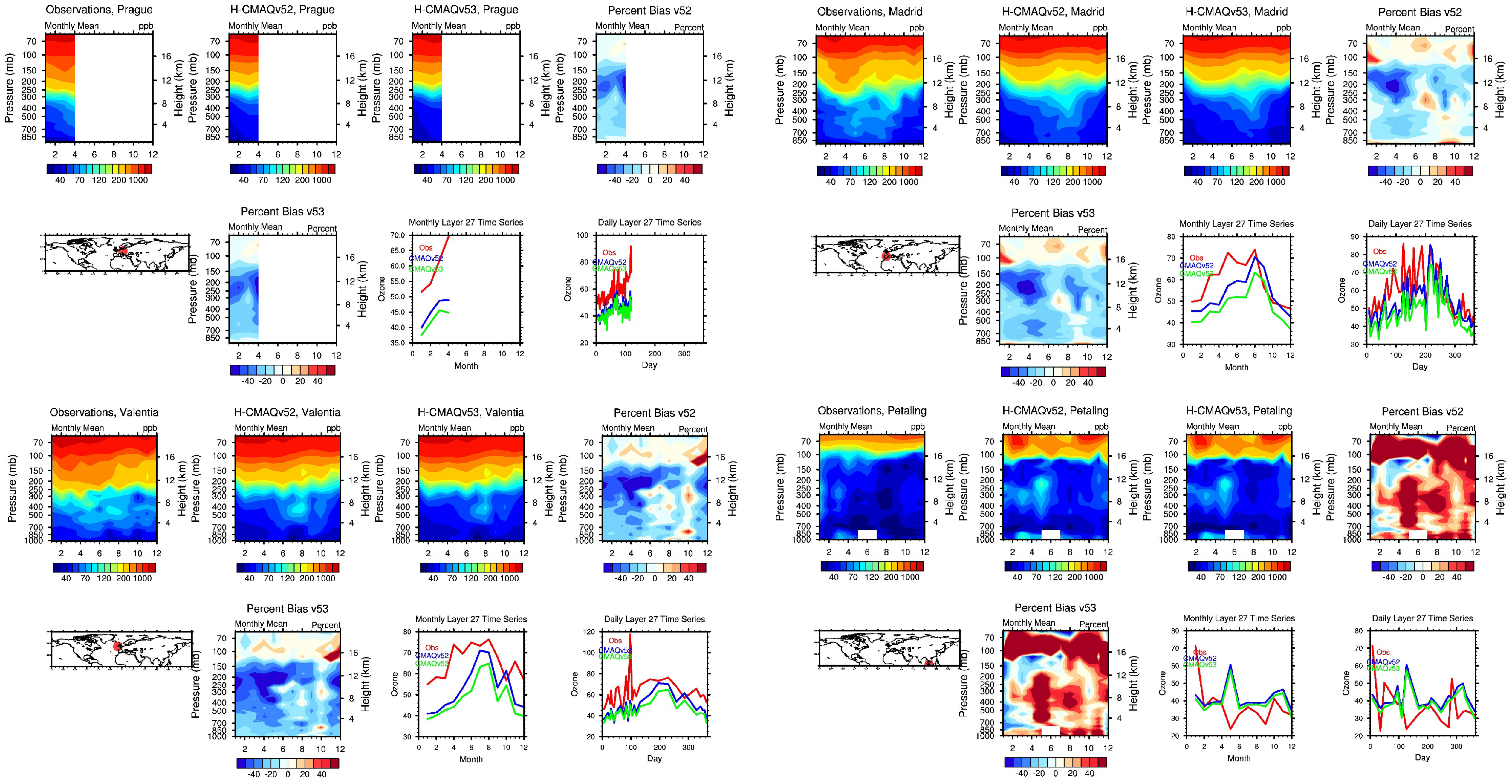

Figure S7. Comparison of ozonesonde data for the Prague, CZ (upper left), Mardrid, SP (upper right), Valentia, SP (lower left), and Petaling, MY (lower right) WOUDC sites. Each panel consists of eight plots: observed O_3 (ppbv; top far left); HCMAQ52 modeled O_3 (ppbv; top middle left); HCMAQ53 modeled O_3 (ppbv; top middle right); HCMAQ52 bias (%; top far right); approximate site location (bottom far left); HCMAQ53 bias (%; bottom middle left); layer 27 monthly average O_3 time series (ppbv; bottom middle right); layer 27 daily average O_3 time series (ppbv; bottom far right).

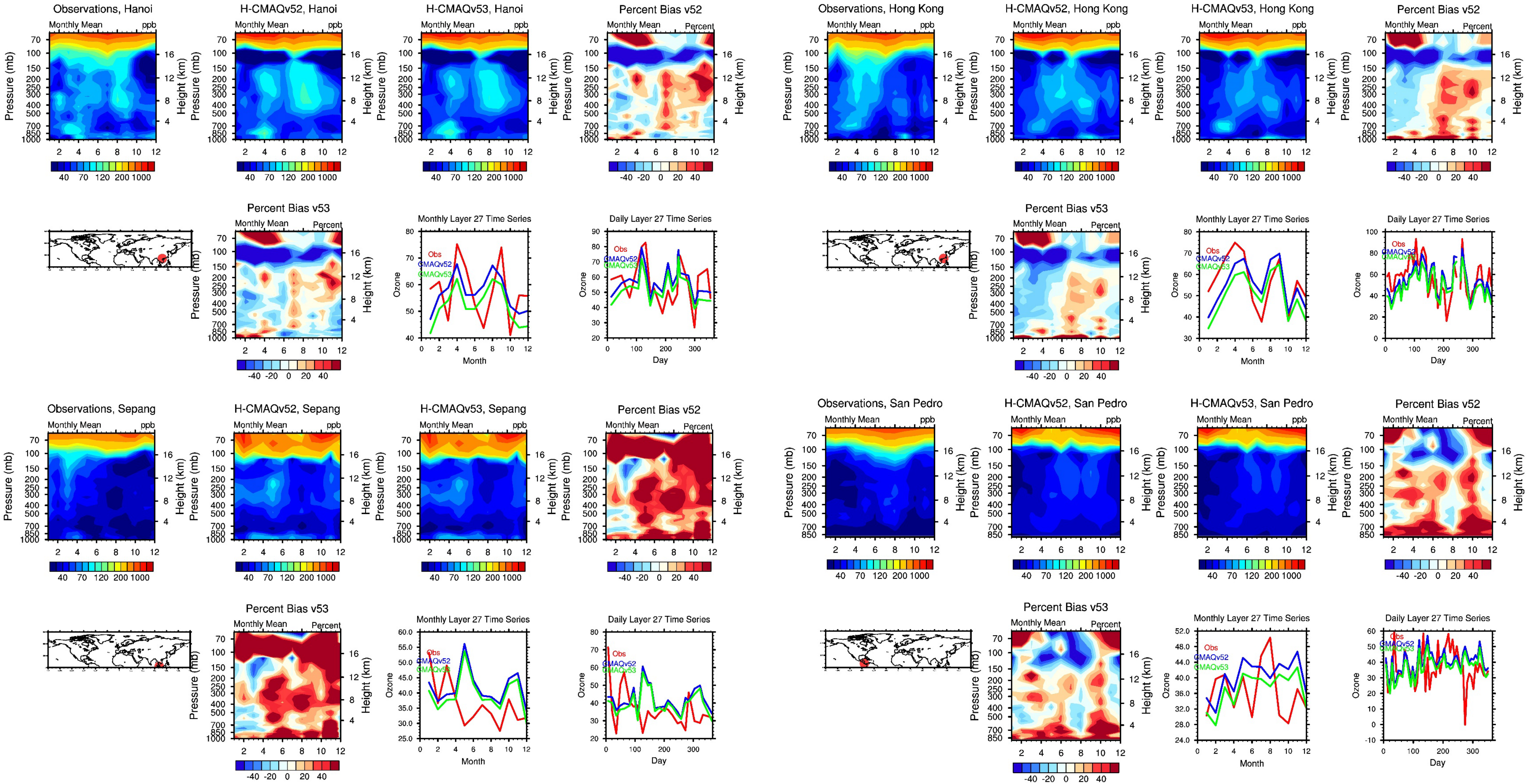

Figure S8. Comparison of ozonesonde data for the Hanoi, VT (upper left), Hong Kong, SAR (upper right), (lower left), and San Pedro, CR (lower right) WOUDC sites. Each panel consists of eight plots: observed O_3 (ppbv; top far left); HCMAQ52 modeled O_3 (ppbv; top middle left); HCMAQ53 modeled O_3 (ppbv; top middle right); HCMAQ52 bias (%; top far right); approximate site location (bottom far left); HCMAQ53 bias (%; bottom middle left); layer 27 monthly average O_3 time series (ppbv; bottom middle right); layer 27 daily average O_3 time series (ppbv; bottom far right).

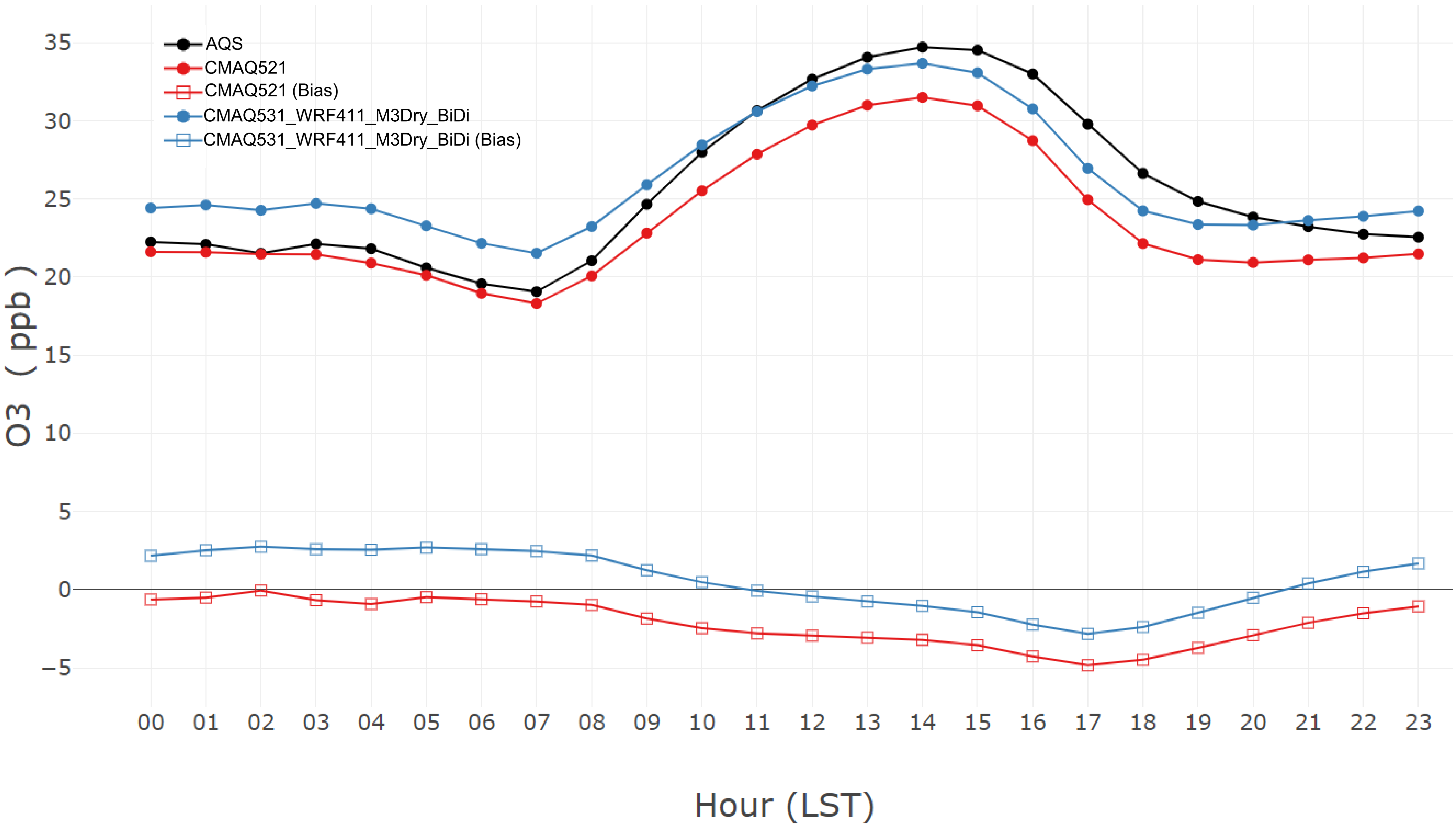

Figure S9. Time series of hourly average O_3 (ppbv; filled circles) and bias (open squares; ppbv) for all AQS sites for winter for the CMAQ521 (red) and CMAQ531_WRF411_M3Dry_BiDi (blue) simulations.

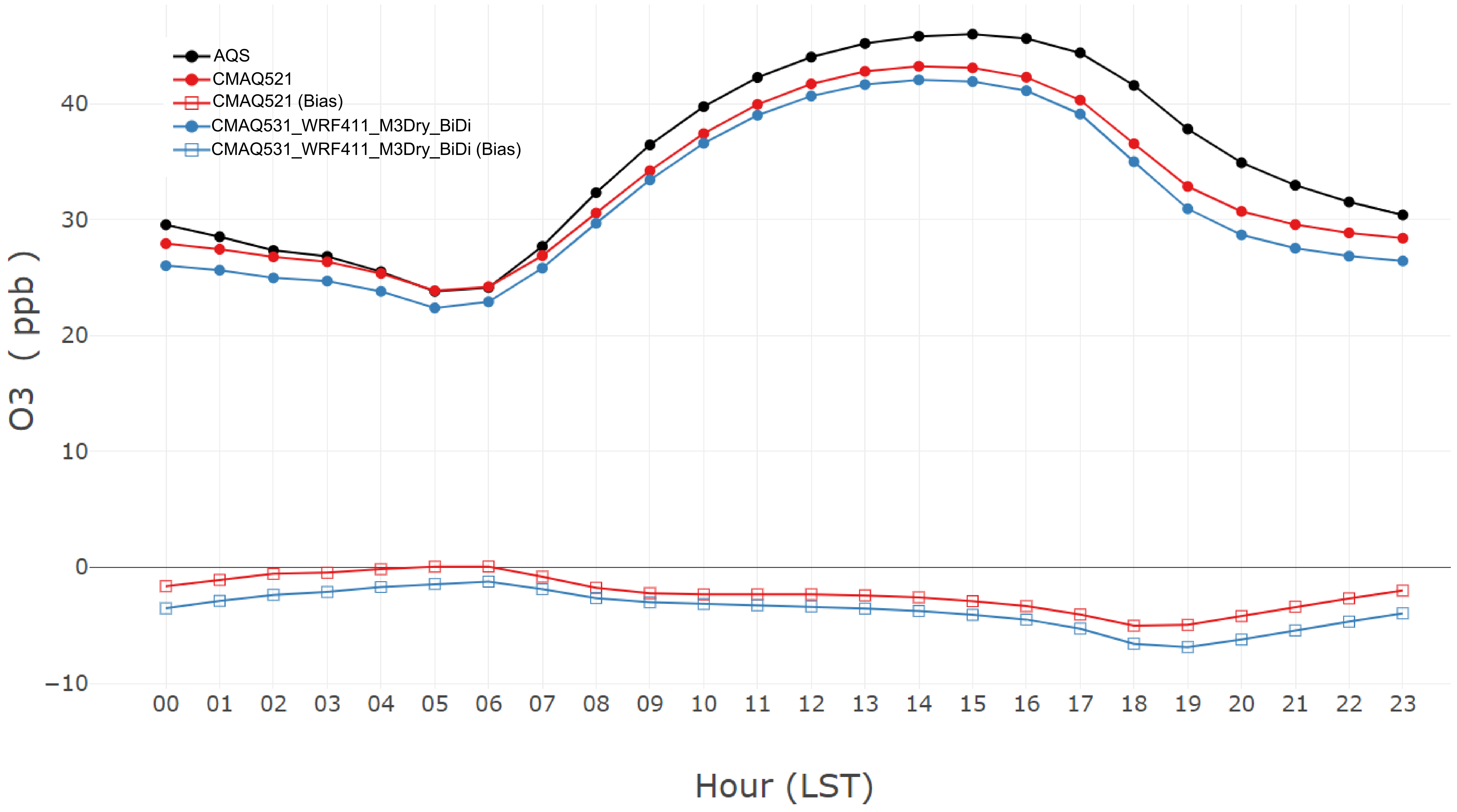

Figure S10. Time series of hourly average O_3 (ppbv; filled circles) and bias (open squares; ppbv) for all AQS sites for spring for the CMAQ521 (red) and CMAQ531_WRF411_M3Dry_BiDi (blue) simulations.

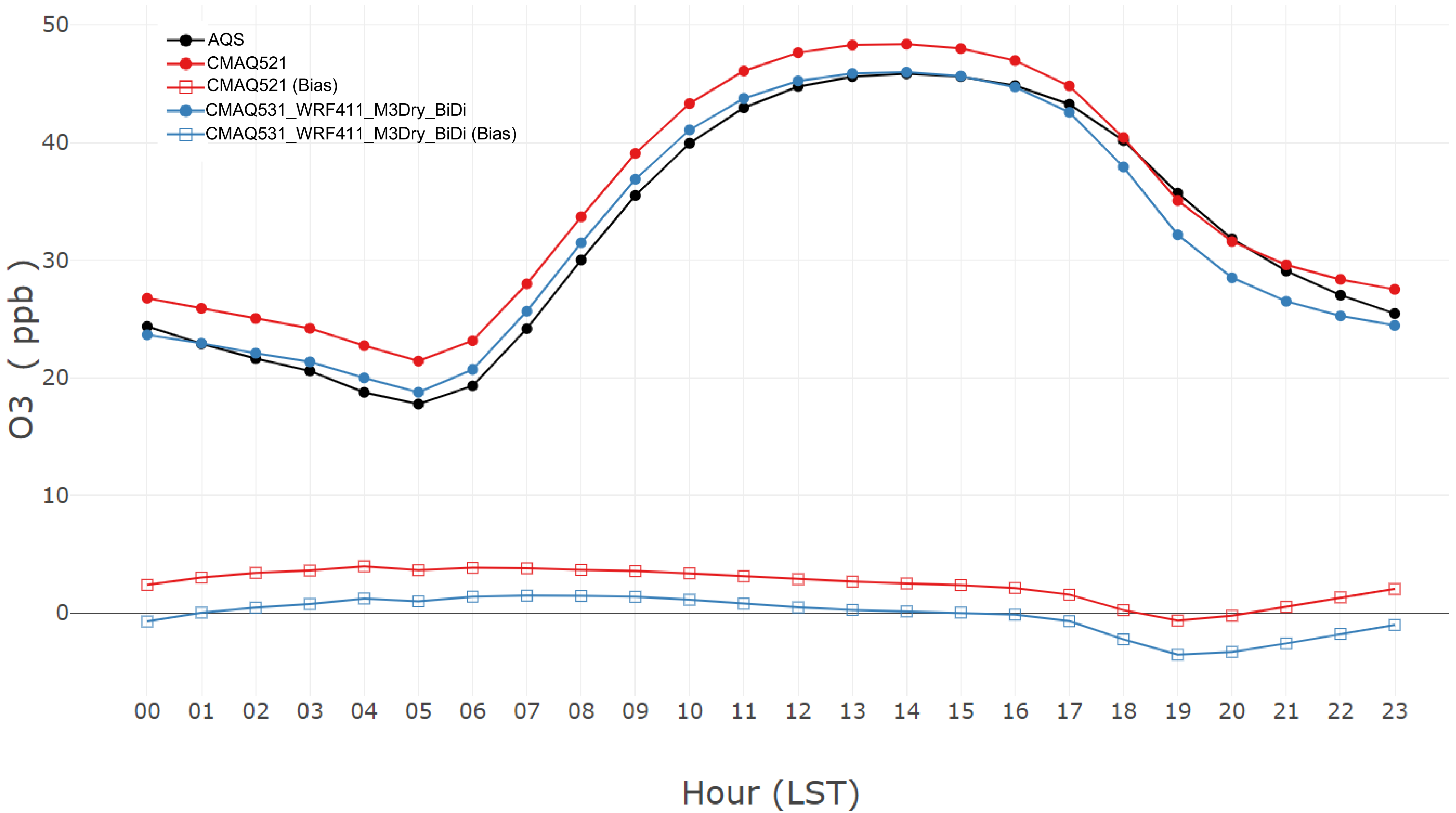

Figure S11. Time series of hourly average O_3 (ppbv; filled circles) and bias (open squares; ppbv) for all AQS sites for summer for the CMAQ521 (red) and CMAQ531_WRF411_M3Dry_BiDi (blue) simulations.

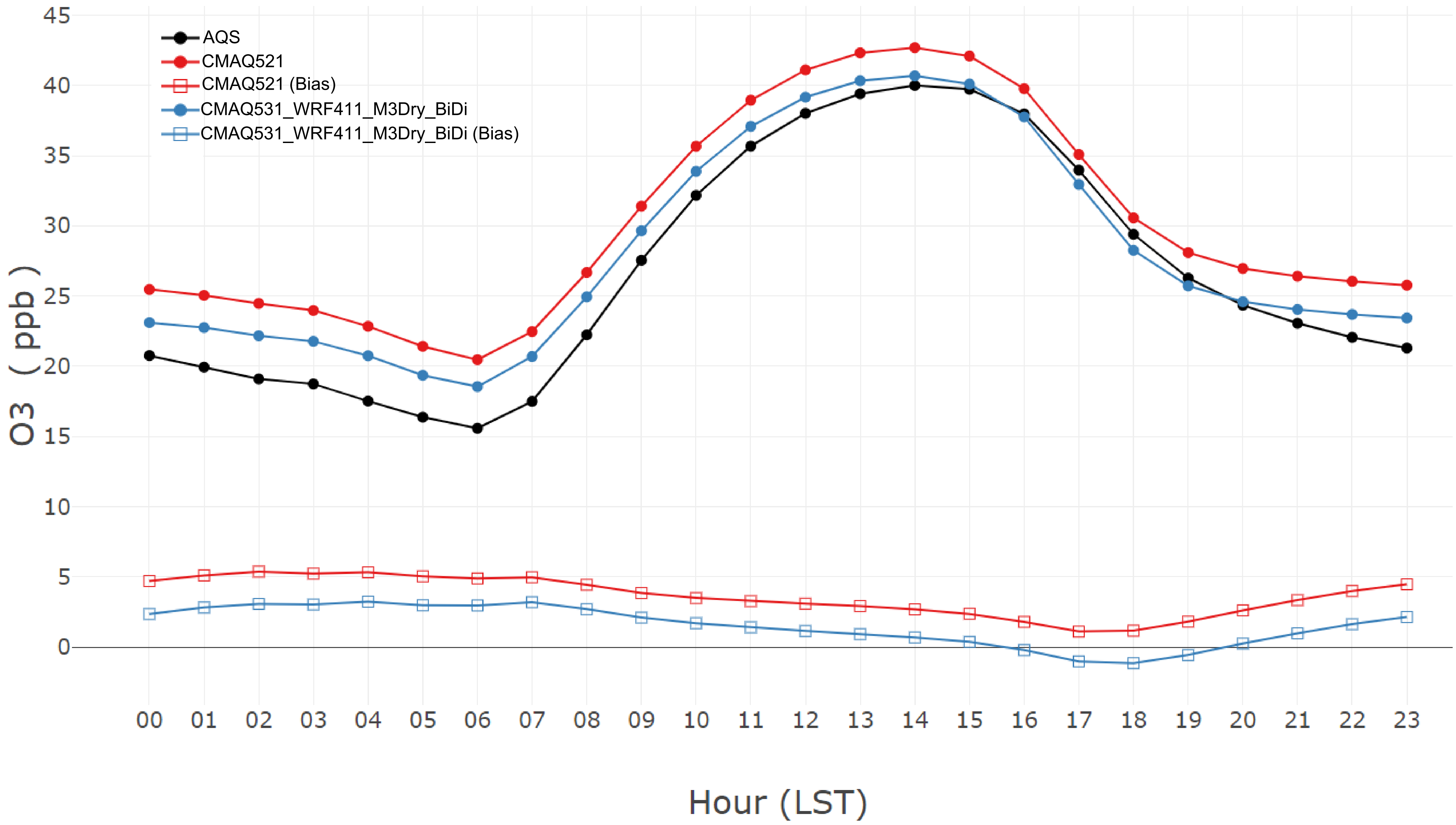

Figure S12. Time series of hourly average O_3 (ppbv; filled circles) and bias (open squares; ppbv) for all AQS sites for fall for the CMAQ521 (red) and CMAQ531_WRF411_M3Dry_BiDi (blue) simulations.

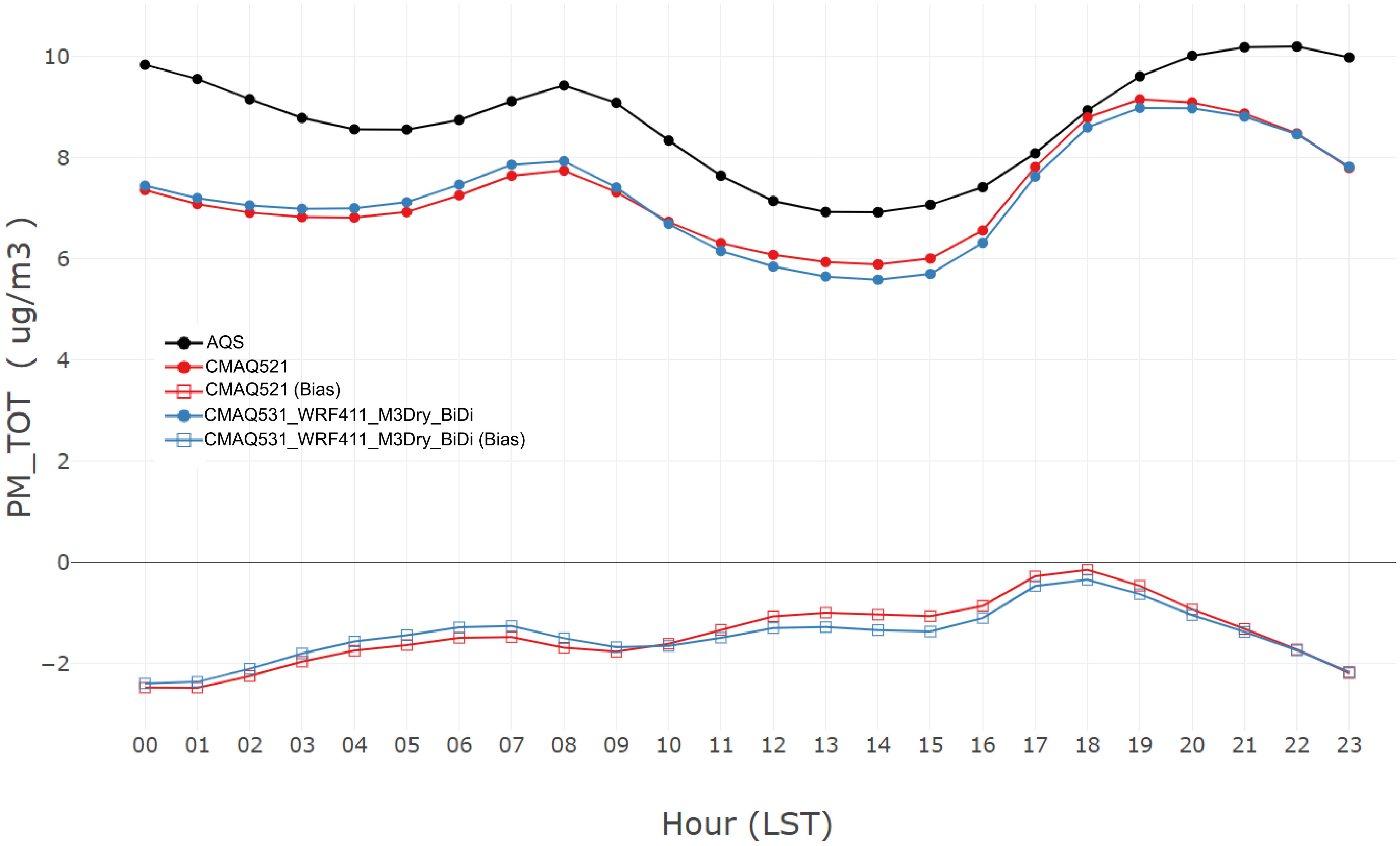

Figure S13. Time series of hourly average $PM_{2.5}$ ($\mu g\ m^{-3}$; filled circles) and bias ($\mu g\ m^{-3}$; open squares) for all AQS sites for winter for the CMAQ521 (red) and CMAQ531_WRF411_M3Dry_BiDi (blue) simulations.

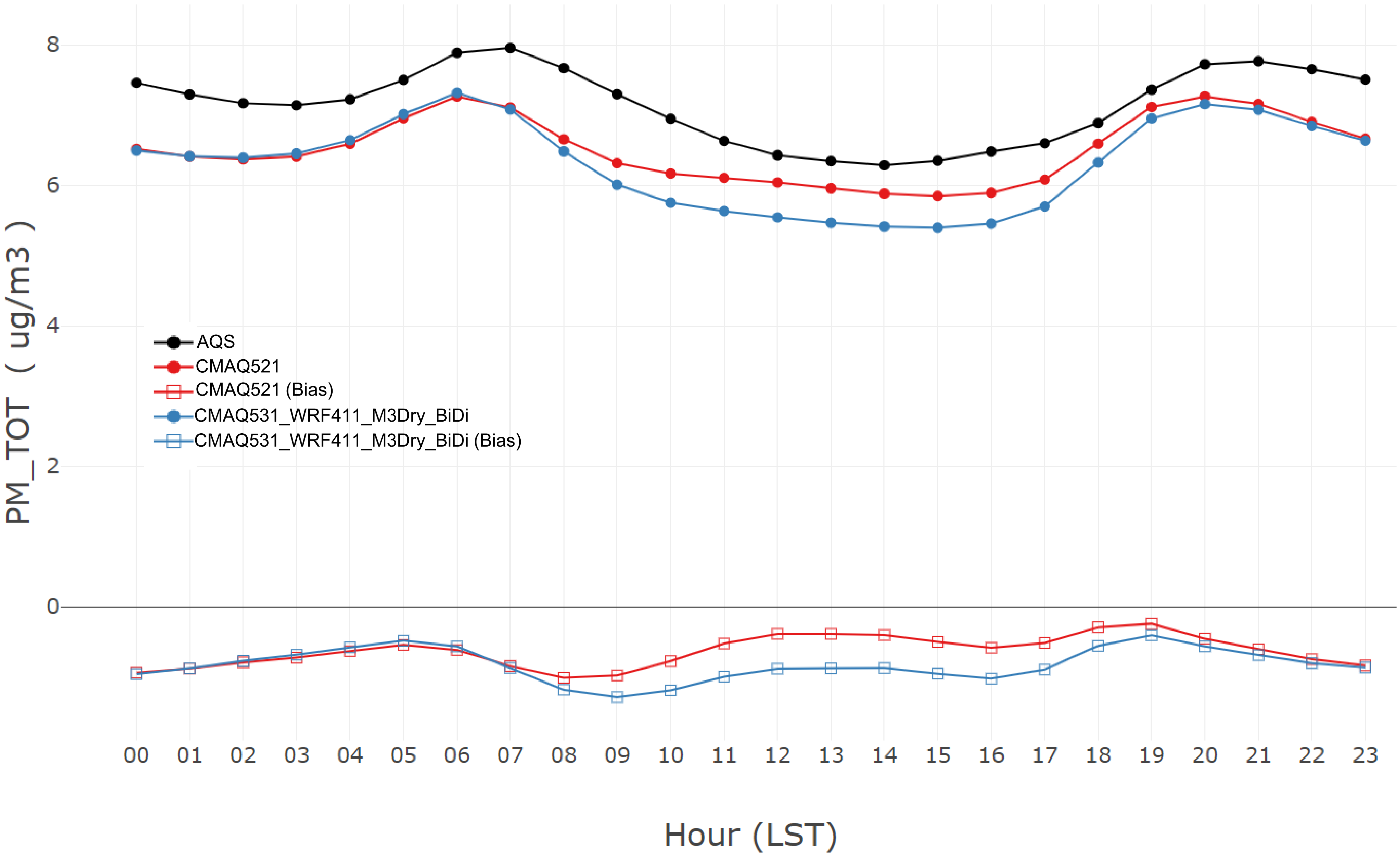

Figure S14. Time series of hourly average $PM_{2.5}$ ($\mu g\ m^{-3}$; filled circles) and bias ($\mu g\ m^{-3}$; open squares) for all AQS sites for spring for the CMAQ521 (red) and CMAQ531_WRF411_M3Dry_BiDi (blue) simulations.

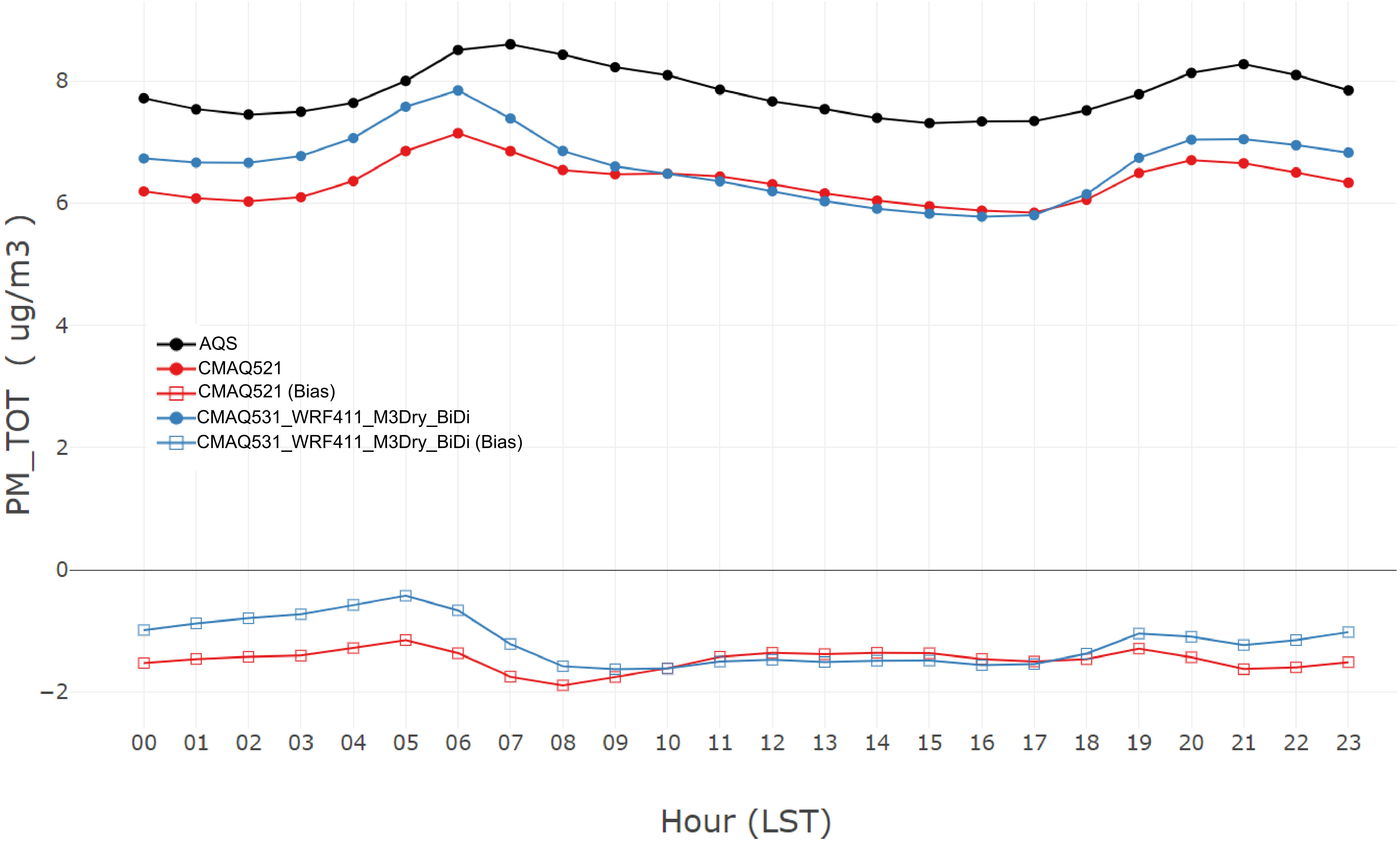

Figure S15. Time series of hourly average $PM_{2.5}$ ($\mu g\ m^{-3}$; filled circles) and bias ($\mu g\ m^{-3}$; open squares) for all AQS sites for summer for the CMAQ521 (red) and CMAQ531_WRF411_M3Dry_BiDi (blue) simulations.

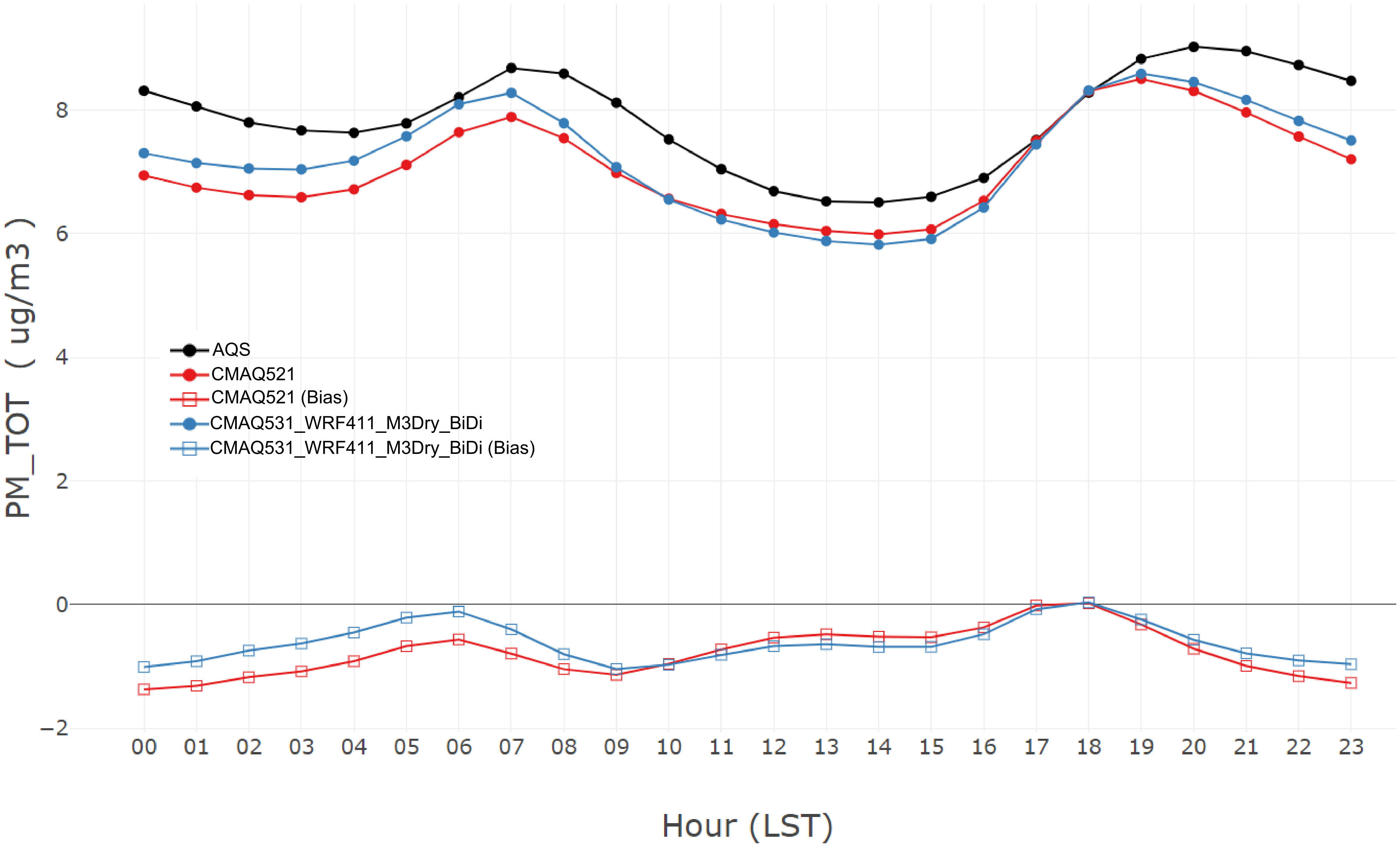

Figure S16. Time series of hourly average $PM_{2.5}$ ($\mu g\ m^{-3}$; filled circles) and bias ($\mu g\ m^{-3}$; open squares) for all AQS sites for fall for the CMAQ521 (red) and CMAQ531_WRF411_M3Dry_BiDi (blue) simulations.

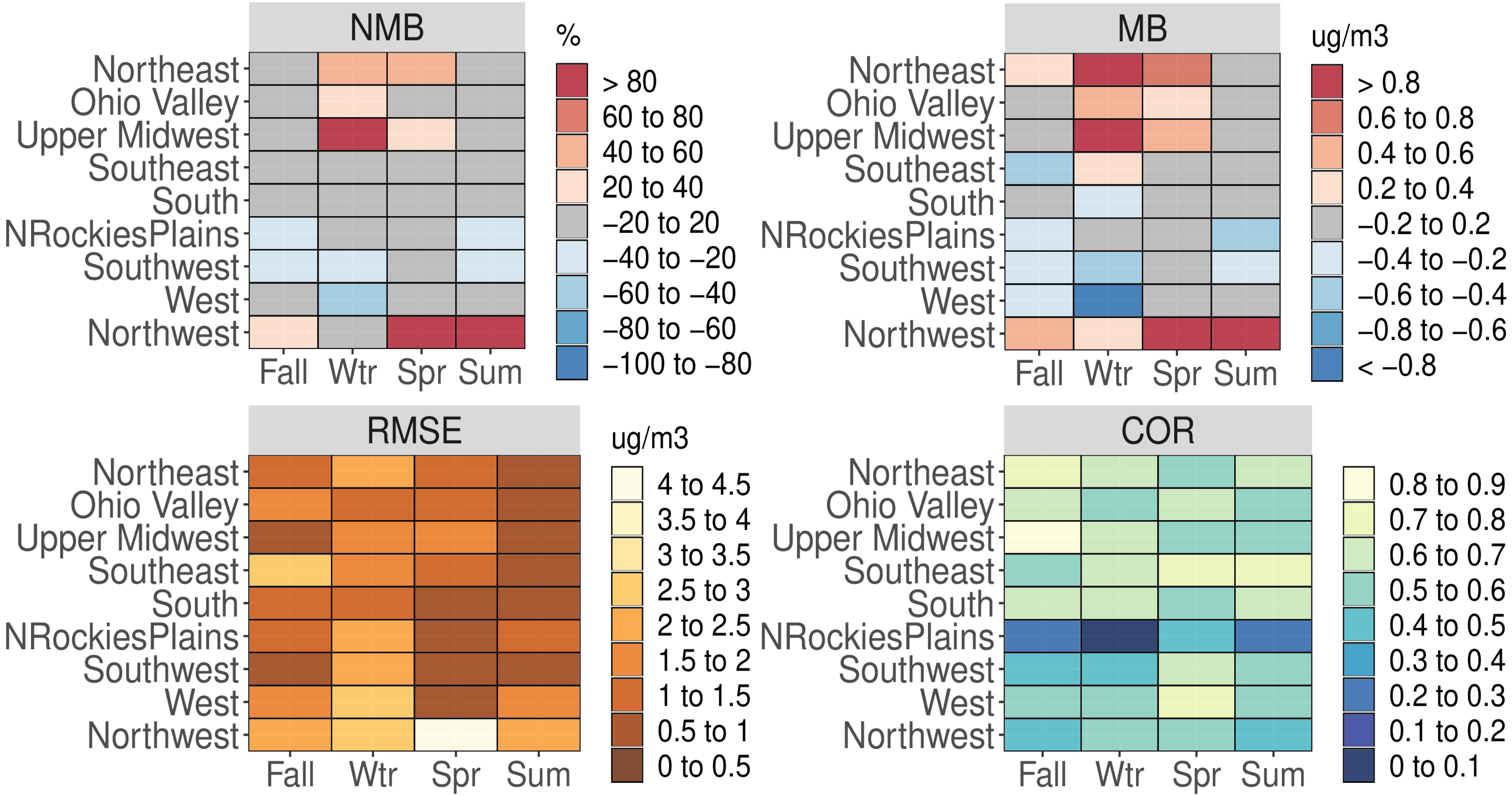

Figure S17. Categorical NMB (%), MB (μg m^{-3}), RMSE (μg m^{-3}), and Pearson correlation values for OC for all CSN sites based on season and NOAA climate region for the CMAQ521 simulation.

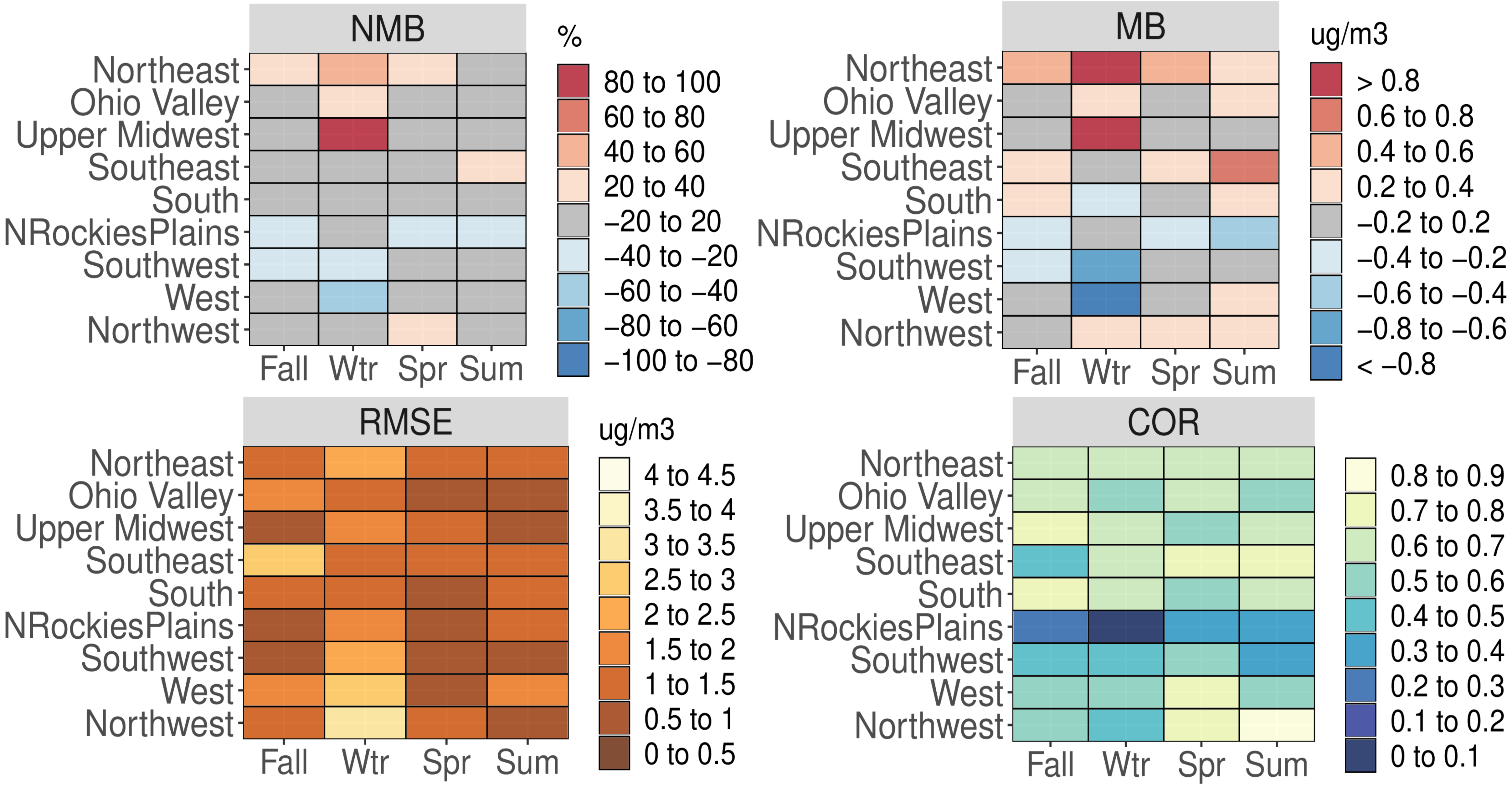

Figure S18. Categorical NMB (%), MB (μg m^{-3}), RMSE (μg m^{-3}), and Pearson correlation values for OC for all CSN sites based on season and NOAA climate region for the CMAQ531_WRF411_M3Dry_BiDi simulation.

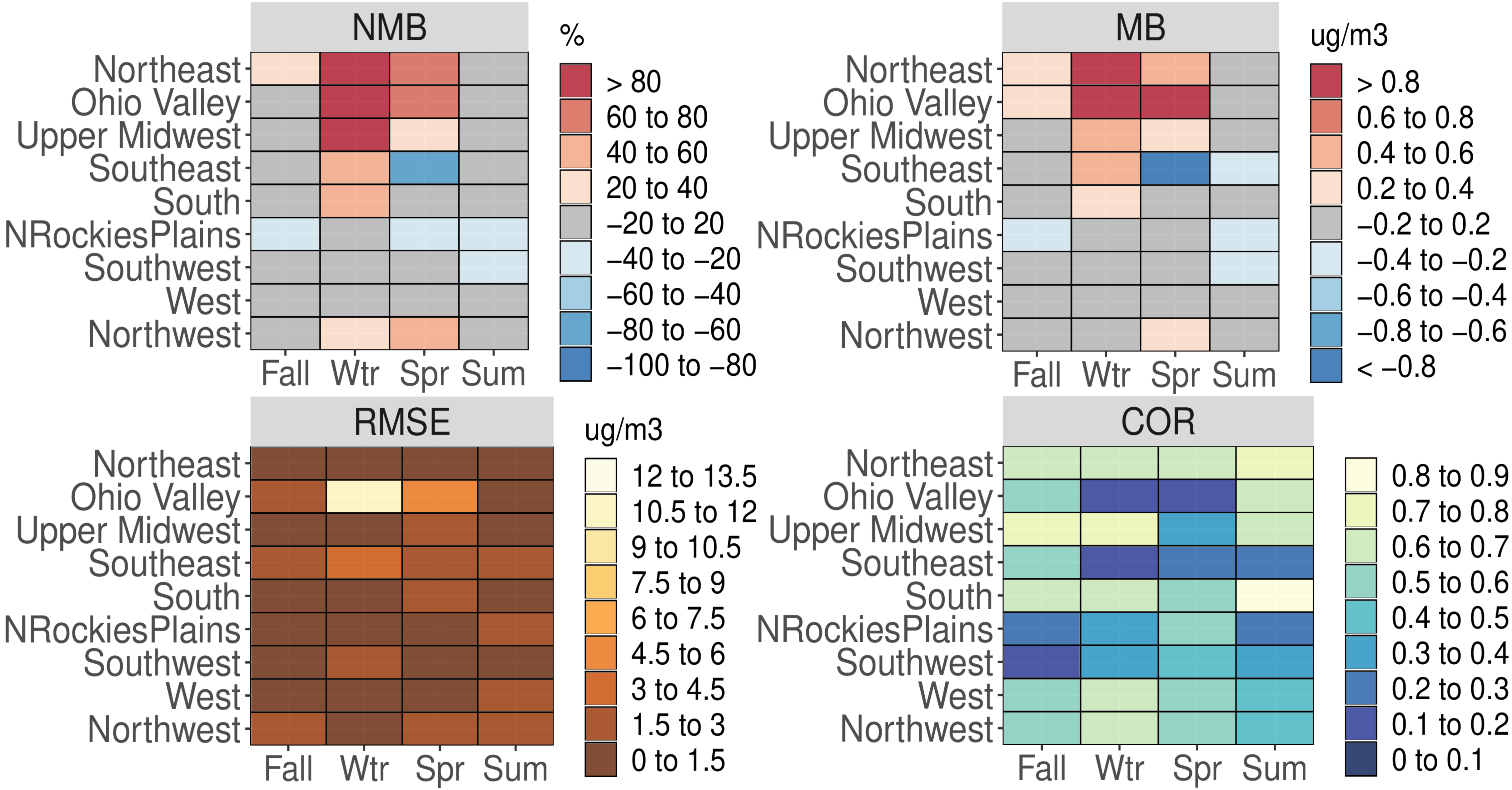

Figure S19. Categorical NMB (%), MB (μg m^{-3}), RMSE (μg m^{-3}), and Pearson correlation values for OC for all CSN sites based on season and NOAA climate region for the CMAQ521 simulation.

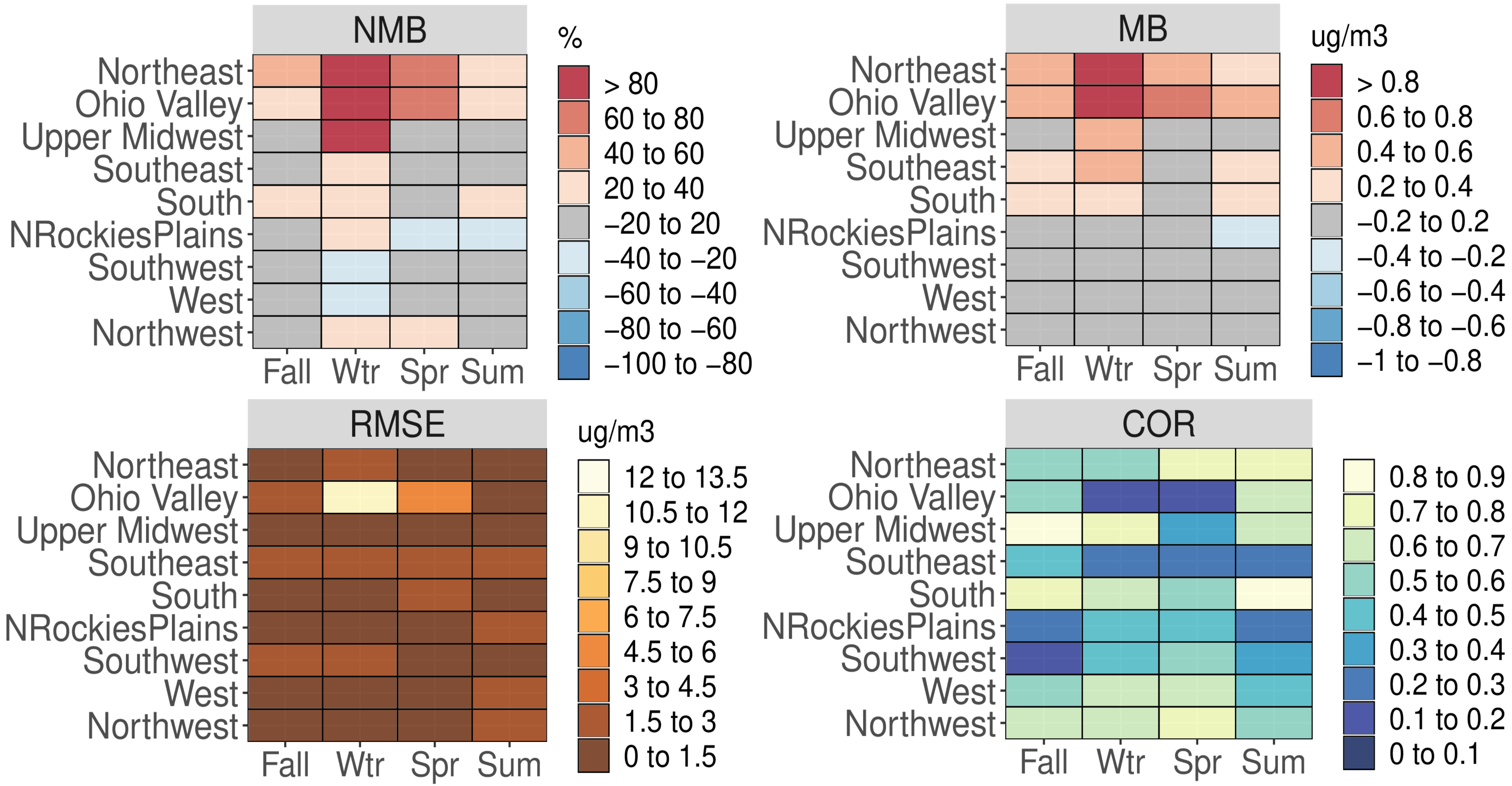

Figure S20. Categorical NMB (%), MB (μg m^{-3}), RMSE (μg m^{-3}), and Pearson correlation values for OC for all IMPROVE sites based on season and NOAA climate region for the CMAQ531_WRF411_M3Dry_BiDi simulation.

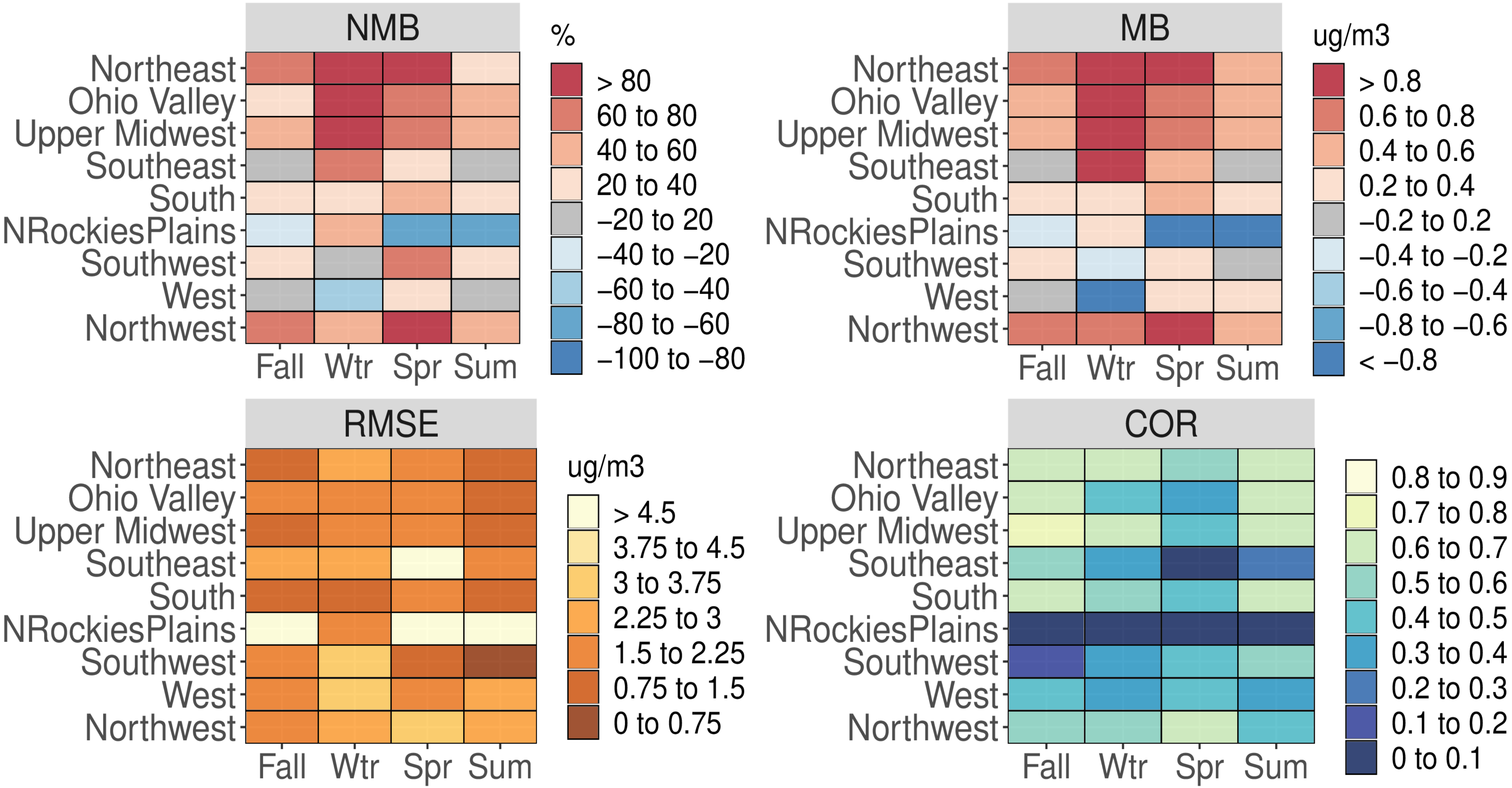

Figure S21. Categorical NMB (%), MB (μg m^{-3}), RMSE (μg m^{-3}), and Pearson correlation values for OC for all AQS sites based on season and NOAA climate region for the CMAQ521 simulation.

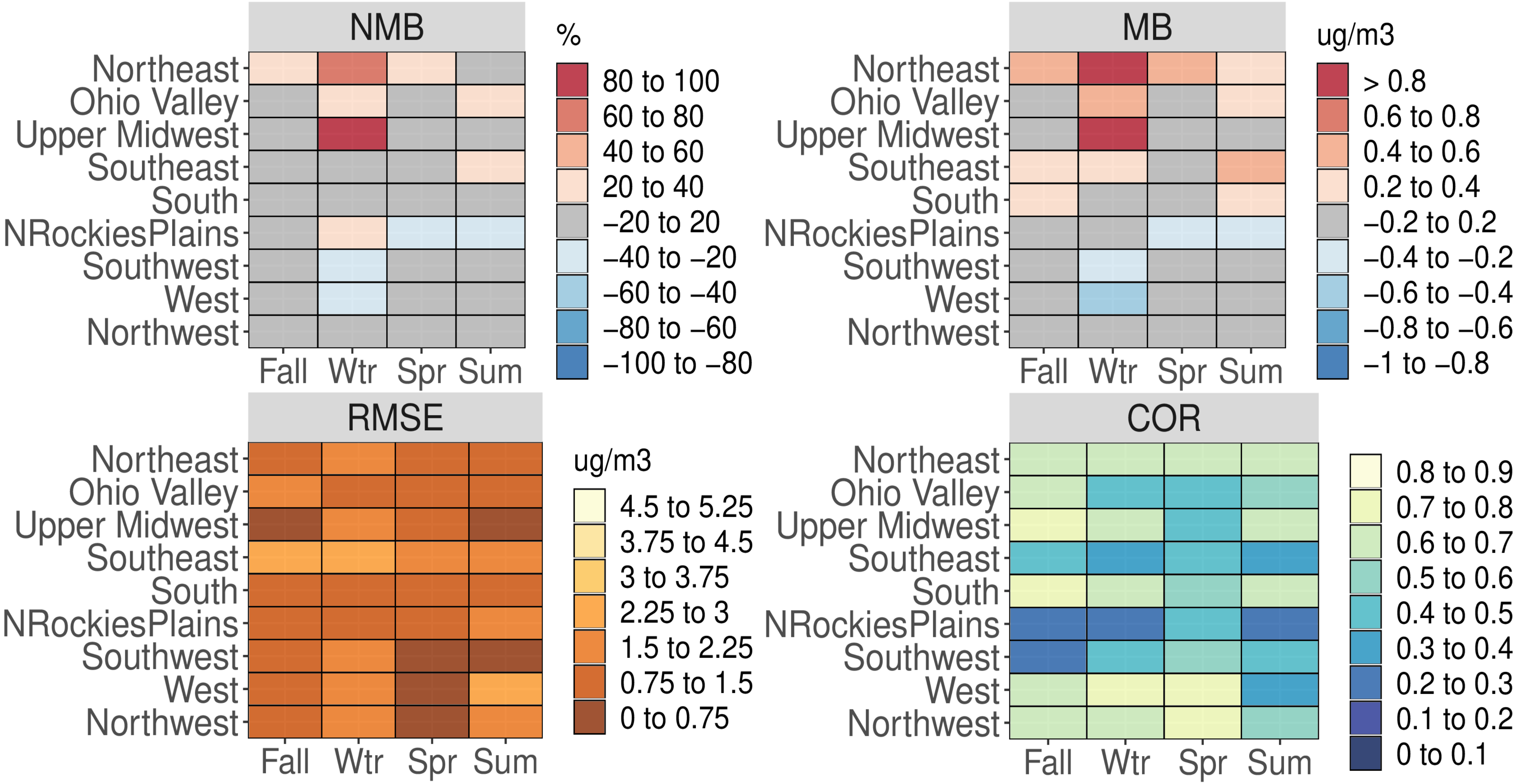

Figure S22. Categorical NMB (%), MB (μg m^{-3}), RMSE (μg m^{-3}), and Pearson correlation values for OC for all AQS sites based on season and NOAA climate region for the CMAQ531_WRF411_M3Dry_BiDi simulation.

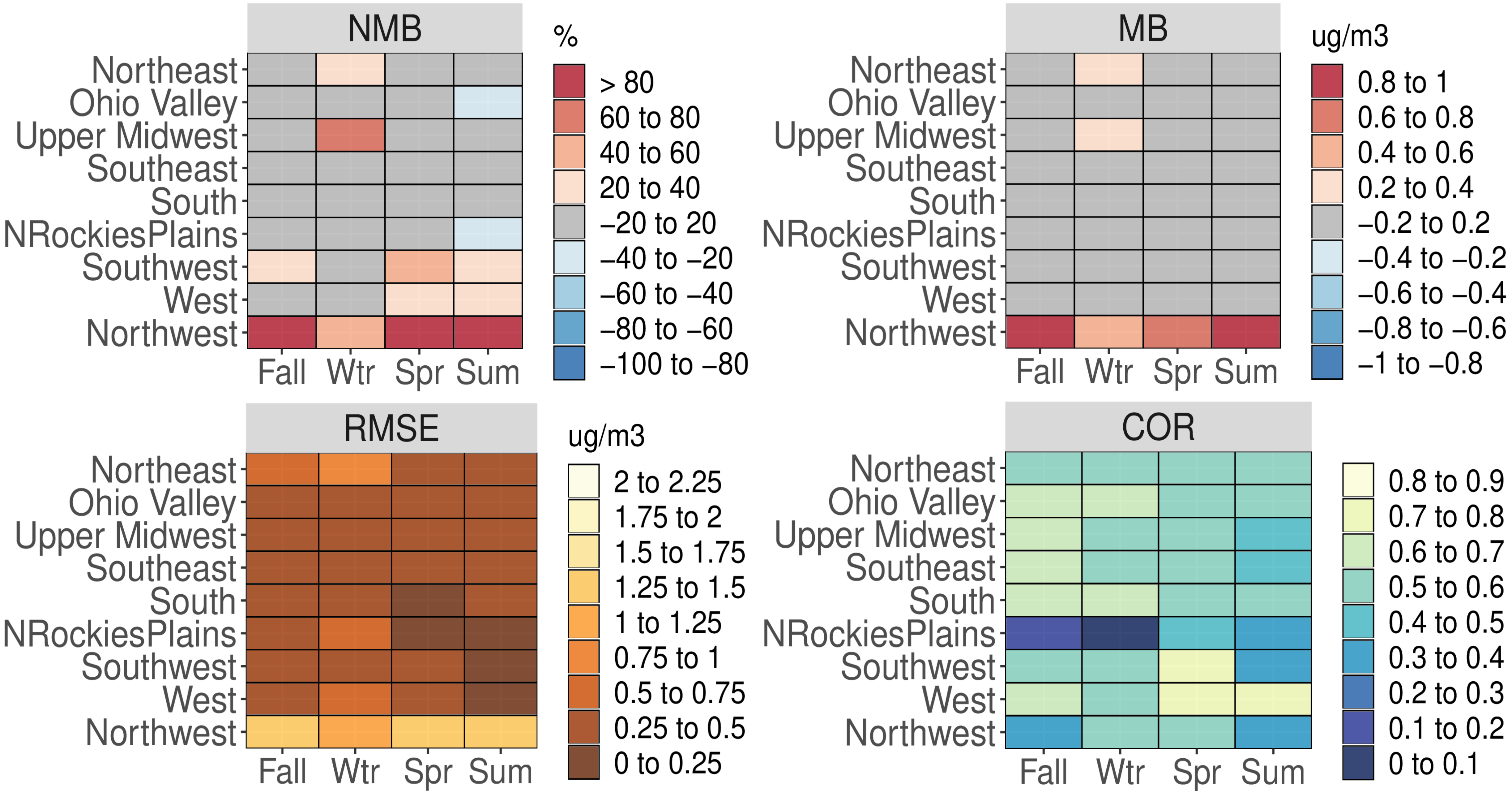

Figure S23. Categorical NMB (%), MB (μg m^{-3}), RMSE (μg m^{-3}), and Pearson correlation values for EC for all CSN sites based on season and NOAA climate region for the CMAQ521 simulation.

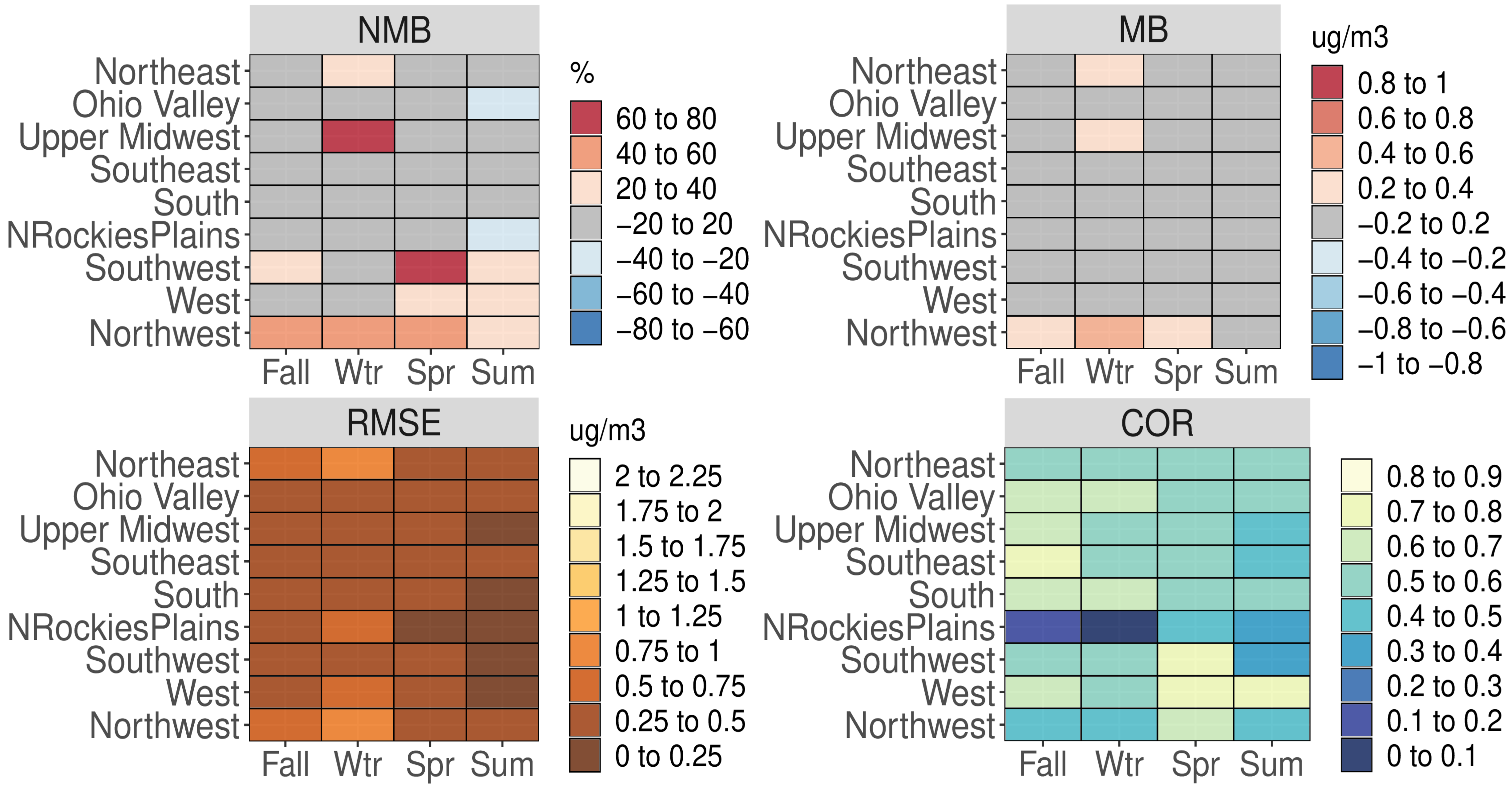

Figure S24. Categorical NMB (%), MB (μg m^{-3}), RMSE (μg m^{-3}), and Pearson correlation values for EC for all CSN sites based on season and NOAA climate region for the CMAQ531_WRF411_M3Dry_BiDi simulation.

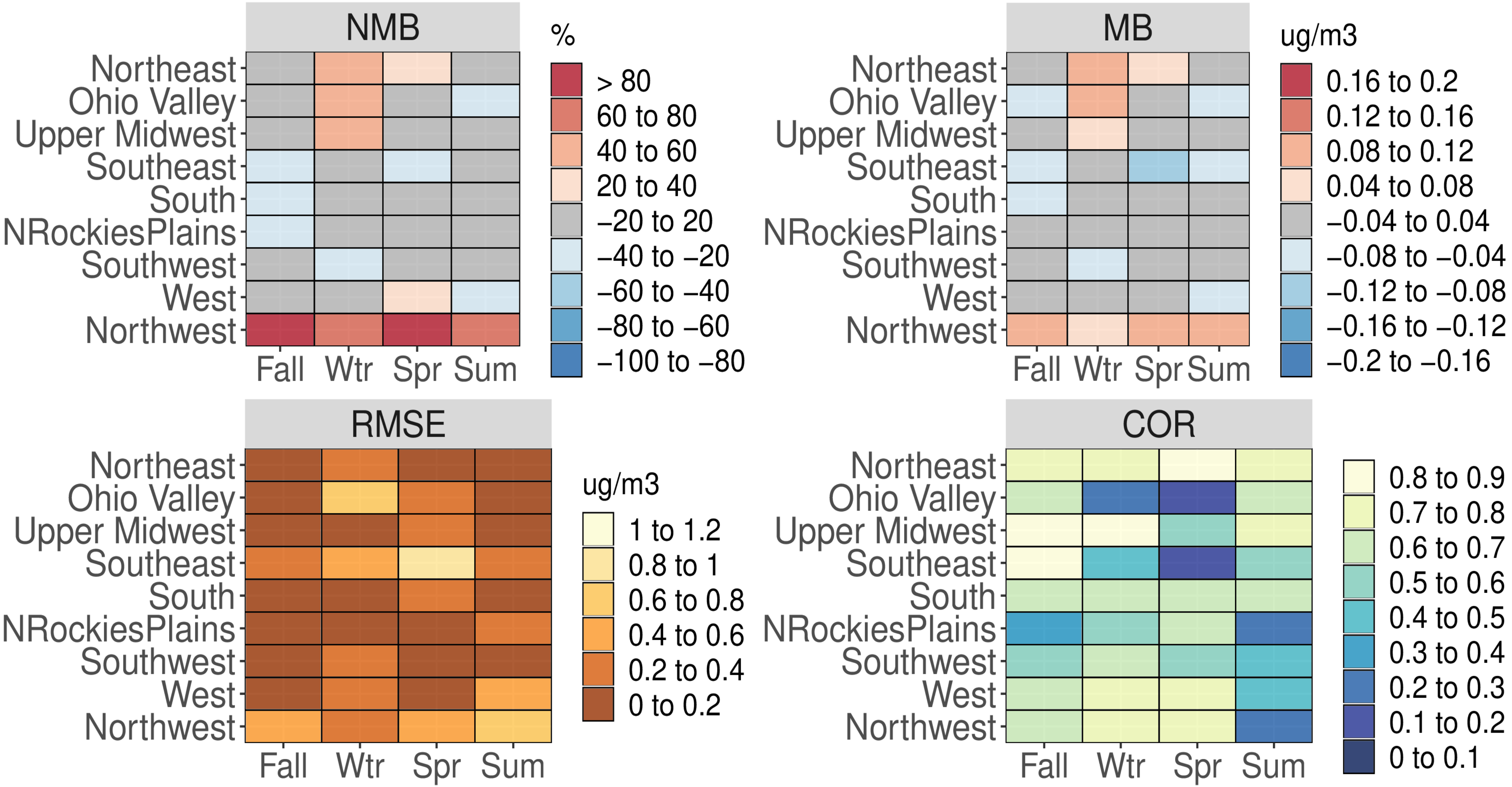

Figure S25. Categorical NMB (%), MB (μg m^{-3}), RMSE (μg m^{-3}), and Pearson correlation values for EC for all IMPROVE sites based on season and NOAA climate region for the CMAQ521 simulation.

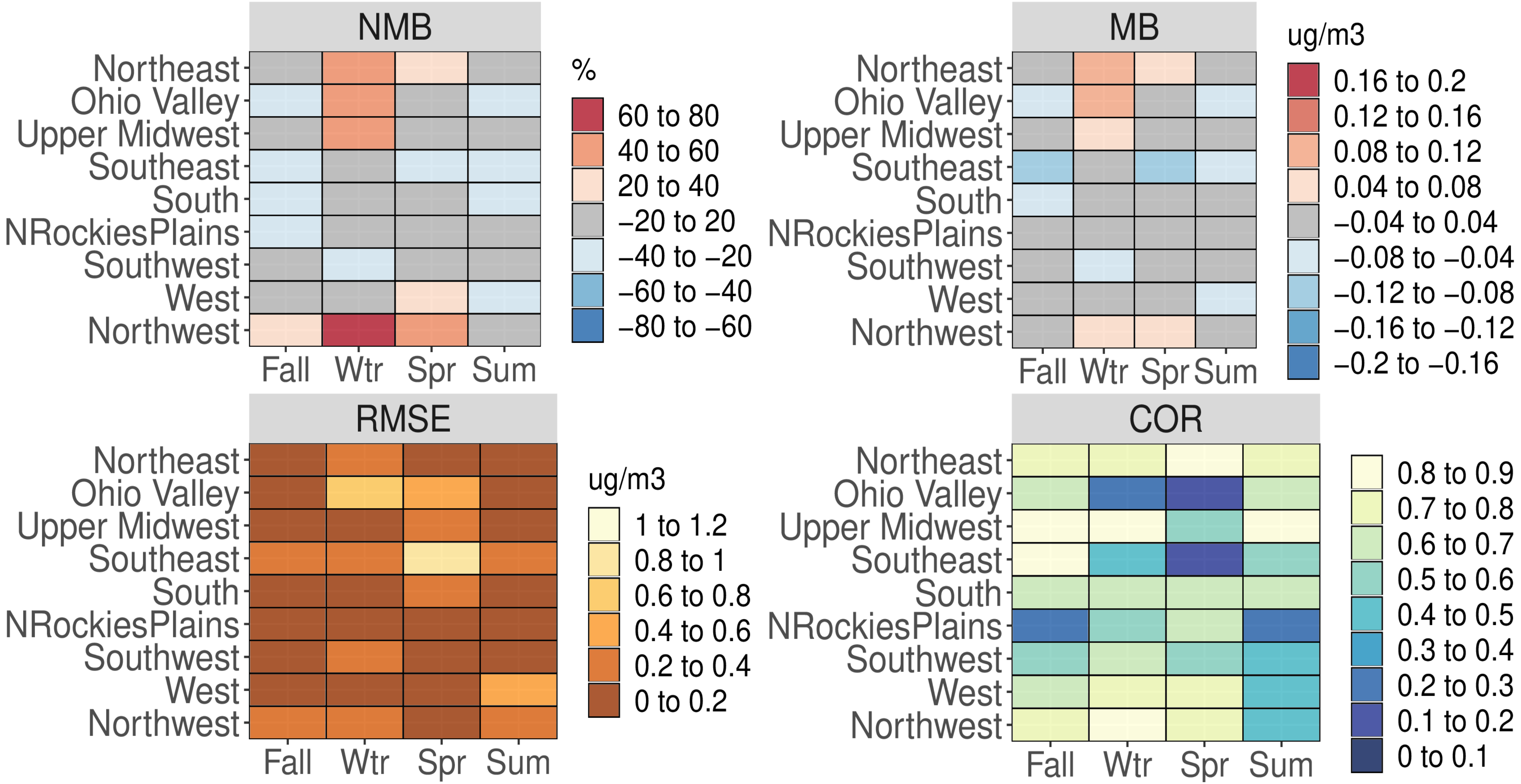

Figure S26. Categorical NMB (%), MB (μg m^{-3}), RMSE (μg m^{-3}), and Pearson correlation values for EC for all IMPROVE sites based on season and NOAA climate region for the CMAQ531_WRF411_M3Dry_BiDi simulation.

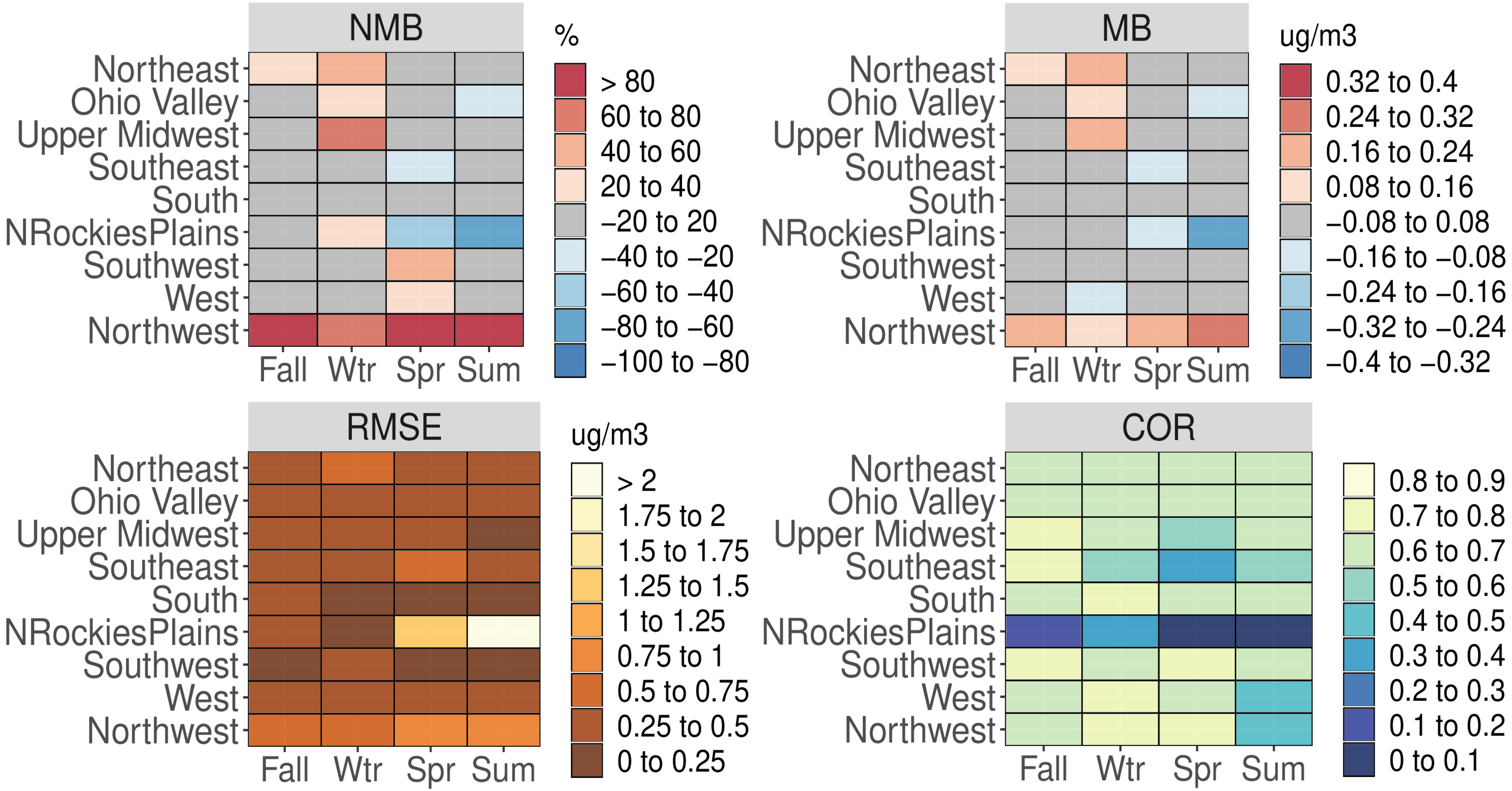

Figure S27. Categorical NMB (%), MB (μg m^{-3}), RMSE (μg m^{-3}), and Pearson correlation values for EC for all AQS sites based on season and NOAA climate region for the CMAQ521 simulation.

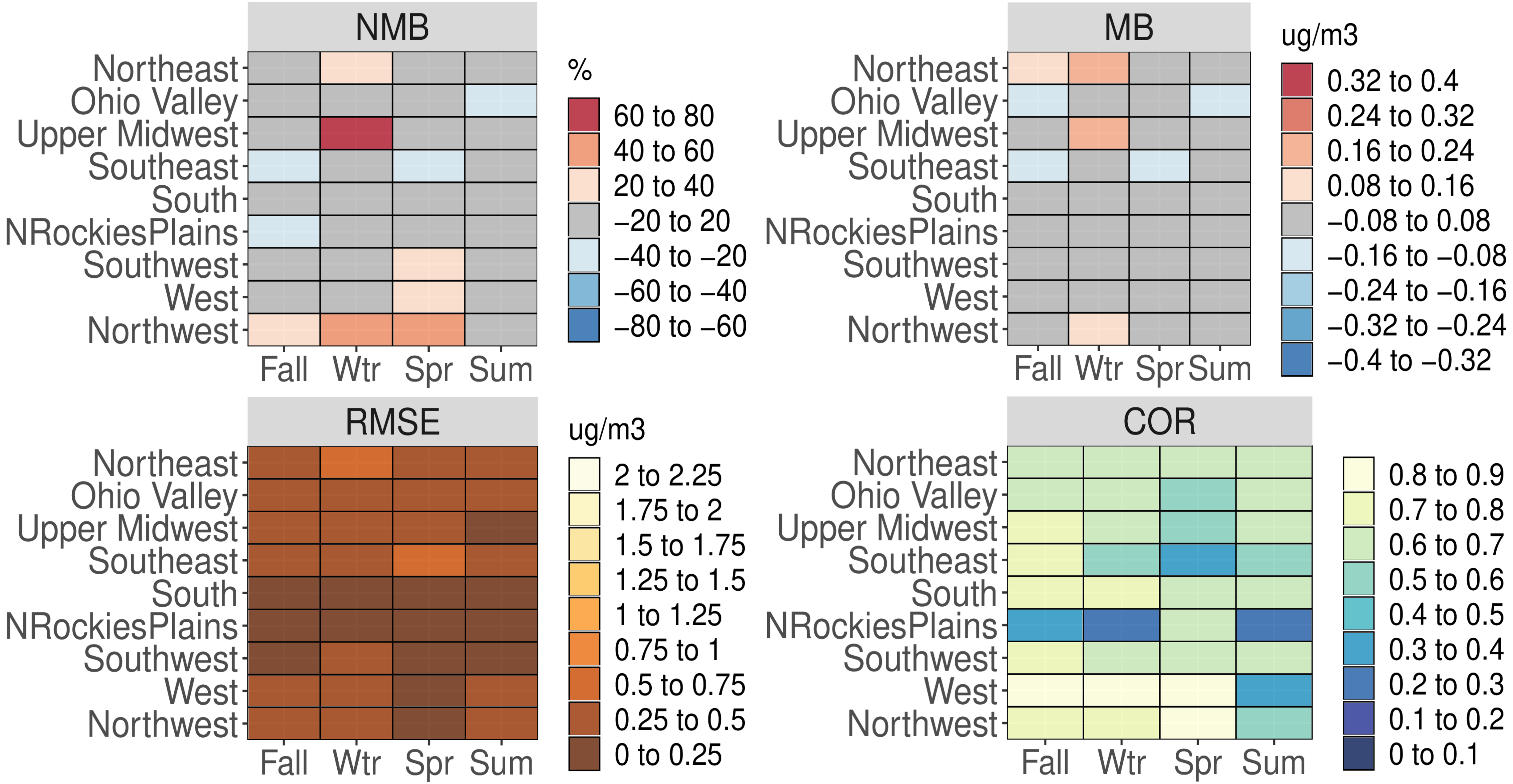

Figure S28. Categorical NMB (%), MB (μg m^{-3}), RMSE (μg m^{-3}), and Pearson correlation values for EC for all AQS sites based on season and NOAA climate region for the CMAQ531_WRF411_M3Dry_BiDi simulation.

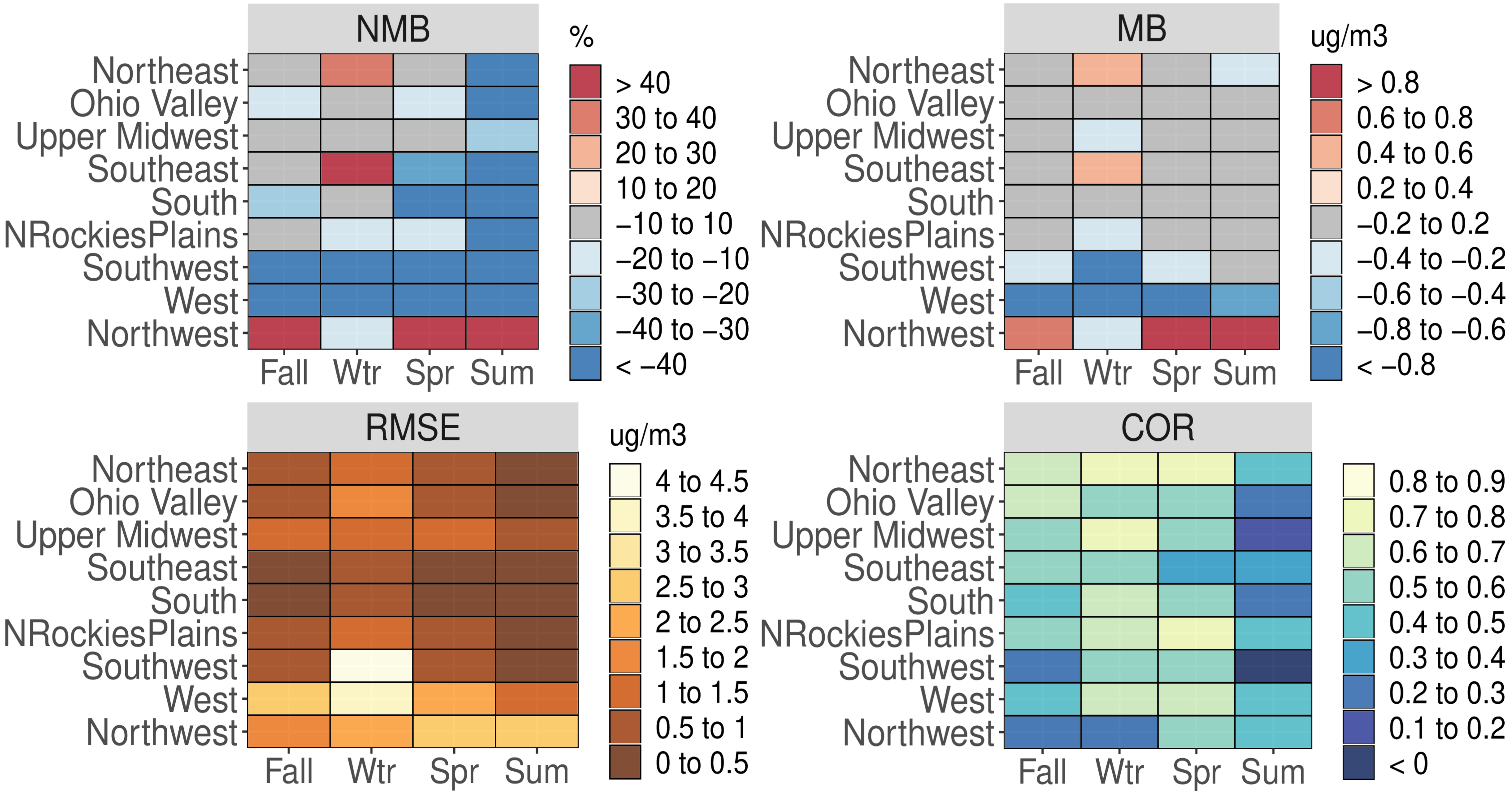

Figure S29. Categorical NMB (%), MB (μg m^{-3}), RMSE (μg m^{-3}), and Pearson correlation values for NO_3^- for all CSN sites based on season and NOAA climate region for the CMAQ521 simulation.

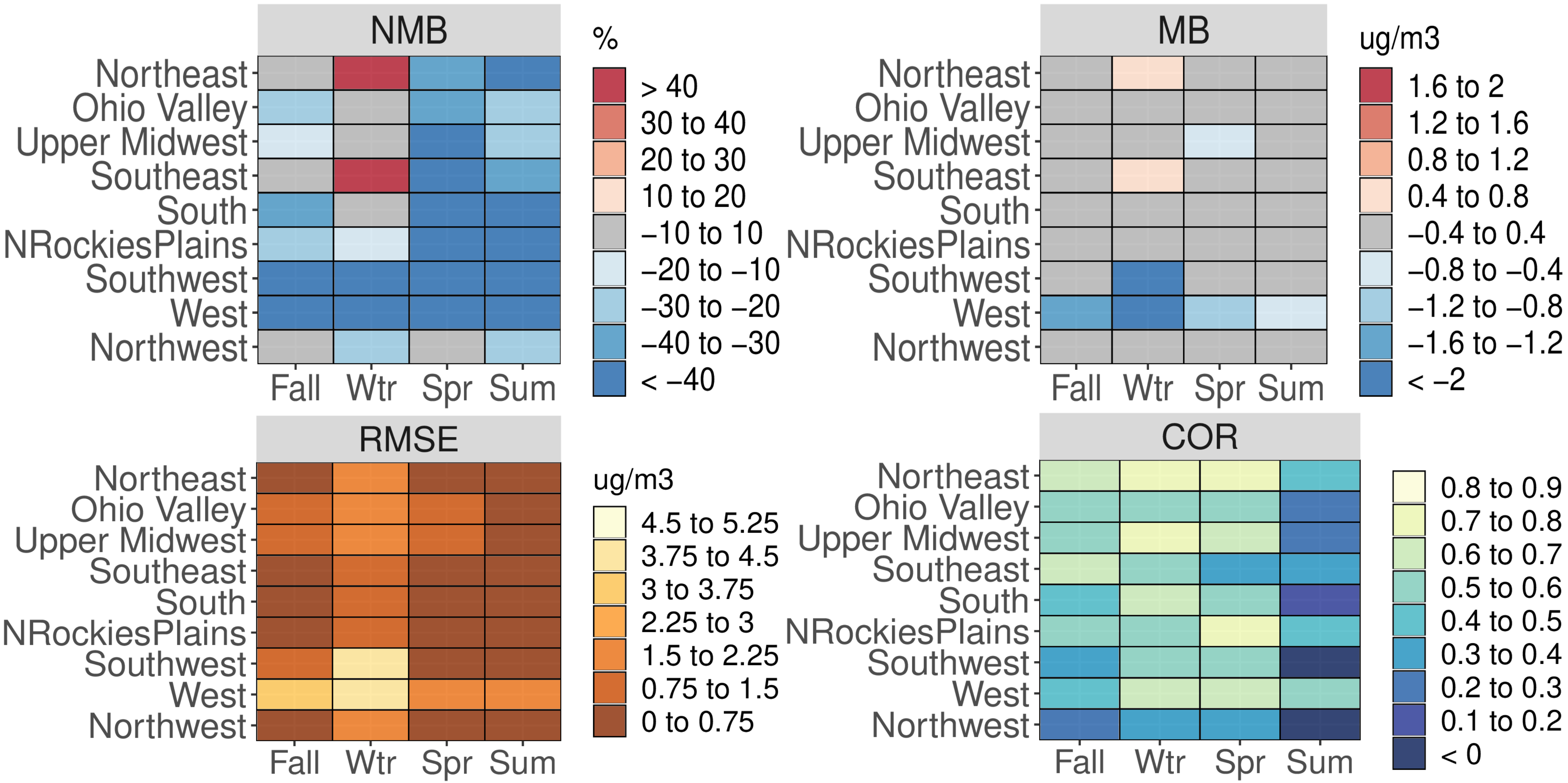

Figure S30. Categorical NMB (%), MB (μg m^{-3}), RMSE (μg m^{-3}), and Pearson correlation values for NO_3^- for all CSN sites based on season and NOAA climate region for the CMAQ531_WRF411_M3Dry_BiDi simulation.

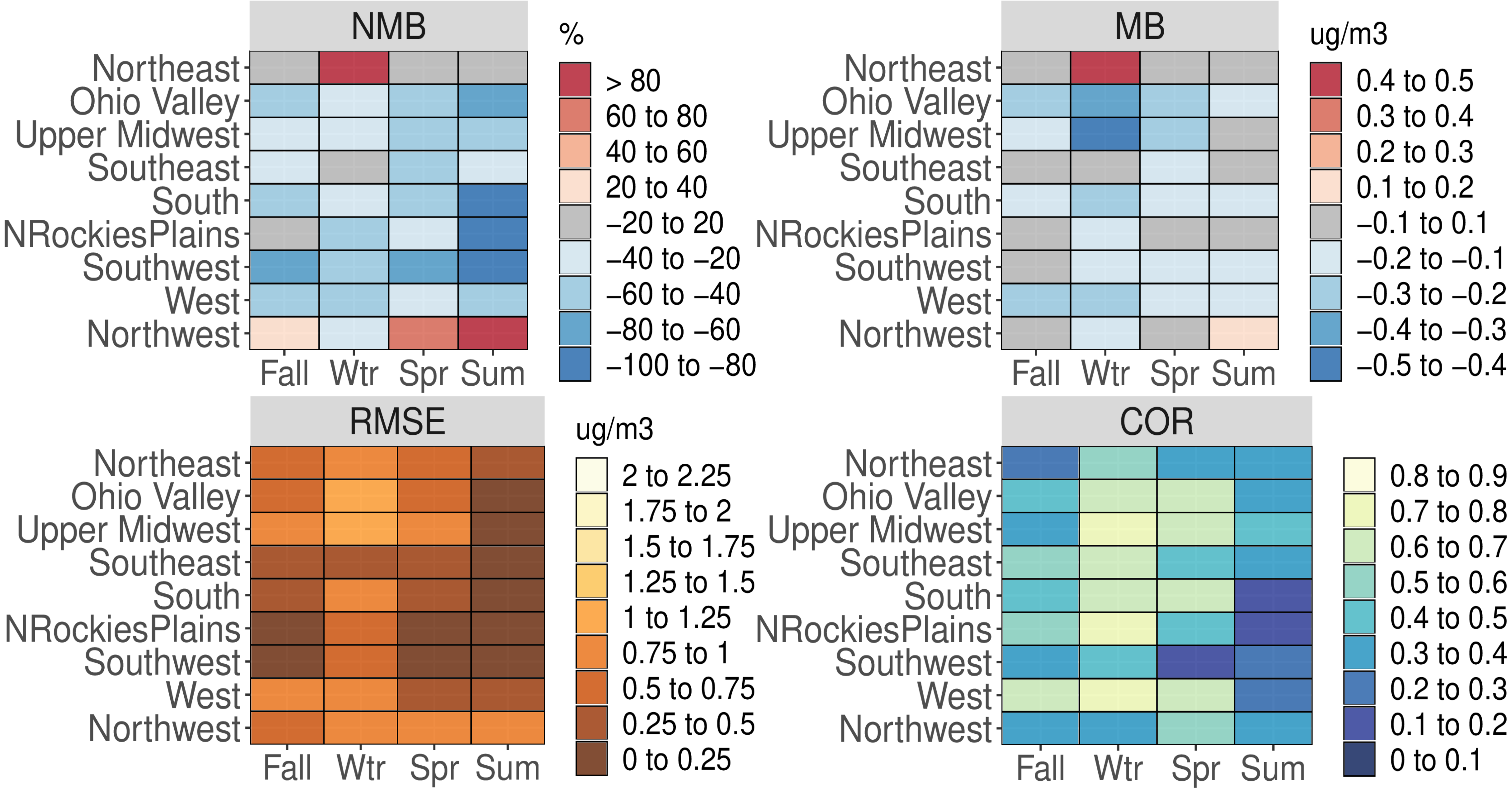

Figure S31. Categorical NMB (%), MB (µg m^{-3}), RMSE (µg m^{-3}), and Pearson correlation values for NO_3^- for all IMPROVE sites based on season and NOAA climate region for the CMAQ521 simulation.

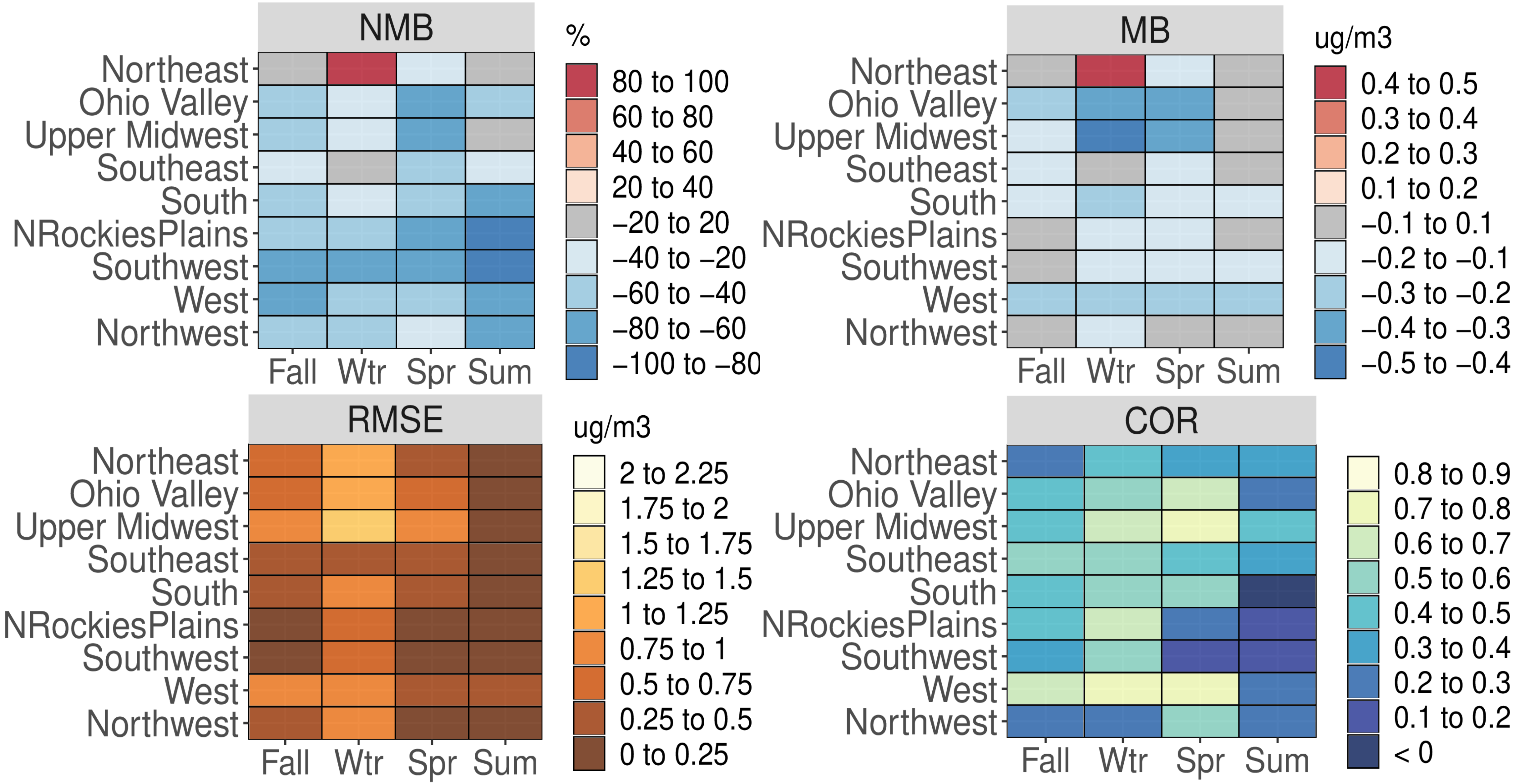

Figure S32. Categorical NMB (%), MB (µg m^{-3}), RMSE (µg m^{-3}), and Pearson correlation values for NO_3^- for all IMPROVE sites based on season and NOAA climate region for the CMAQ531_WRF411_M3Dry_BiDi simulation.

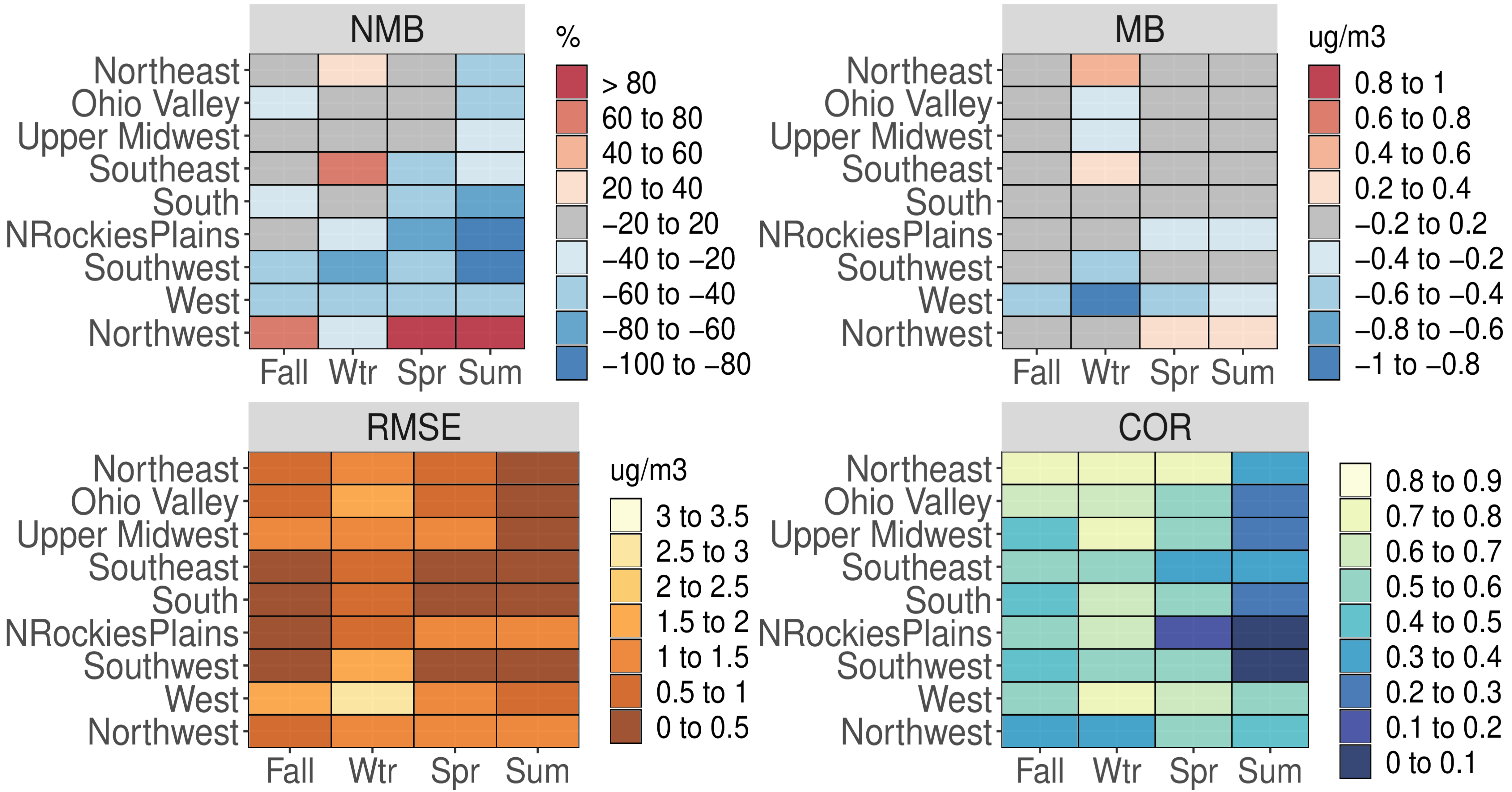

Figure S33. Categorical NMB (%), MB (μg m^{-3}), RMSE (μg m^{-3}), and Pearson correlation values for NO_3^- for all AQS sites based on season and NOAA climate region for the CMAQ521 simulation.

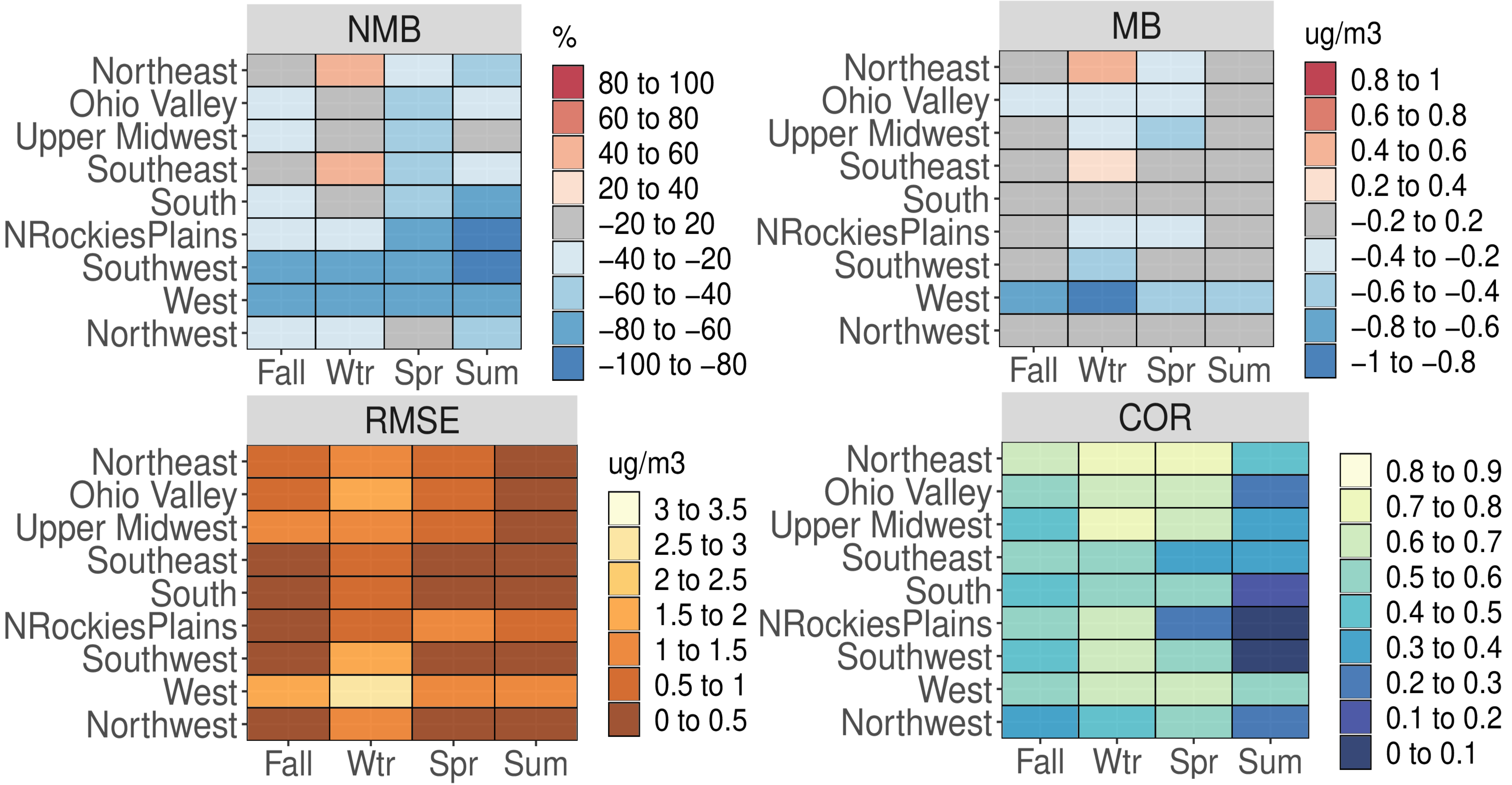

Figure S34. Categorical NMB (%), MB (µg m^{-3}), RMSE (µg m^{-3}), and Pearson correlation values for NO_3^- for all AQS sites based on season and NOAA climate region for the CMAQ531_WRF411_M3Dry_BiDi simulation.

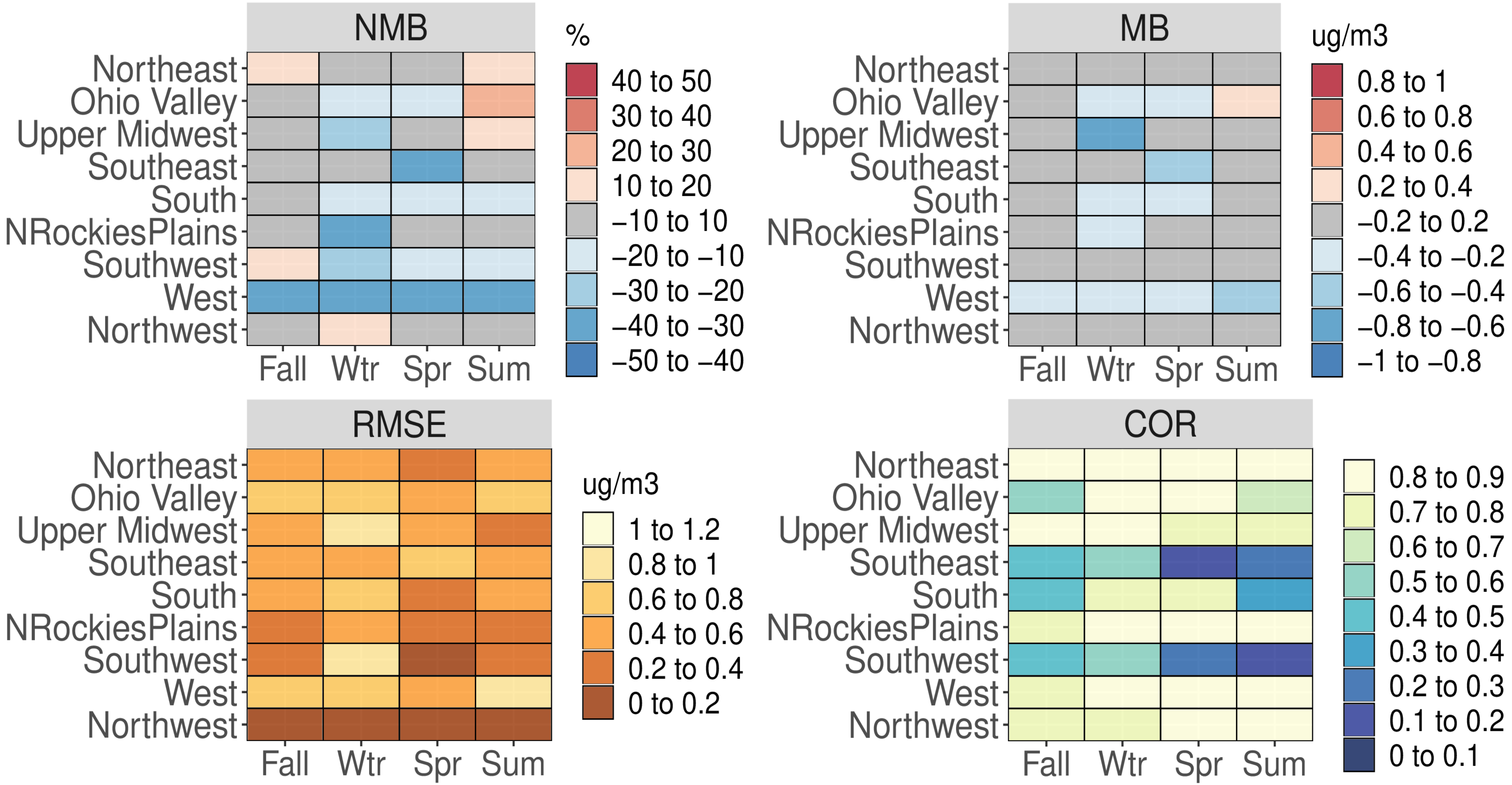

Figure S35. Categorical NMB (%), MB (μg m^{-3}), RMSE (μg m^{-3}), and Pearson correlation values for TNO_3^- for all CASTNet sites based on season and NOAA climate region for the CMAQ521 simulation.

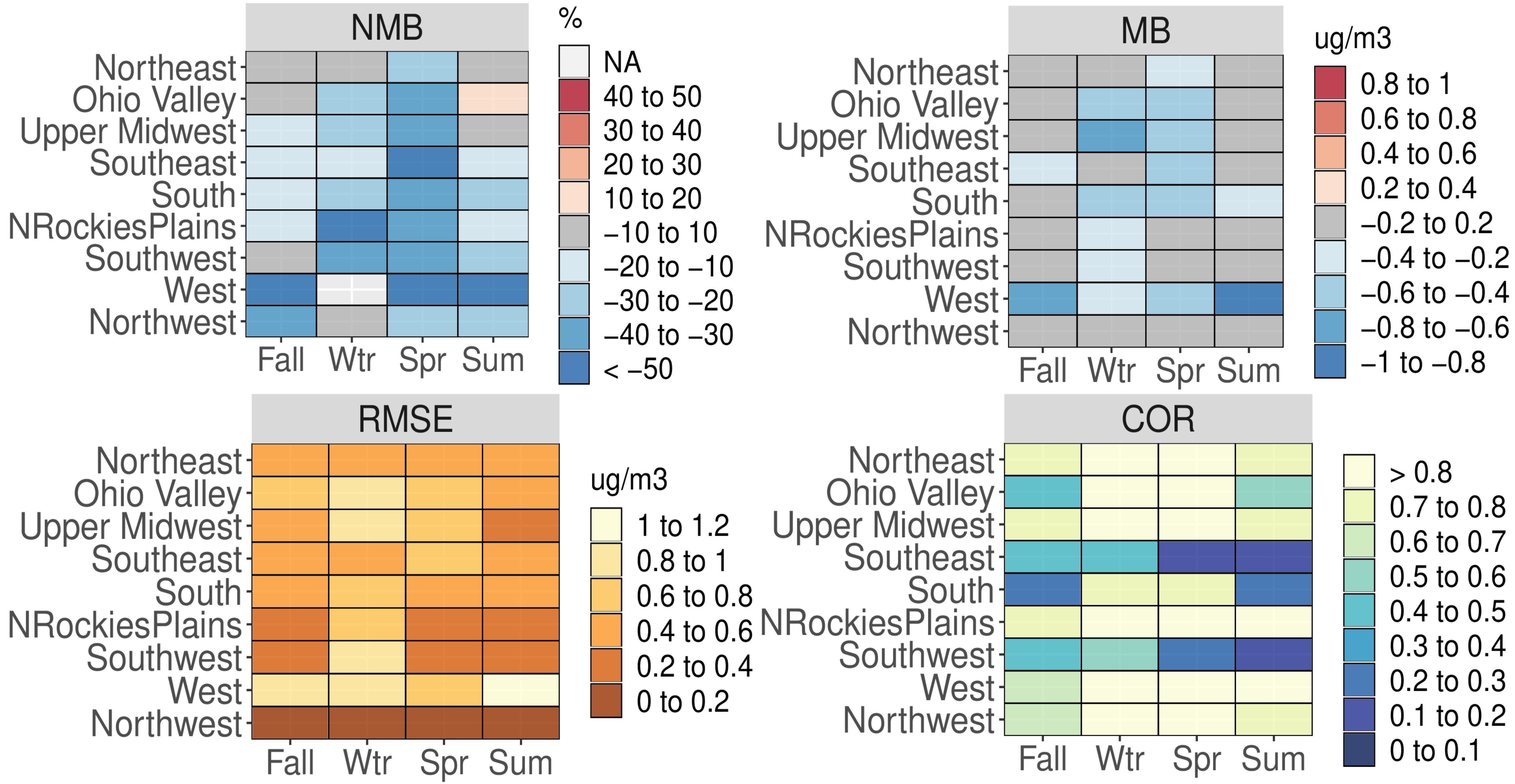

Figure S36. Categorical NMB (%), MB (μg m^{-3}), RMSE (μg m^{-3}), and Pearson correlation values for TNO_3^- for all CASTNet sites based on season and NOAA climate region for the CMAQ531_WRF411_M3Dry_BiDi simulation.

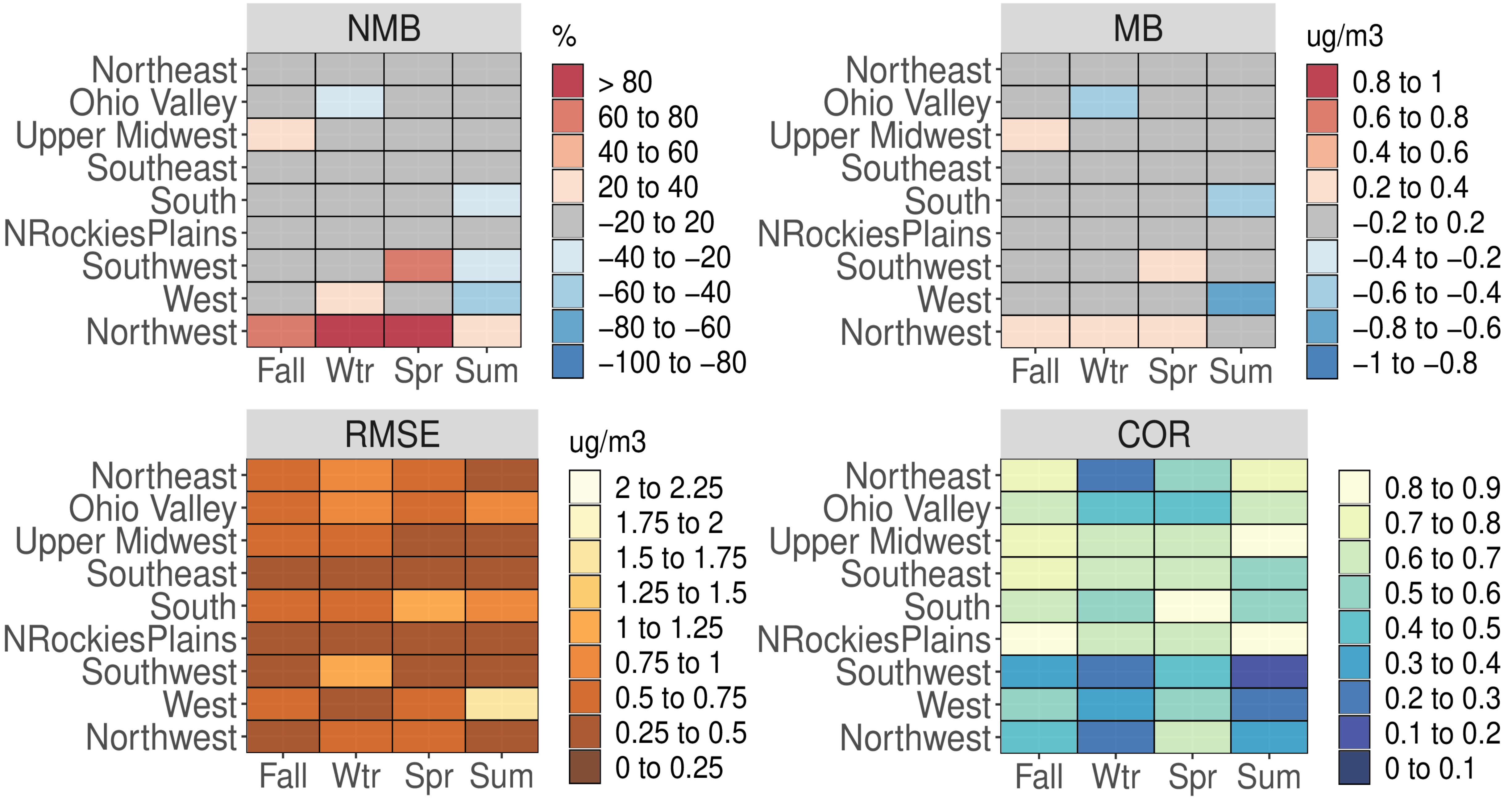

Figure S37. Categorical NMB (%), MB (µg m^{-3}), RMSE (µg m^{-3}), and Pearson correlation values for SO_4^{2-} for all CSN sites based on season and NOAA climate region for the CMAQ521 simulation.

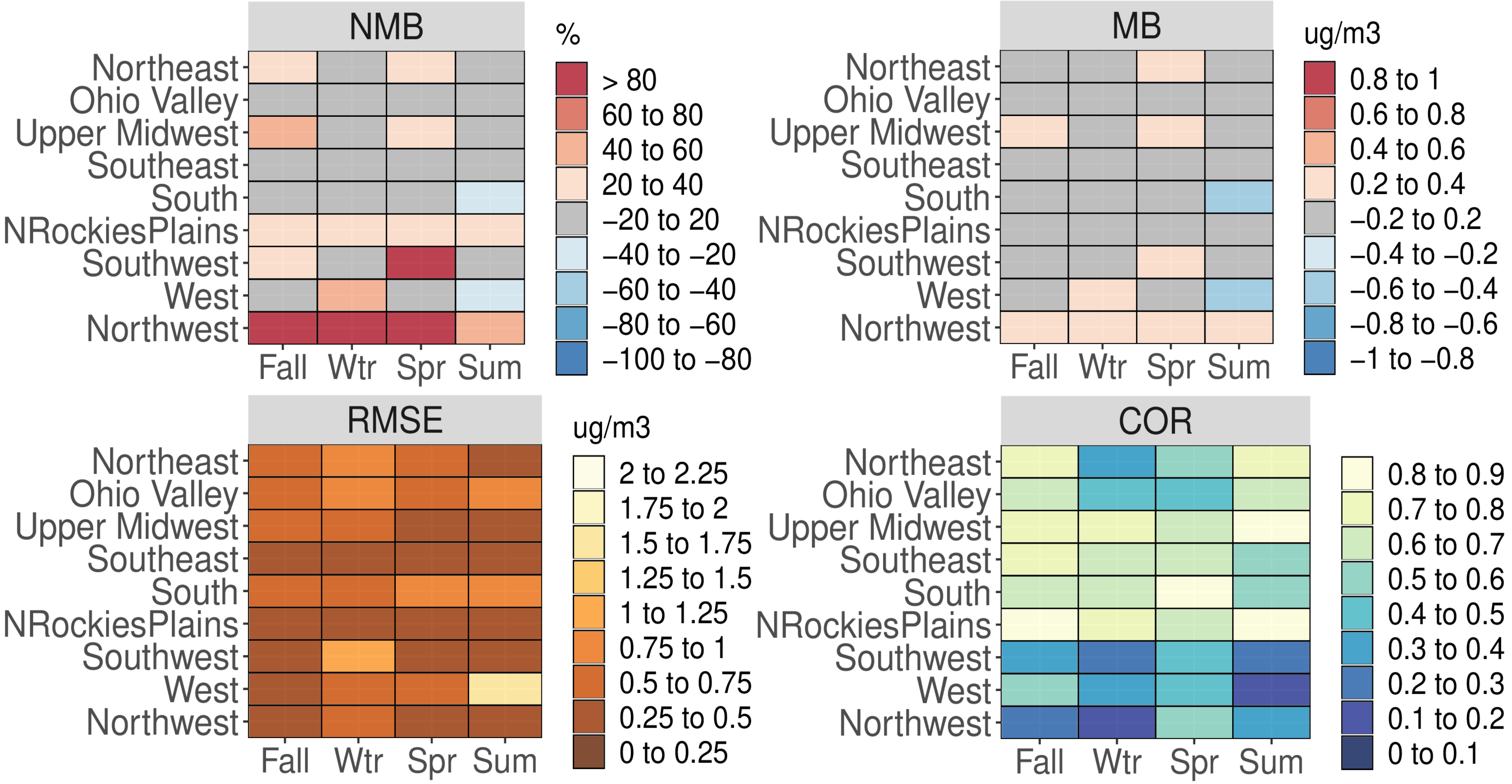

Figure S38. Categorical NMB (%), MB (µg m^{-3}), RMSE (µg m^{-3}), and Pearson correlation values for SO_4^{2-} for all CSN sites based on season and NOAA climate region for the CMAQ531_WRF411_M3Dry_BiDi simulation.

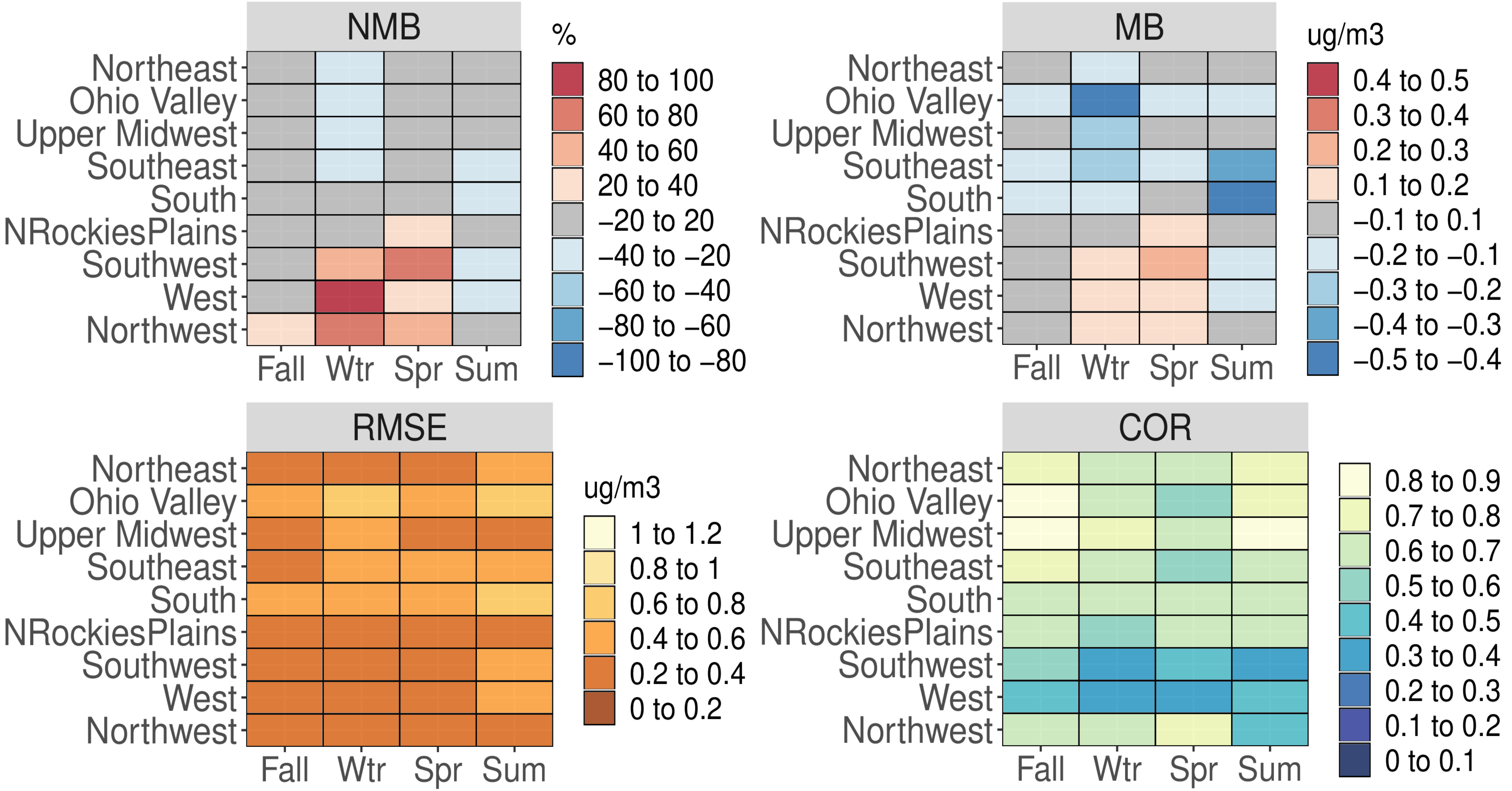

Figure S39. Categorical NMB (%), MB (μg m^{-3}), RMSE (μg m^{-3}), and Pearson correlation values for SO_4^{2-} for all IMPROVE sites based on season and NOAA climate region for the CMAQ521 simulation.

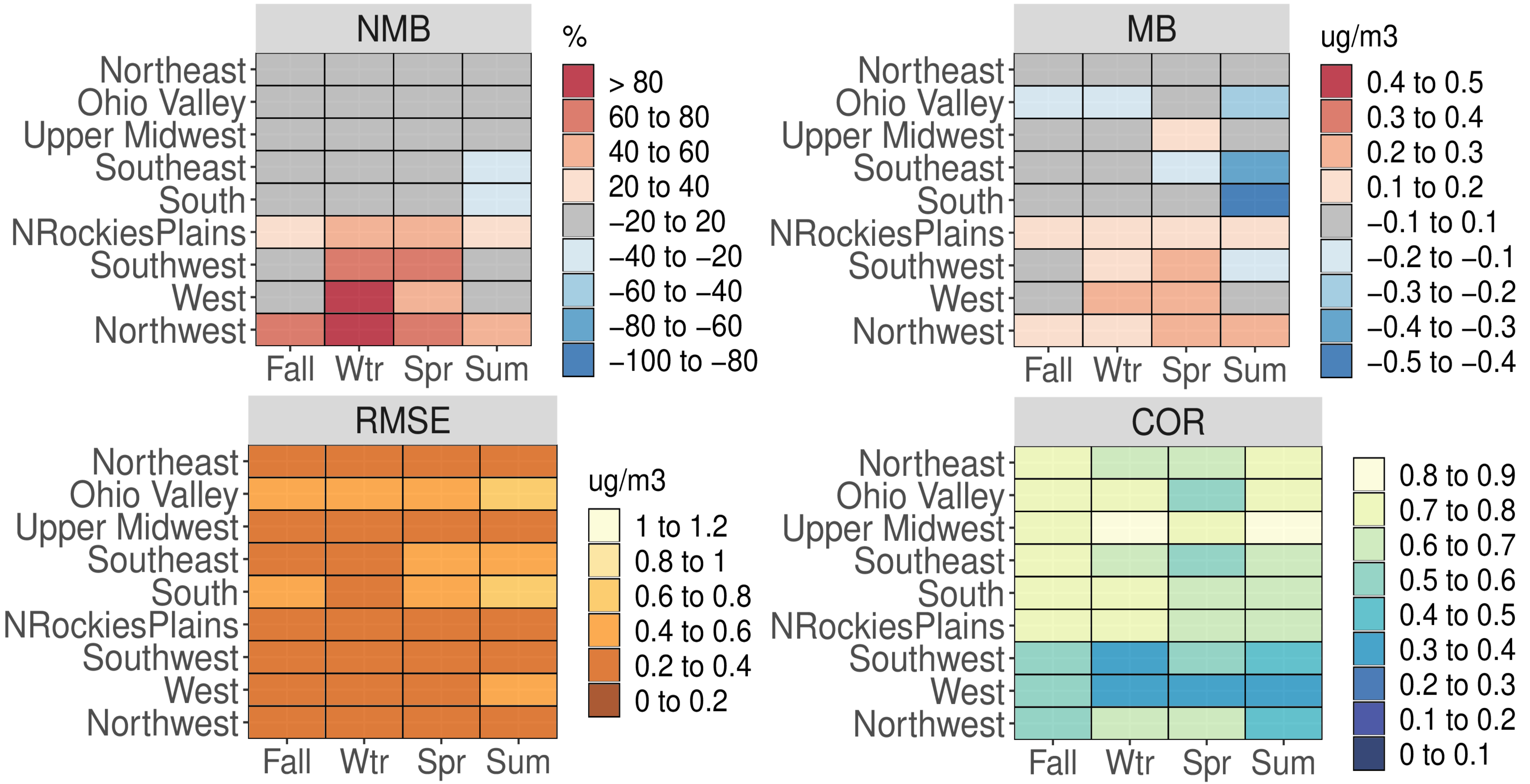

Figure S40. Categorical NMB (%), MB (μg m^{-3}), RMSE (μg m^{-3}), and Pearson correlation values for SO_4^{2-} for all IMPROVE sites based on season and NOAA climate region for the CMAQ531_WRF411_M3Dry_BiDi simulation.

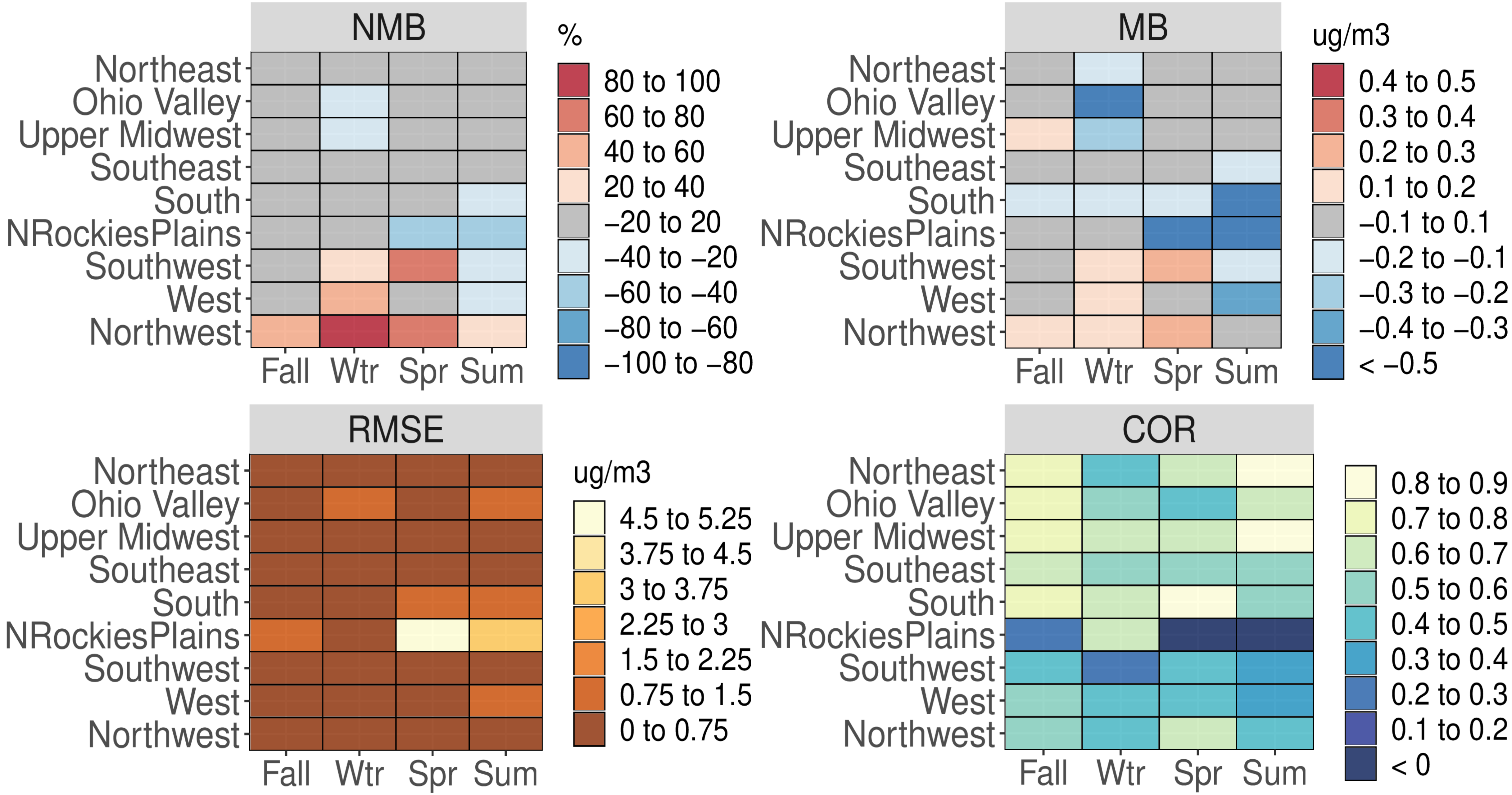

Figure S41. Categorical NMB (%), MB (μg m^{-3}), RMSE (μg m^{-3}), and Pearson correlation values for SO_4^{2-} for all AQS sites based on season and NOAA climate region for the CMAQ521 simulation.

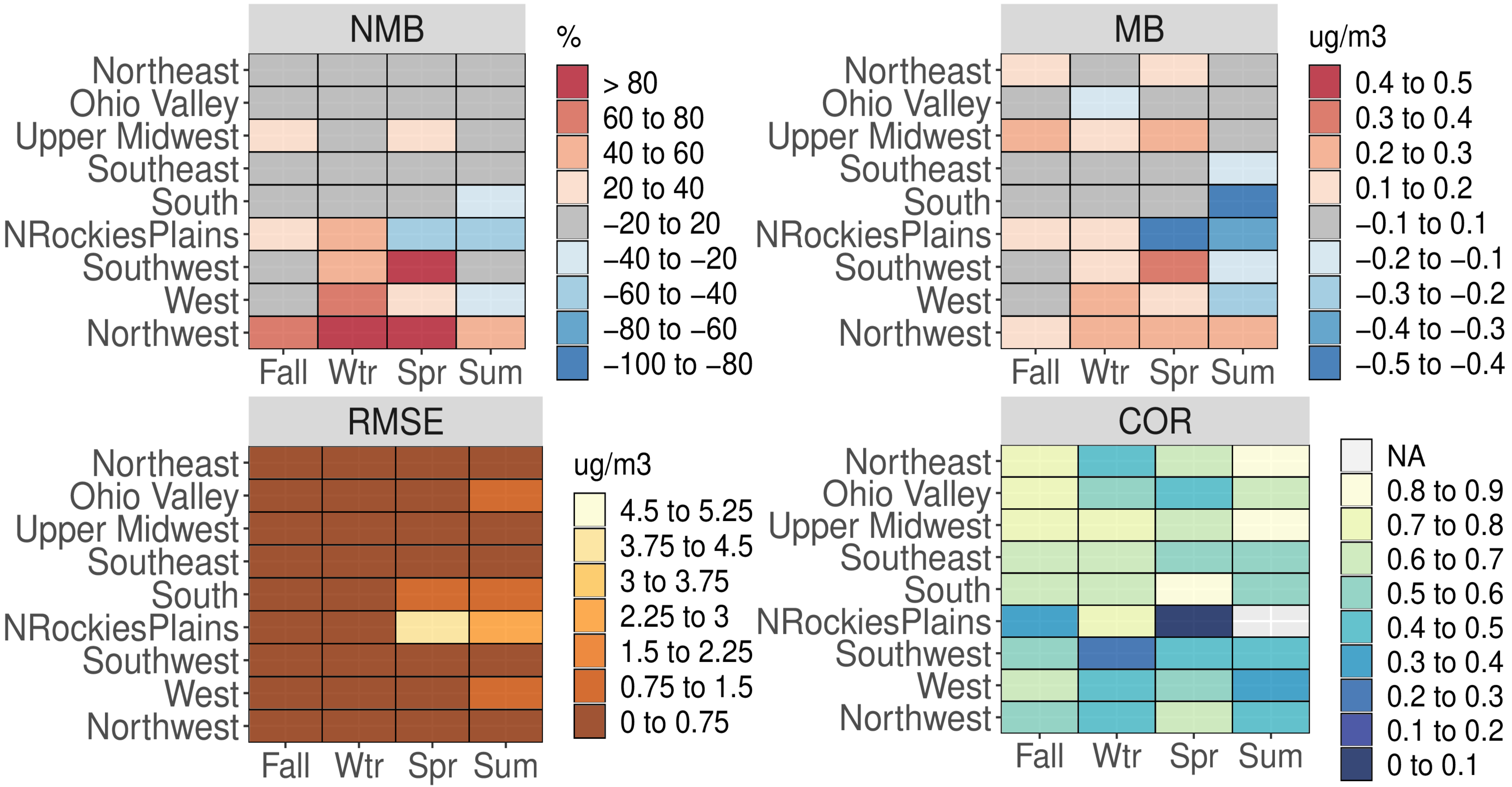

Figure S42. Categorical NMB (%), MB (μg m^{-3}), RMSE (μg m^{-3}), and Pearson correlation values for SO_4^{2-} for all AQS sites based on season and NOAA climate region for the CMAQ531_WRF411_M3Dry_BiDi simulation.

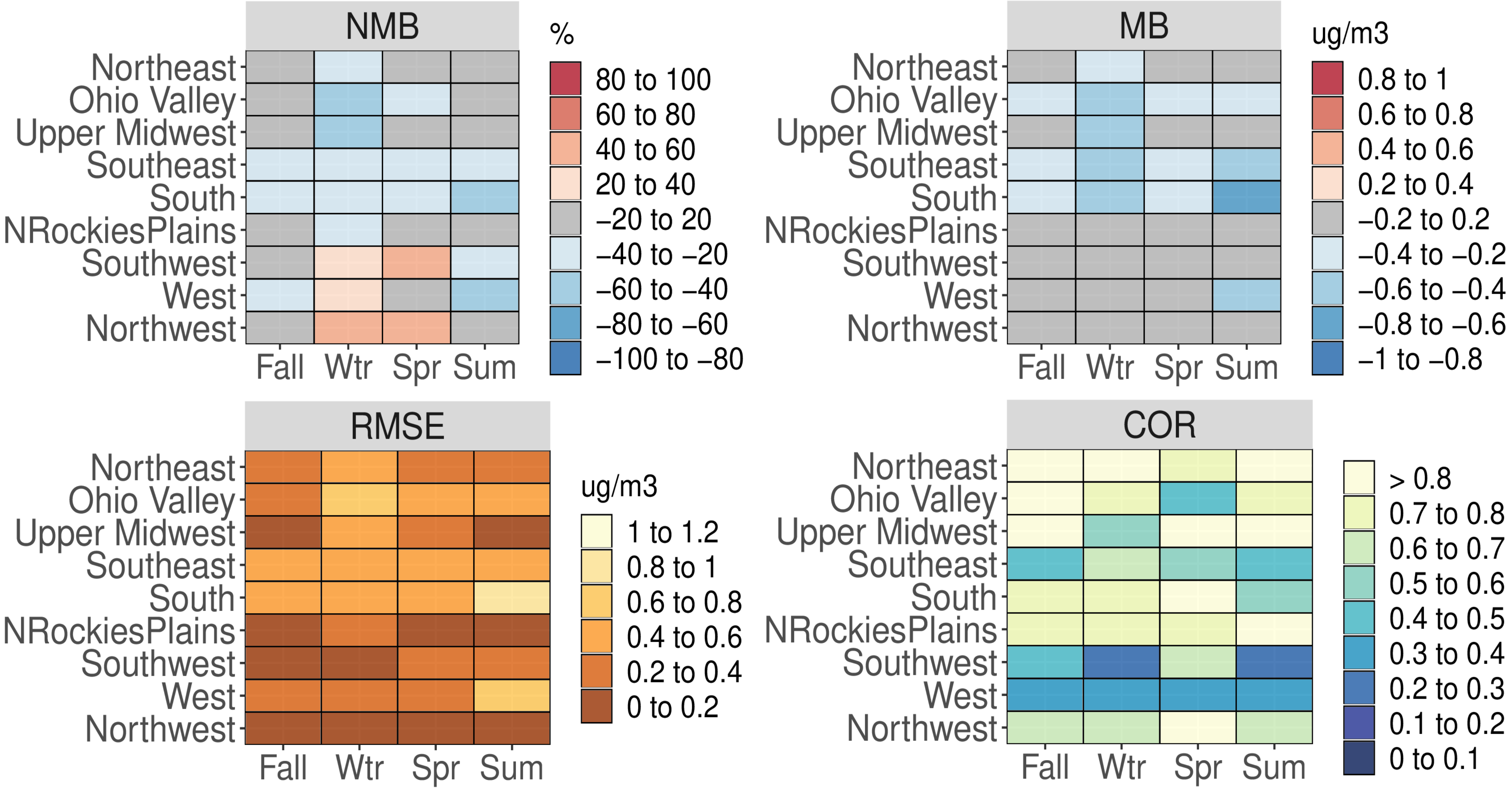

Figure S43. Categorical NMB (%), MB (μg m^{-3}), RMSE (μg m^{-3}), and Pearson correlation values for SO_4^{2-} for all CASTNet sites based on season and NOAA climate region for the CMAQ521 simulation.

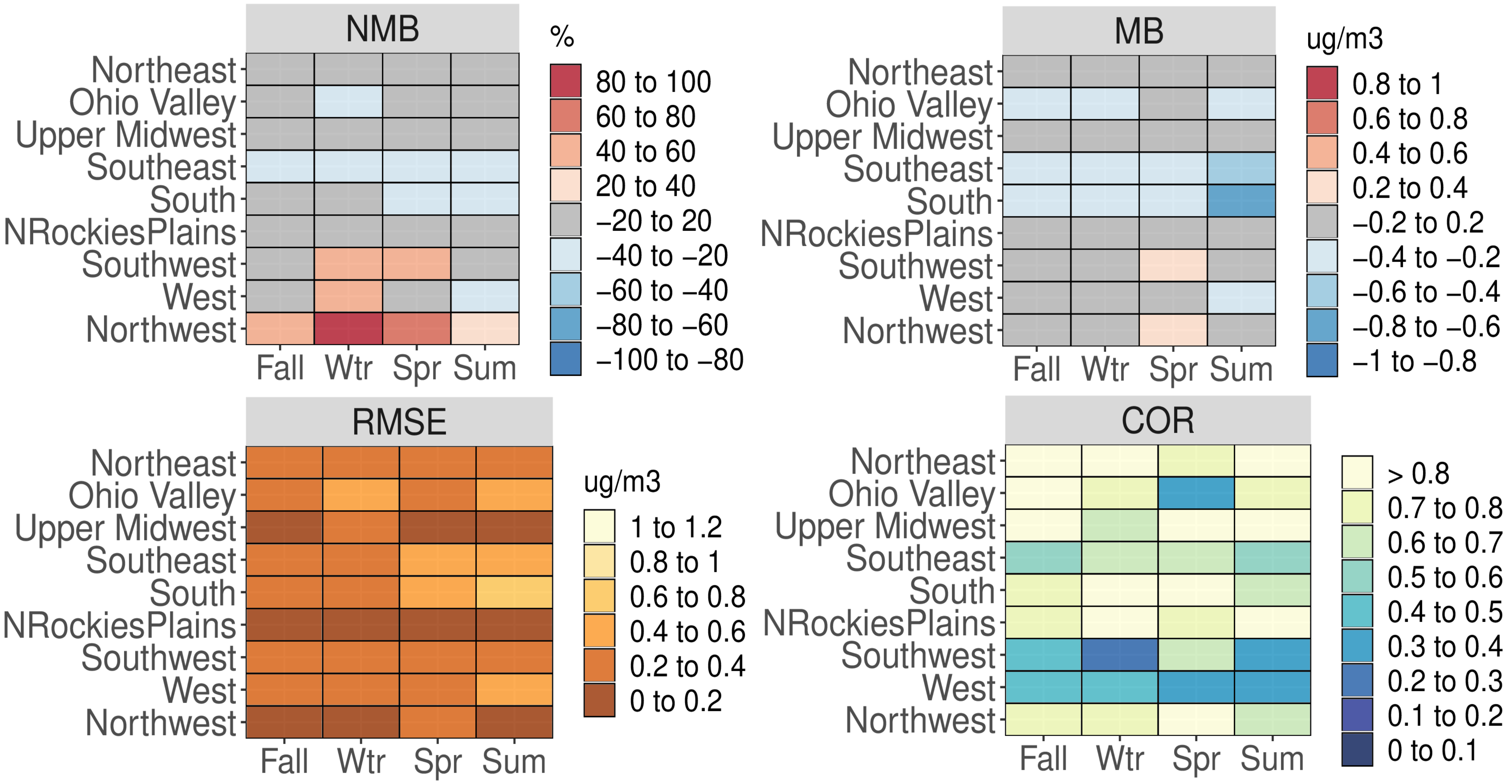

Figure S44. Categorical NMB (%), MB (μg m^{-3}), RMSE (μg m^{-3}), and Pearson correlation values for SO_4^{2-} for all CASTNet sites based on season and NOAA climate region for the CMAQ531_WRF411_M3Dry_BiDi simulation.

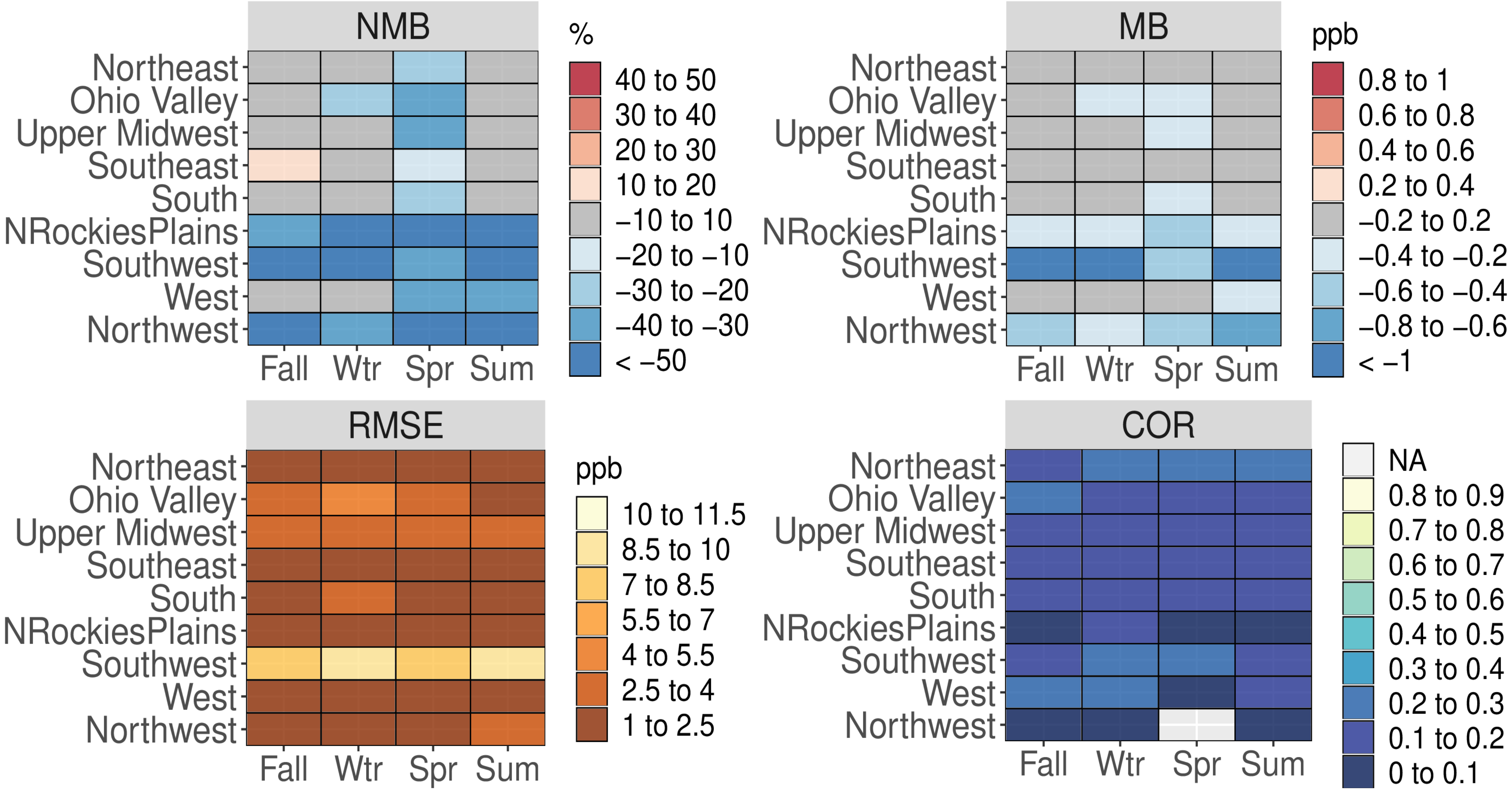

Figure S45. Categorical NMB (%), MB (ppbv), RMSE (ppbv), and Pearson correlation values for SO_2 (hourly) for all AQS sites based on season and NOAA climate region for the CMAQ521 simulation.

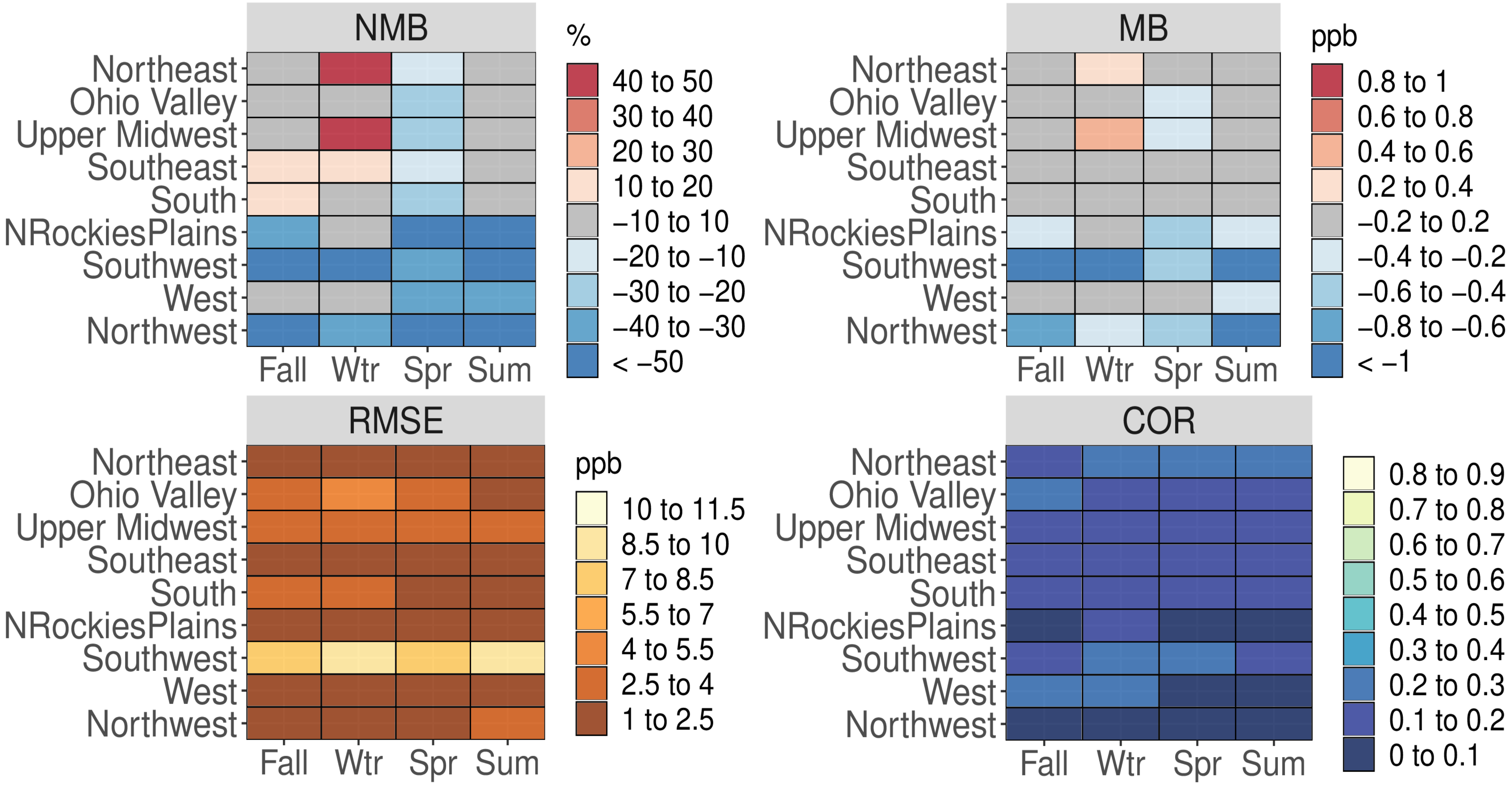

Figure S46. Categorical NMB (%), MB (ppbv), RMSE (ppbv), and Pearson correlation values for SO_2 (hourly) for all AQS sites based on season and NOAA climate region for the CMAQ531_WRF411_M3Dry_BiDi simulation.

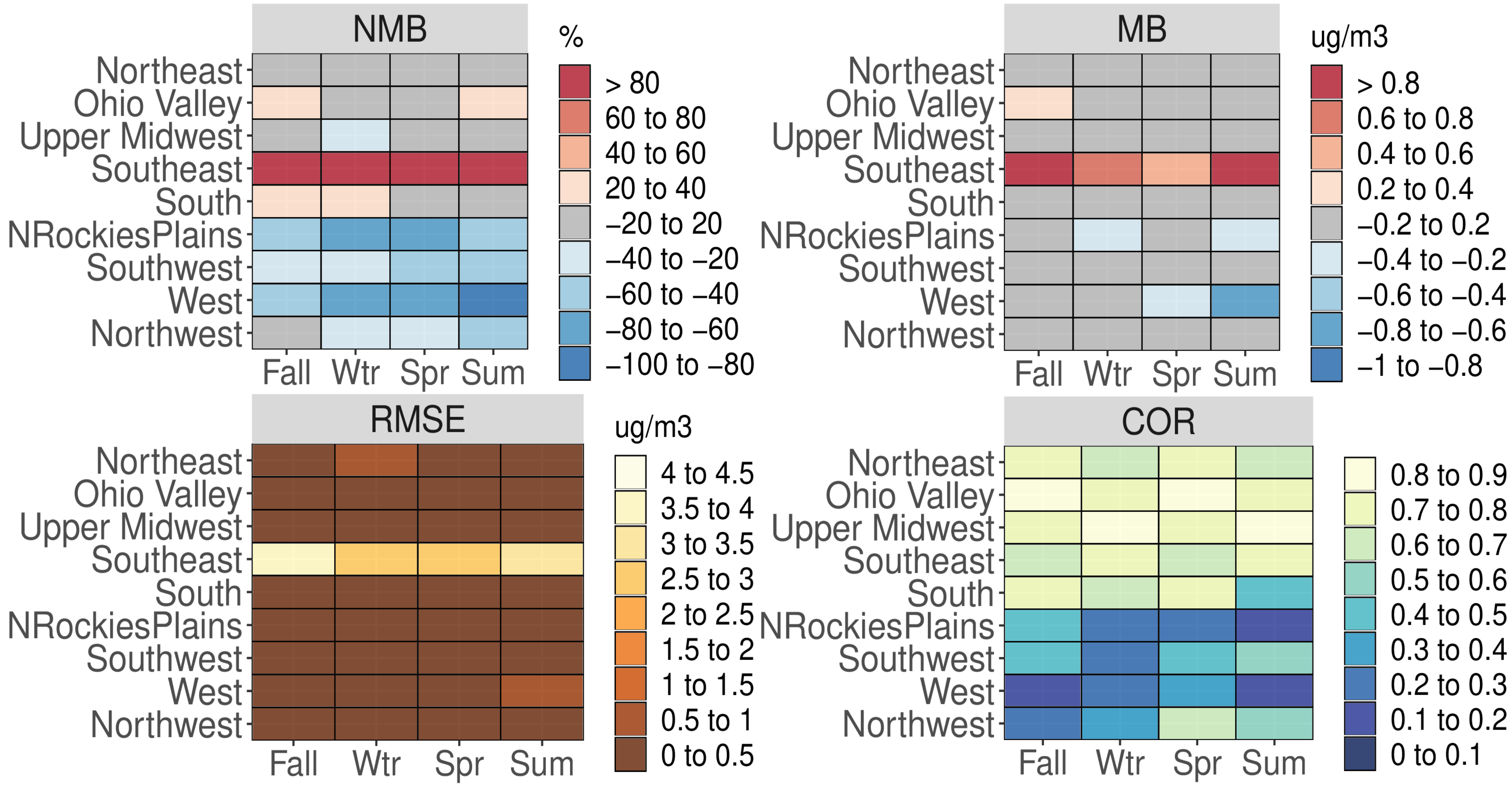

Figure S47. Categorical NMB (%), MB (μg m^{-3}), RMSE (μg m^{-3}), and Pearson correlation values for SO_2 (weekly) for all CASTNET sites based on season and NOAA climate region for the CMAQ521 simulation.

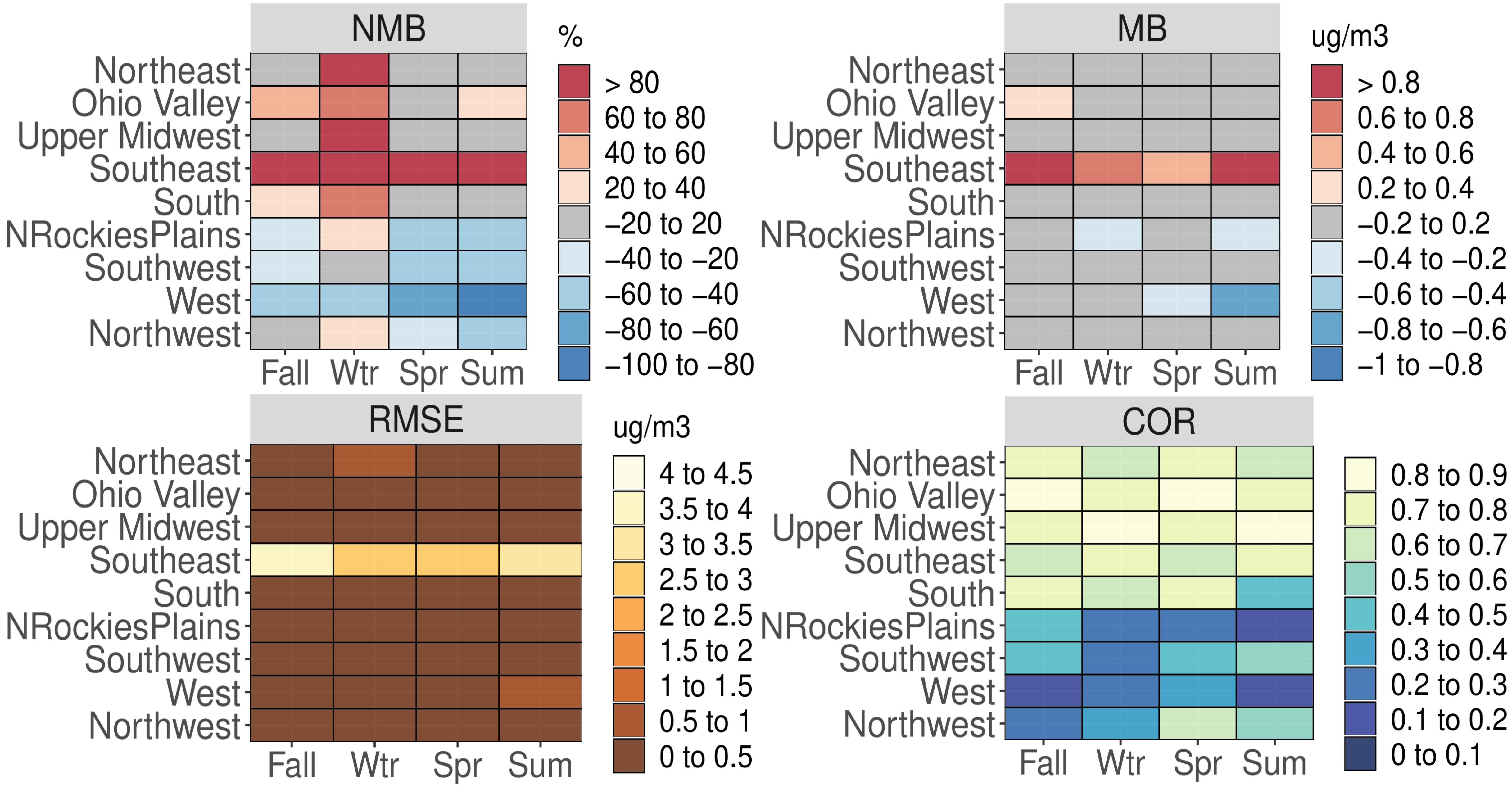

Figure S48. Categorical NMB (%), MB (μg m^{-3}), RMSE (μg m^{-3}), and Pearson correlation values for SO_2 (weekly) for all CASTNET sites based on season and NOAA climate region for the CMAQ531_WRF411_M3Dry_BiDi simulation.

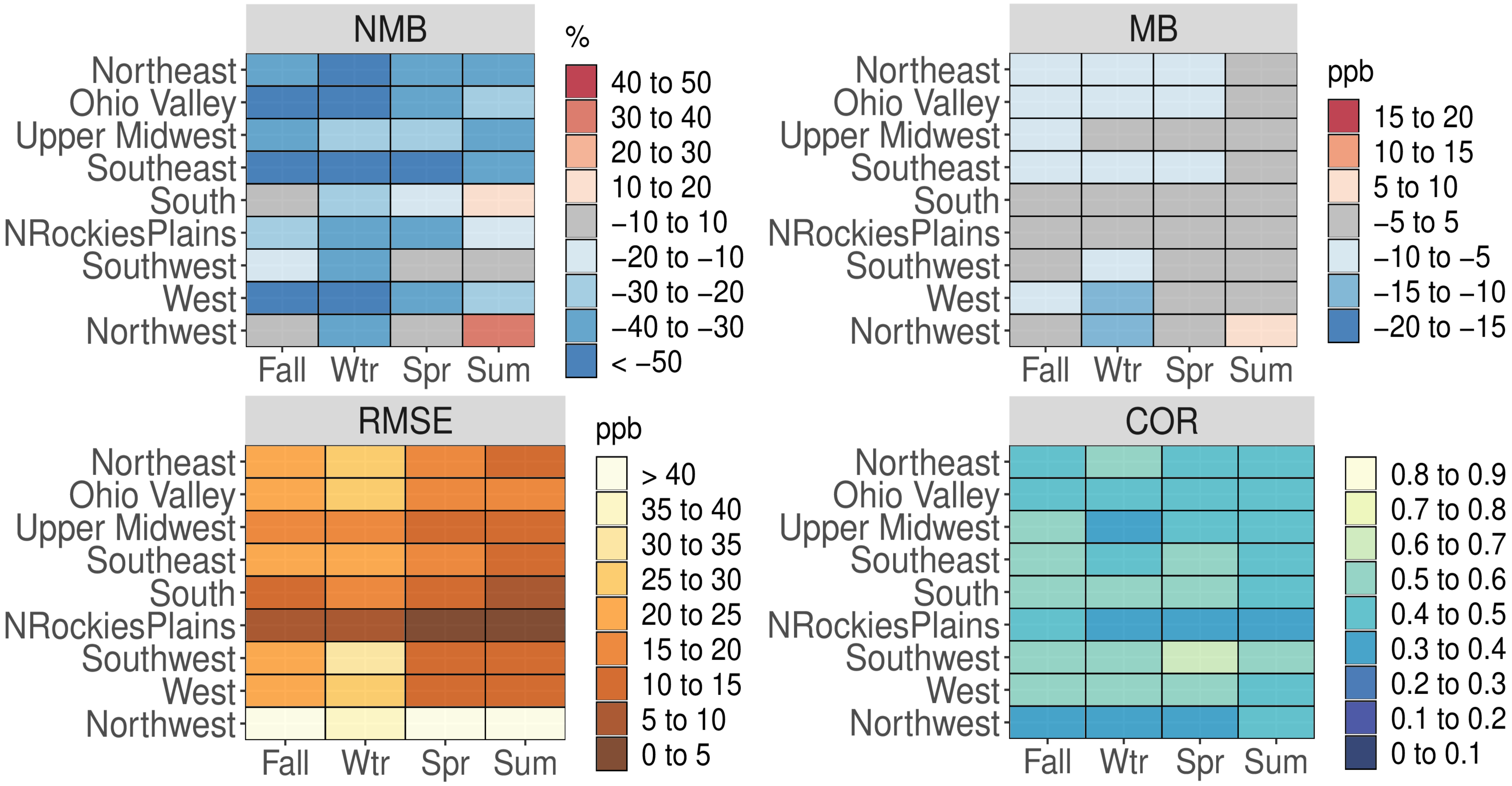

Figure S49. Categorical NMB (%), MB (ppbv), RMSE (ppbv), and Pearson correlation values for NO_X for all AQS sites based on season and NOAA climate region for the CMAQ521 simulation.

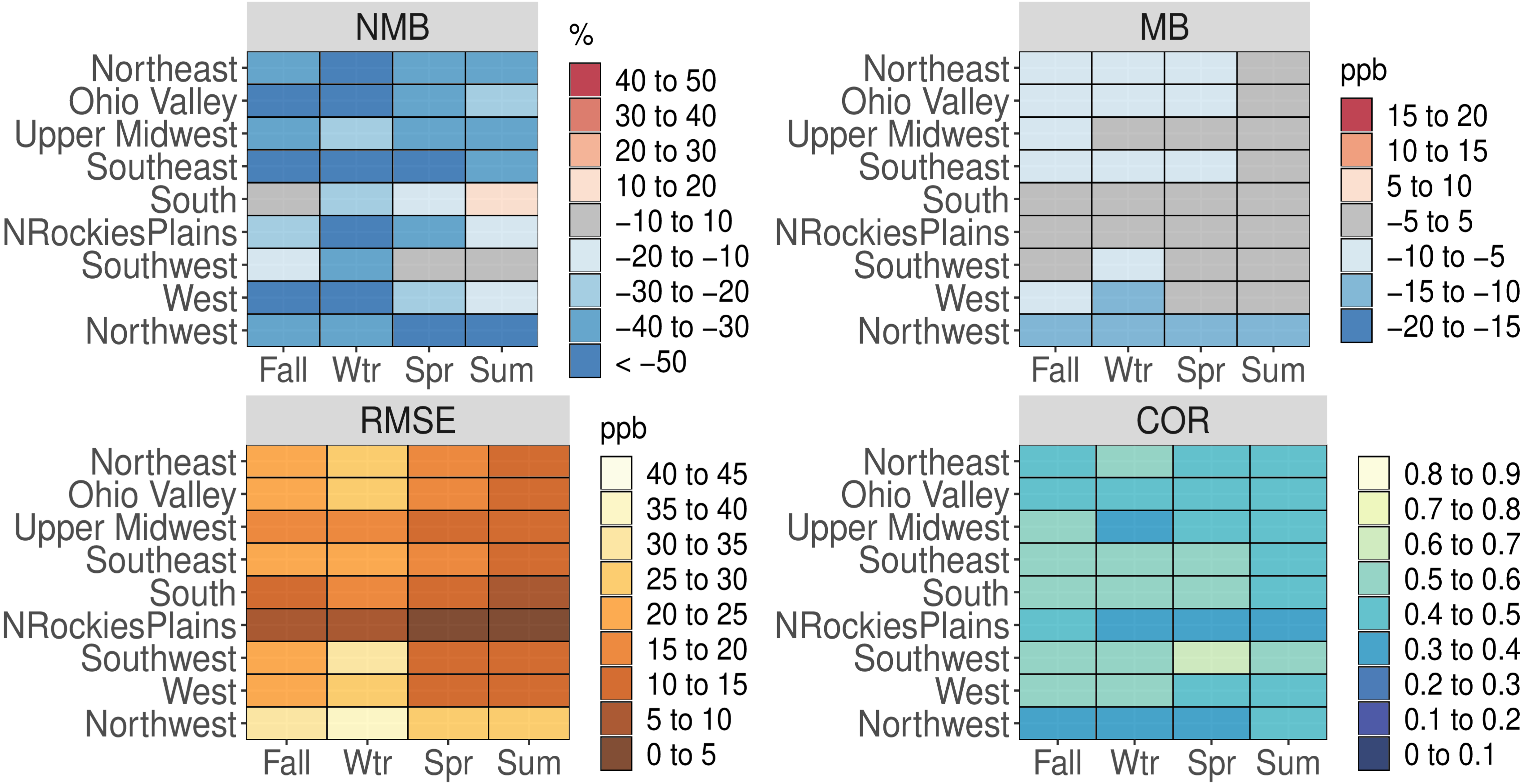

Figure S50. Categorical NMB (%), MB (ppbv), RMSE (ppbv), and Pearson correlation values for NO_X for all AQS sites based on season and NOAA climate region for the CMAQ531_WRF411_M3Dry_BiDi simulation.

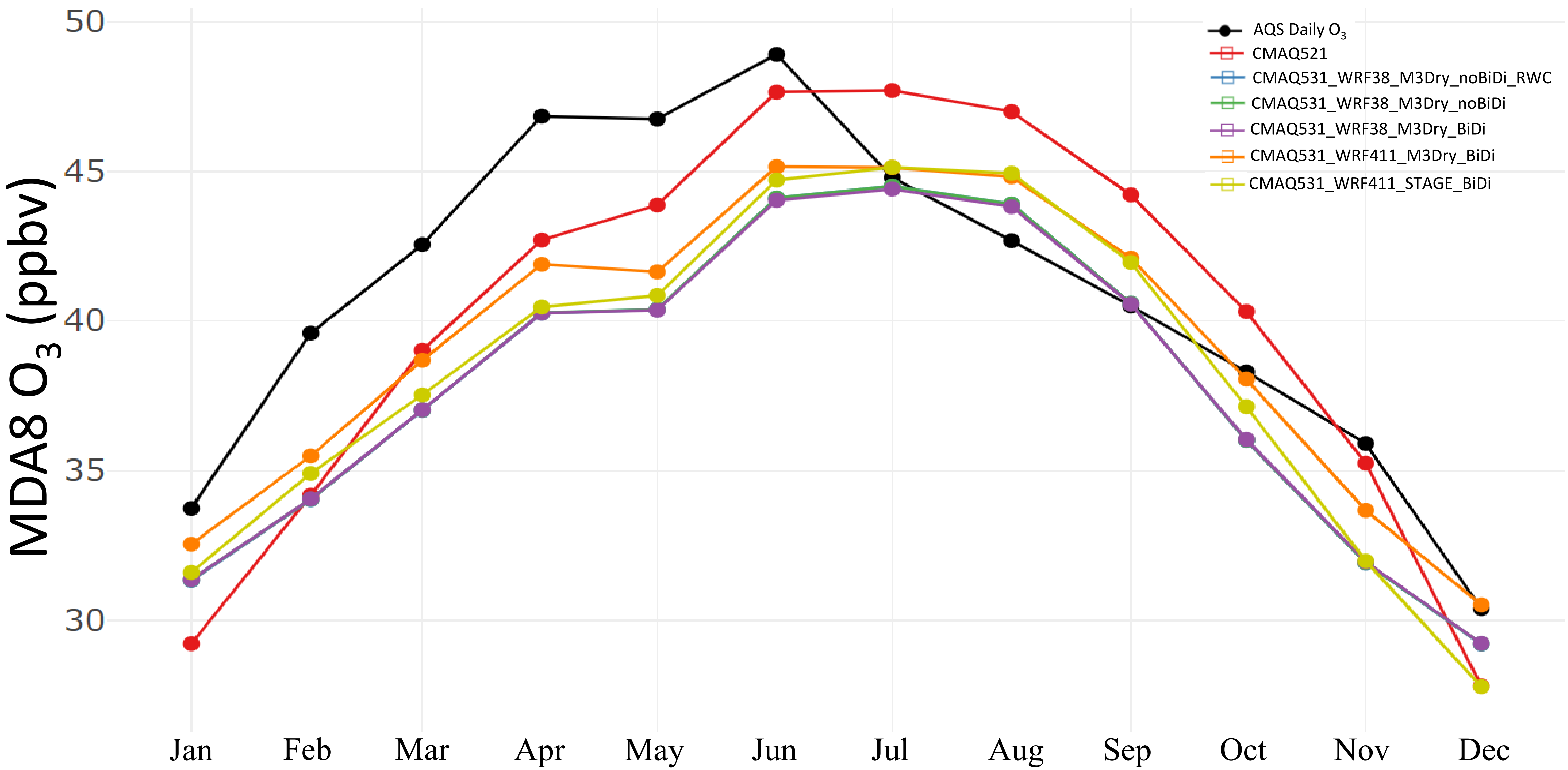

Figure S51. Time series of monthly average MDA8 O_3 mixing ratio (ppbv) for all AQS sites (black), CMAQ521 (red), CMAQ531_WRF38_M3Dry_noBiDi_RWC (blue), CMAQ531_WRF38_M3Dry_noBiDi (green), CMAQ531_WRF38_M3Dry_BiDi (purple), CMAQ531_WRF411_M3Dry_BiDi (orange), and CMAQ531_WRF411_STAGE_BiDi (yellow).

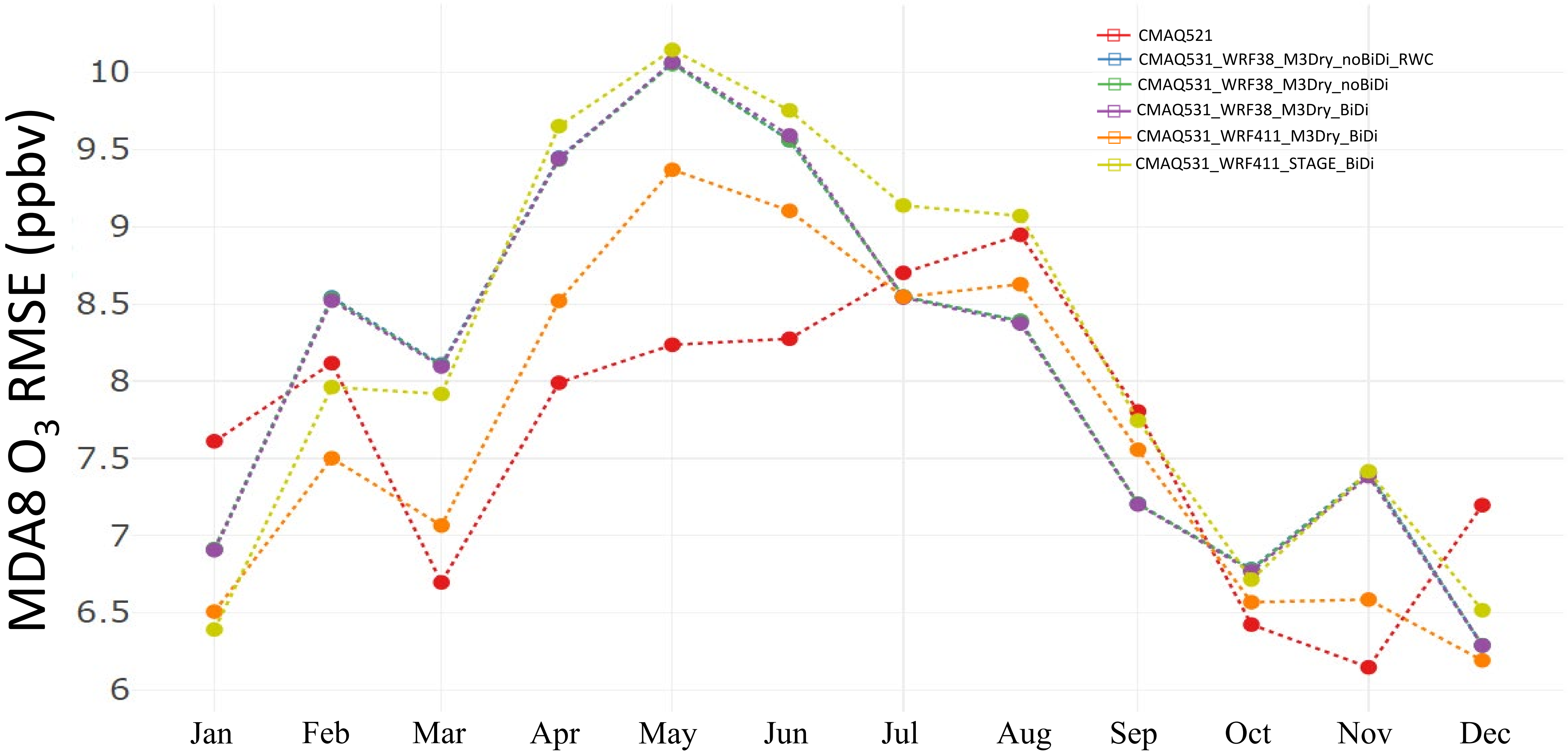

Figure S52. Time series of monthly average MDA8 O_3 RMSE (ppbv) for all AQS sites for CMAQ521 (red), CMAQ531_WRF38_M3Dry_noBiDi_RWC (blue), CMAQ531_WRF38_M3Dry_noBiDi (green), CMAQ531_WRF38_M3Dry_BiDi (purple), CMAQ531_WRF411_M3Dry_BiDi (orange), and CMAQ531_WRF411_STAGE_BiDi (yellow).

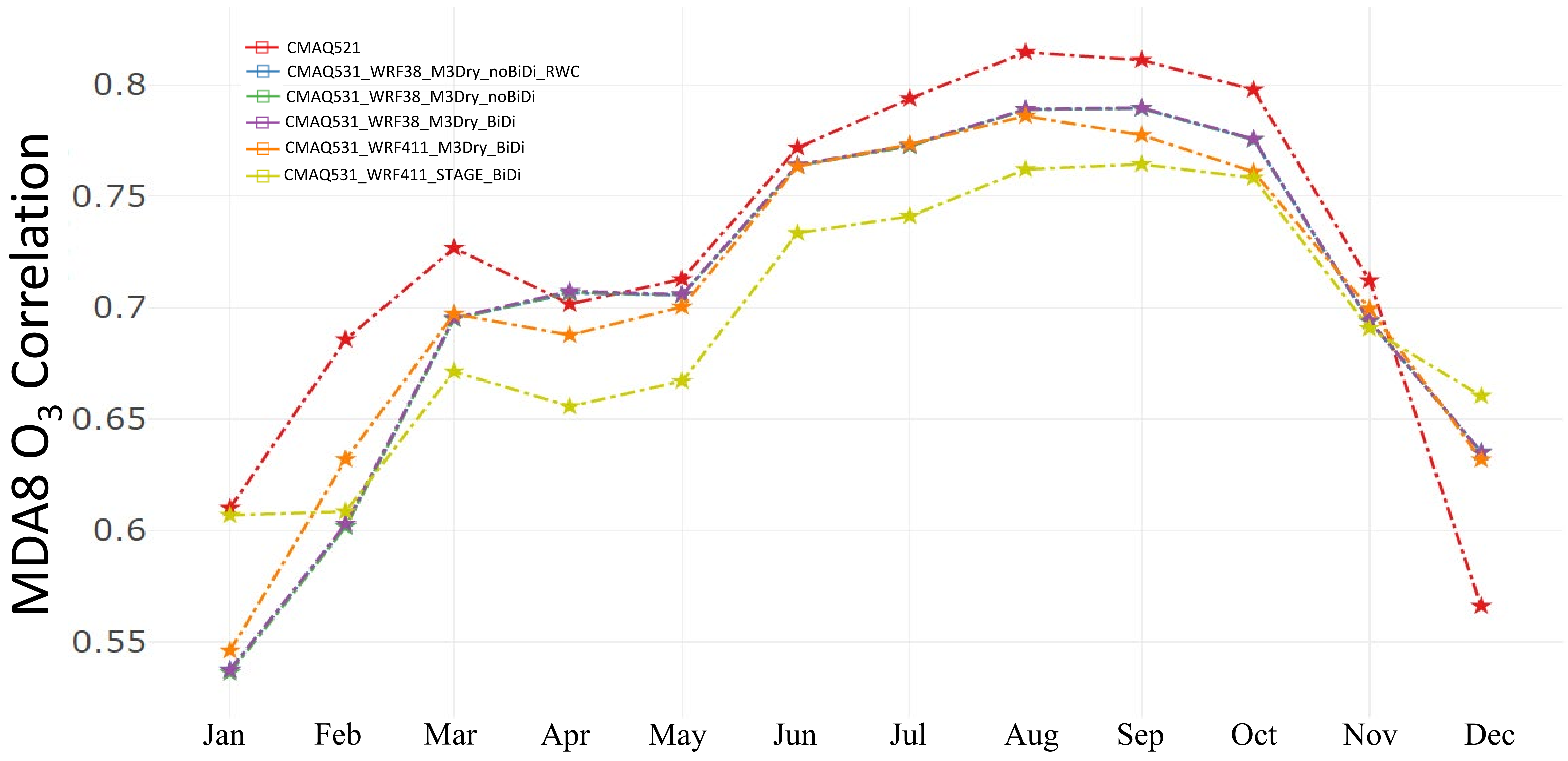

Figure S53. Time series of monthly average MDA8 O_3 Pearson correlation for all AQS sites for CMAQ521 (red), CMAQ531_WRF38_M3Dry_noBiDi_RWC (blue), CMAQ531_WRF38_M3Dry_noBiDi (green), CMAQ531_WRF38_M3Dry_BiDi (purple), CMAQ531_WRF411_M3Dry_BiDi (orange), and CMAQ531_WRF411_STAGE_BiDi (yellow).

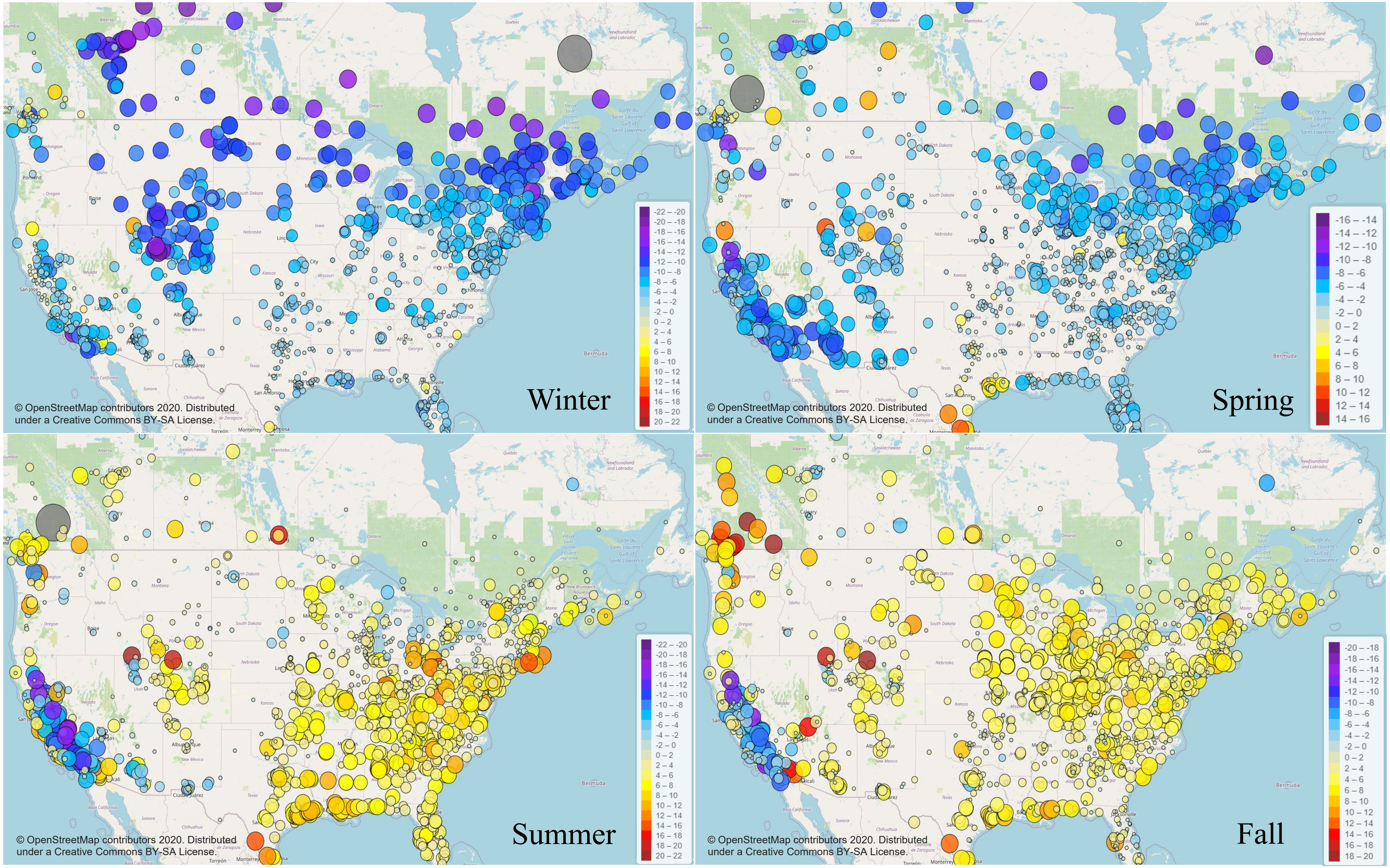

Figure S54. Seasonal average MDA8 O_3 bias (ppbv) for AQS and NAPS sites for the CMAQ521 simulation.

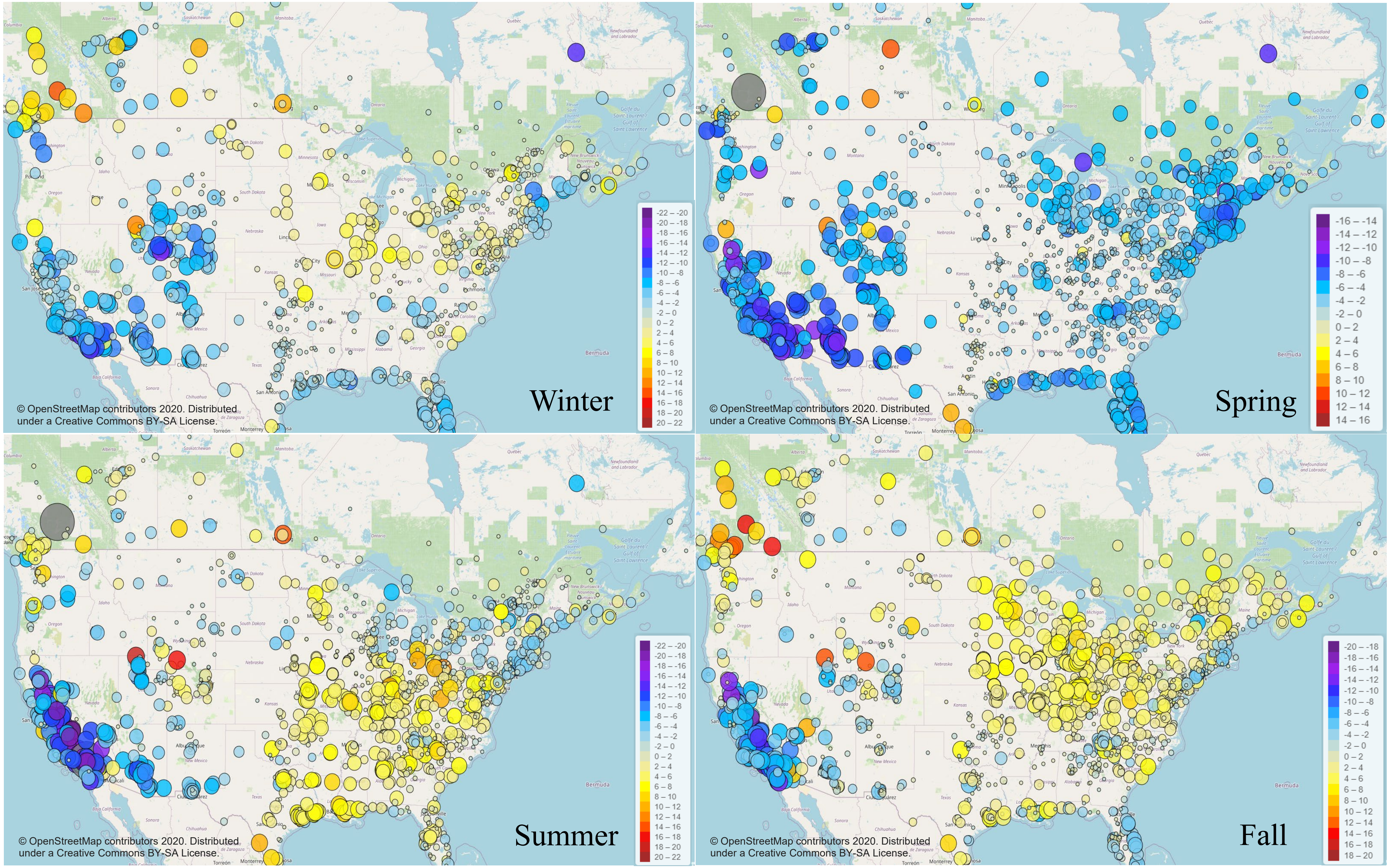

Figure S55. Seasonal average MDA8 O_3 bias (ppbv) for AQS and NAPS sites for the CMAQ531_WRF411_M3Dry_BiDi simulation.

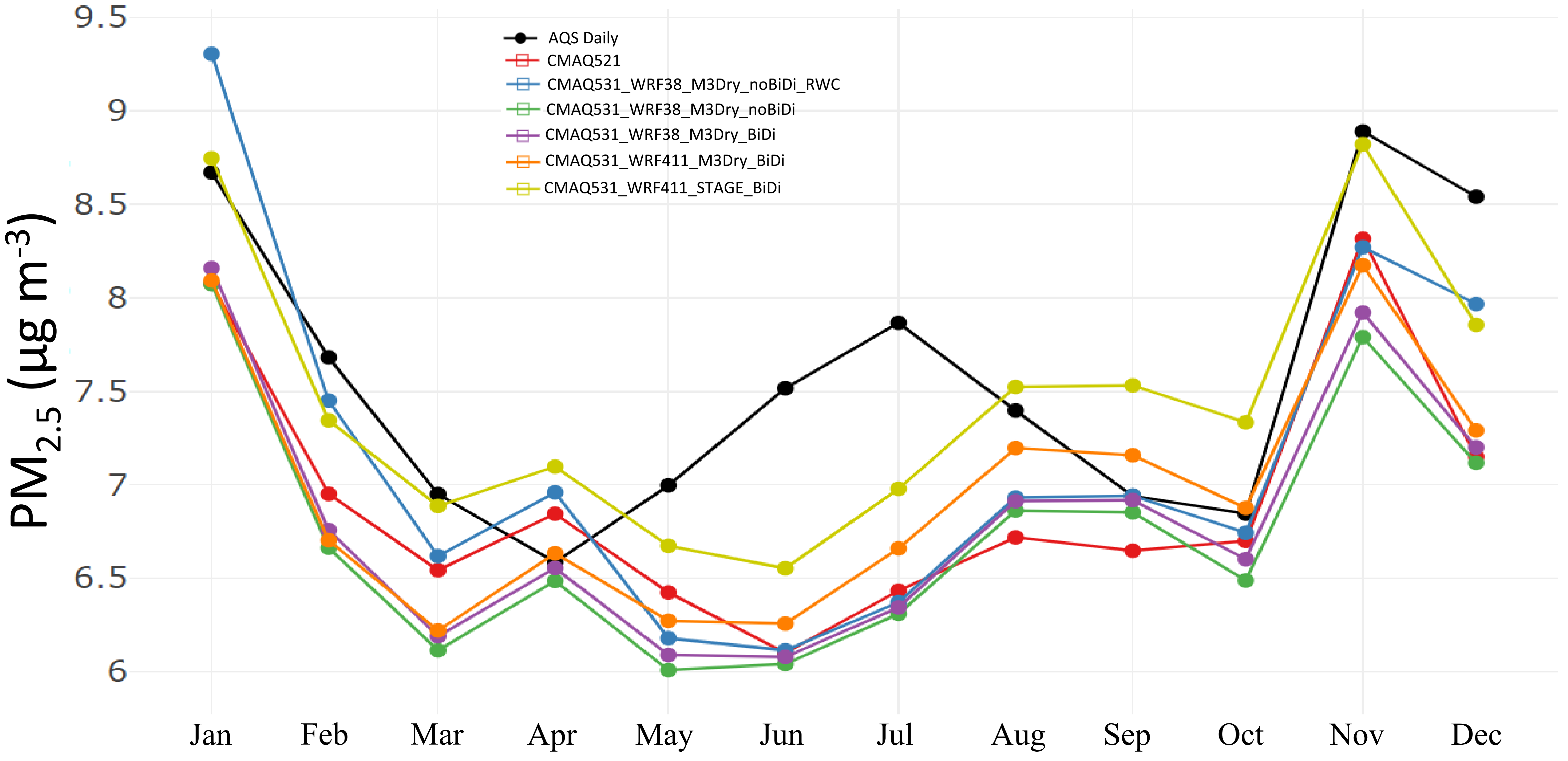

Figure S56. Time series of monthly average $PM_{2.5}$ ($\mu g\ m^{-3}$) for all AQS sites (black), CMAQ521 (red), CMAQ531_WRF38_M3Dry_noBiDi_RWC (blue), CMAQ531_WRF38_M3Dry_noBiDi (green), CMAQ531_WRF38_M3Dry_BiDi (purple), CMAQ531_WRF411_M3Dry_BiDi (orange), and CMAQ531_WRF411_STAGE_BiDi (yellow).

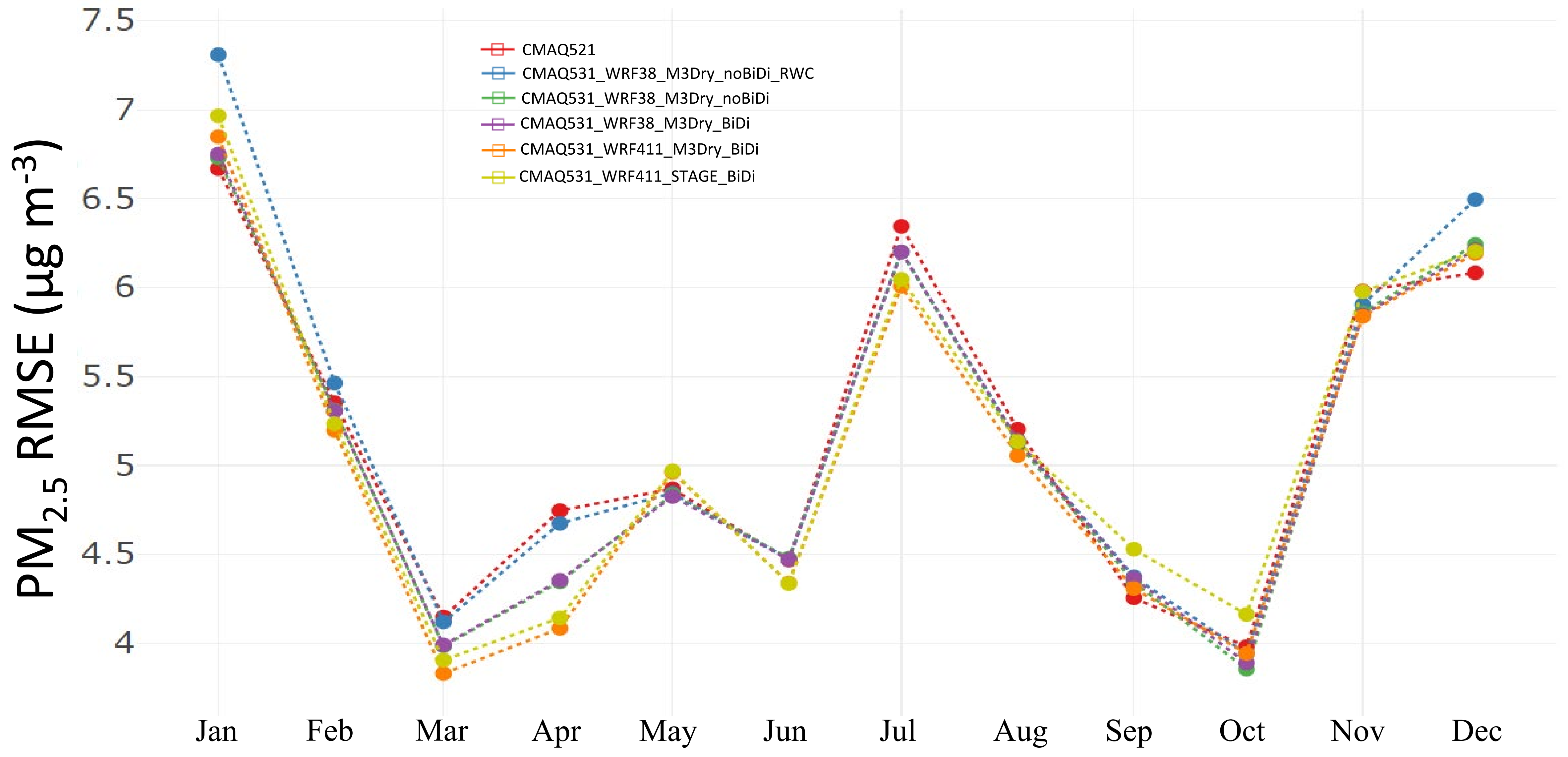

Figure S57. Time series of monthly average $PM_{2.5}$ RMSE ($\mu g\ m^{-3}$) for all AQS sites for CMAQ521 (red), CMAQ531_WRF38_M3Dry_noBiDi_RWC (blue), CMAQ531_WRF38_M3Dry_noBiDi (green), CMAQ531_WRF38_M3Dry_BiDi (purple), CMAQ531_WRF411_M3Dry_BiDi (orange), and CMAQ531_WRF411_STAGE_BiDi (yellow).

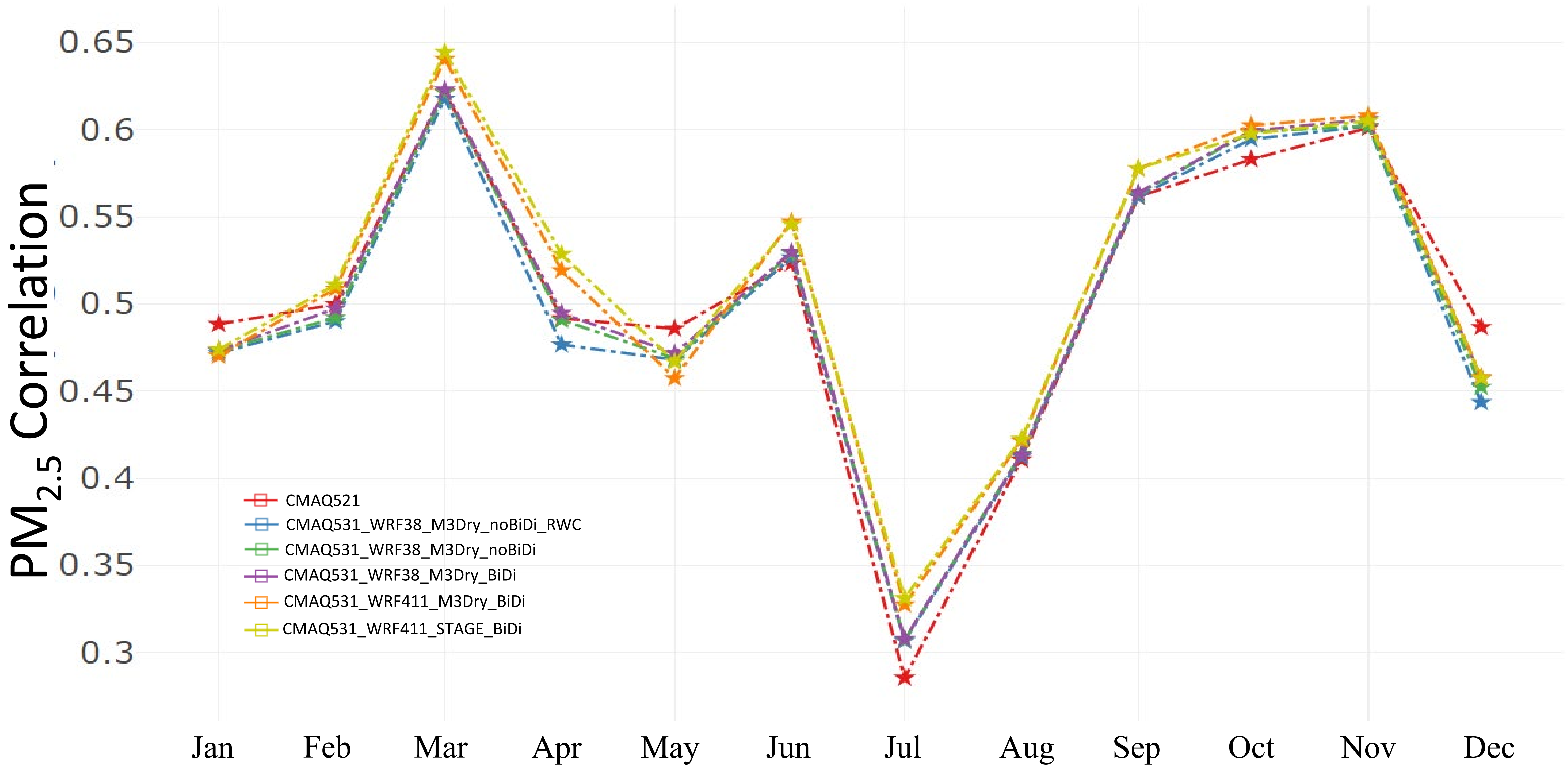

Figure S58. Time series of monthly average $PM_{2.5}$ Pearson correlation for all AQS sites for CMAQ521 (red), CMAQ531_WRF38_M3Dry_noBiDi_RWC (blue), CMAQ531_WRF38_M3Dry_noBiDi (green), CMAQ531_WRF38_M3Dry_BiDi (purple), CMAQ531_WRF411_M3Dry_BiDi (orange), and CMAQ531_WRF411_STAGE_BiDi (yellow).

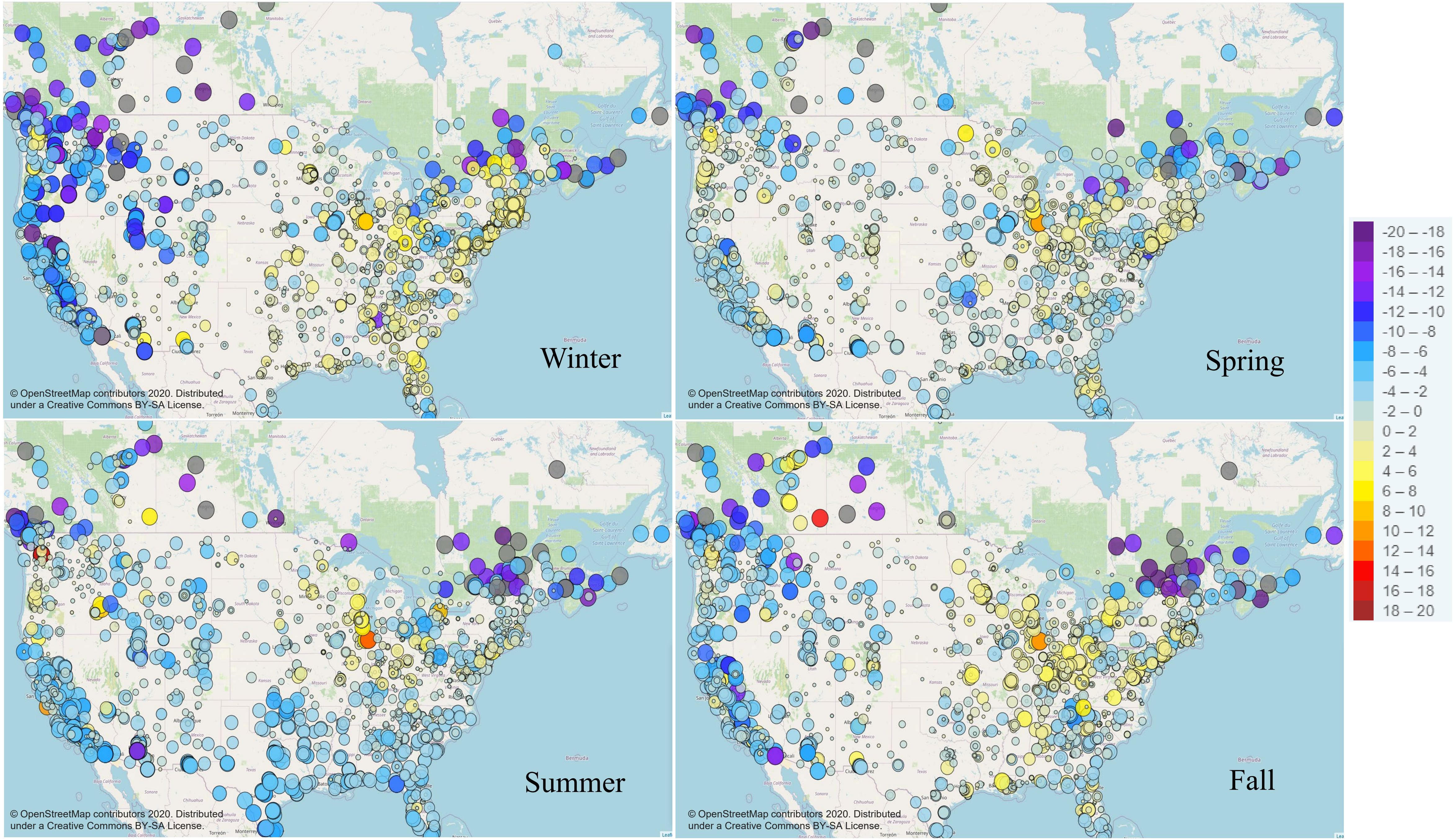

Figure S59. Seasonal average $PM_{2.5}$ bias (μg m^{-3}) for AQS and NAPS sites for the CMAQ521 simulation. The symbol size is commensurate with the absolute value of the bias. Gray symbols indicate values outside the color scale (i.e. outliers).

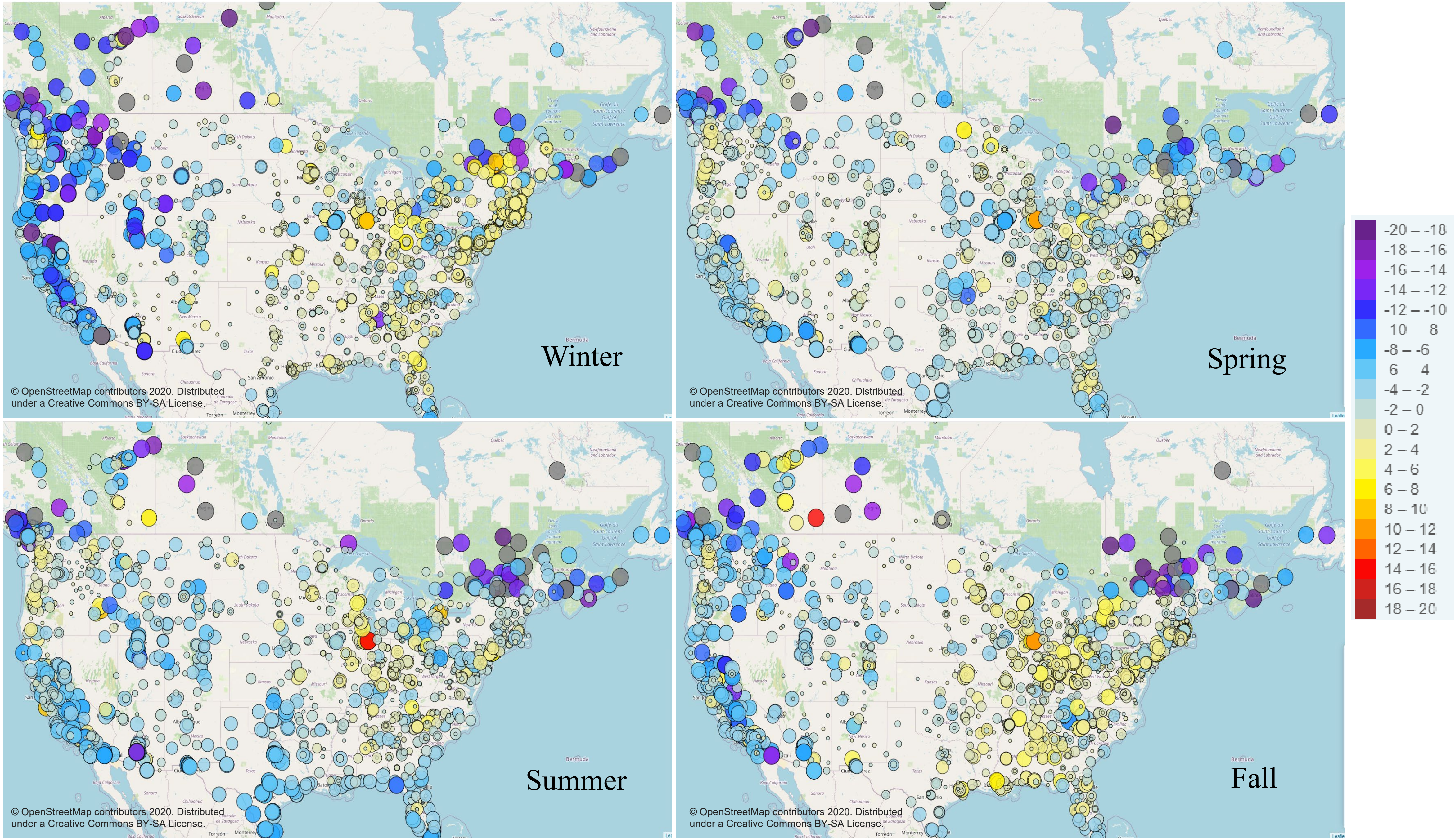

Figure S60. Seasonal average $PM_{2.5}$ bias ($\mu g\ m^{-3}$) for AQS and NAPS sites for the CMAQ531_WRF411_M3Dry_BiDi simulation. The symbol size is commensurate with the absolute value of the bias. Gray symbols indicate values outside the color scale (i.e. outliers).

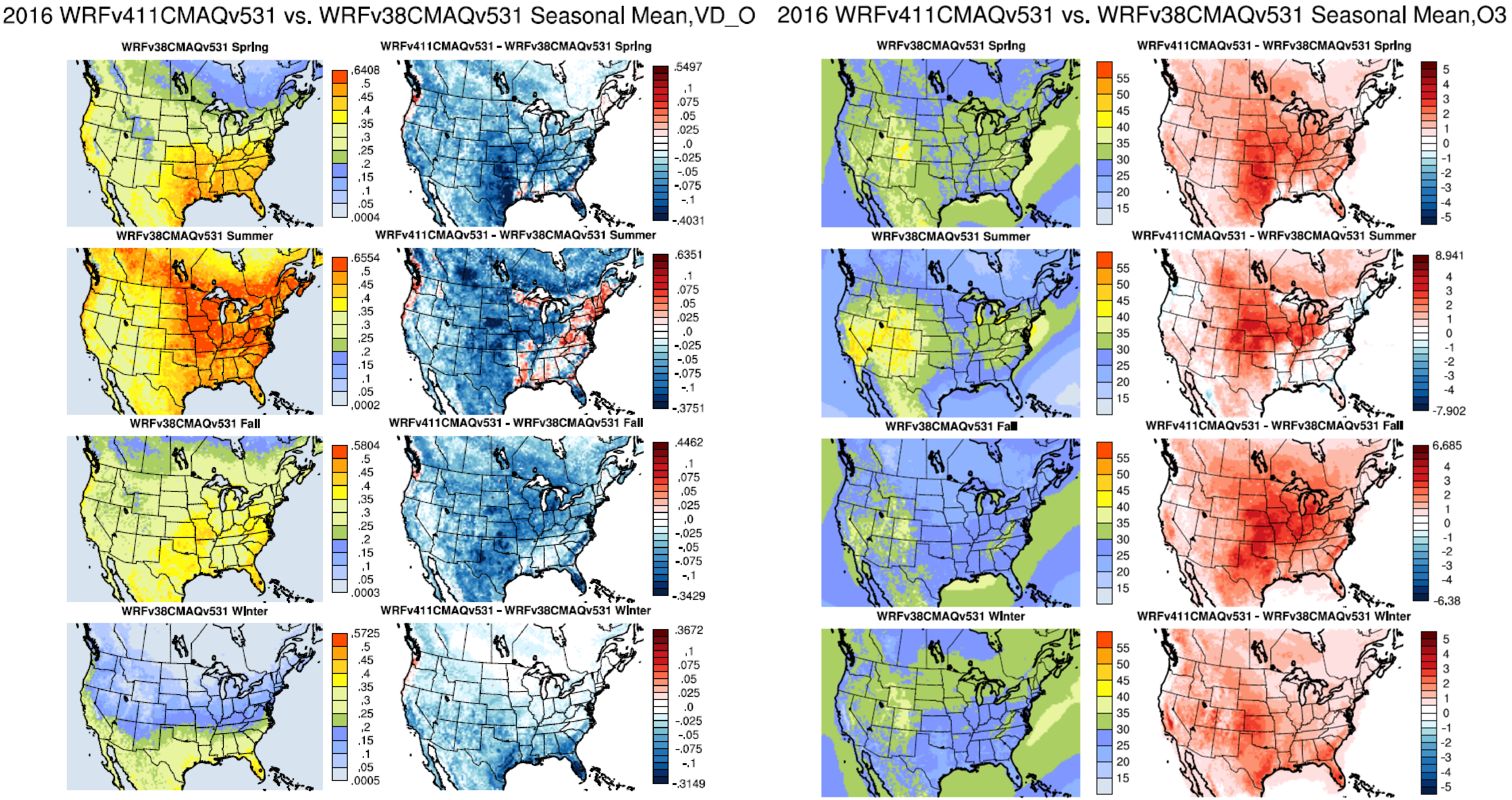

Figure S61. Seasonal O_3 deposition velocity (VD_O_3; cm s^{-1}; left) and O_3 mixing ratio (ppbv; right) for the CMAQ531_WRF38_M3Dry_BiDi simulation along with the difference in VD_O_3 and mixing ratio between the CMAQ531_WRF38_M3Dry_Bidi and CMAQ531_WRF411_M3Dry_BiDi simulations (WRF411 – WRF38).

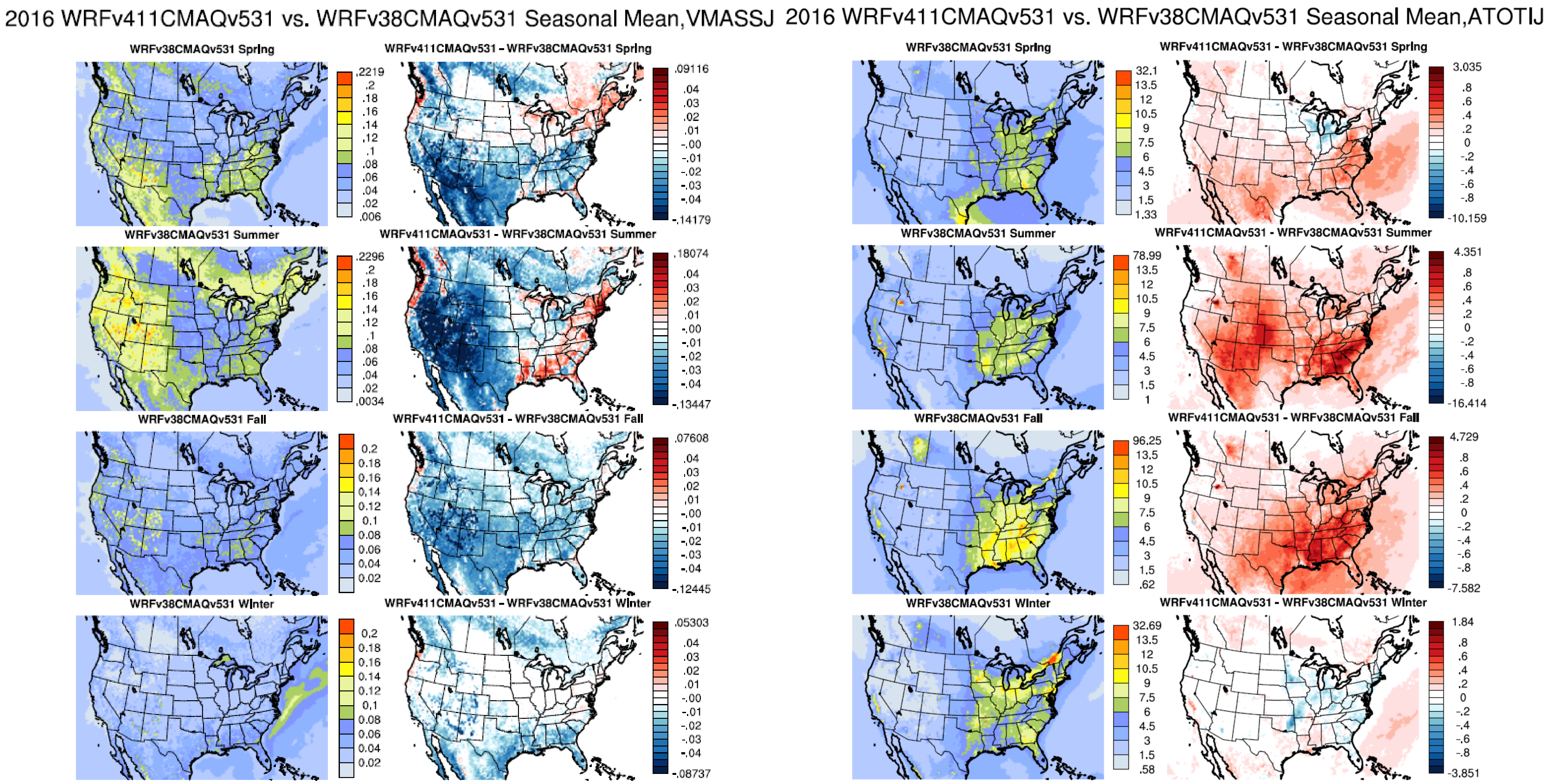

Figure S62. Seasonal accumulation mode deposition velocity (VMASSJ; cm s^{-1}; left) and $PM_{2.5}$ concentration (μg m^{-3}) for the CMAQ531_WRF38_M3Dry_BiDi simulation along with the difference in VMASSJ and $PM_{2.5}$ concentration between the CMAQ531_WRF38_M3Dry_Bidi and CMAQ531_WRF411_M3Dry_BiDi simulations (WRF411 – WRF38).

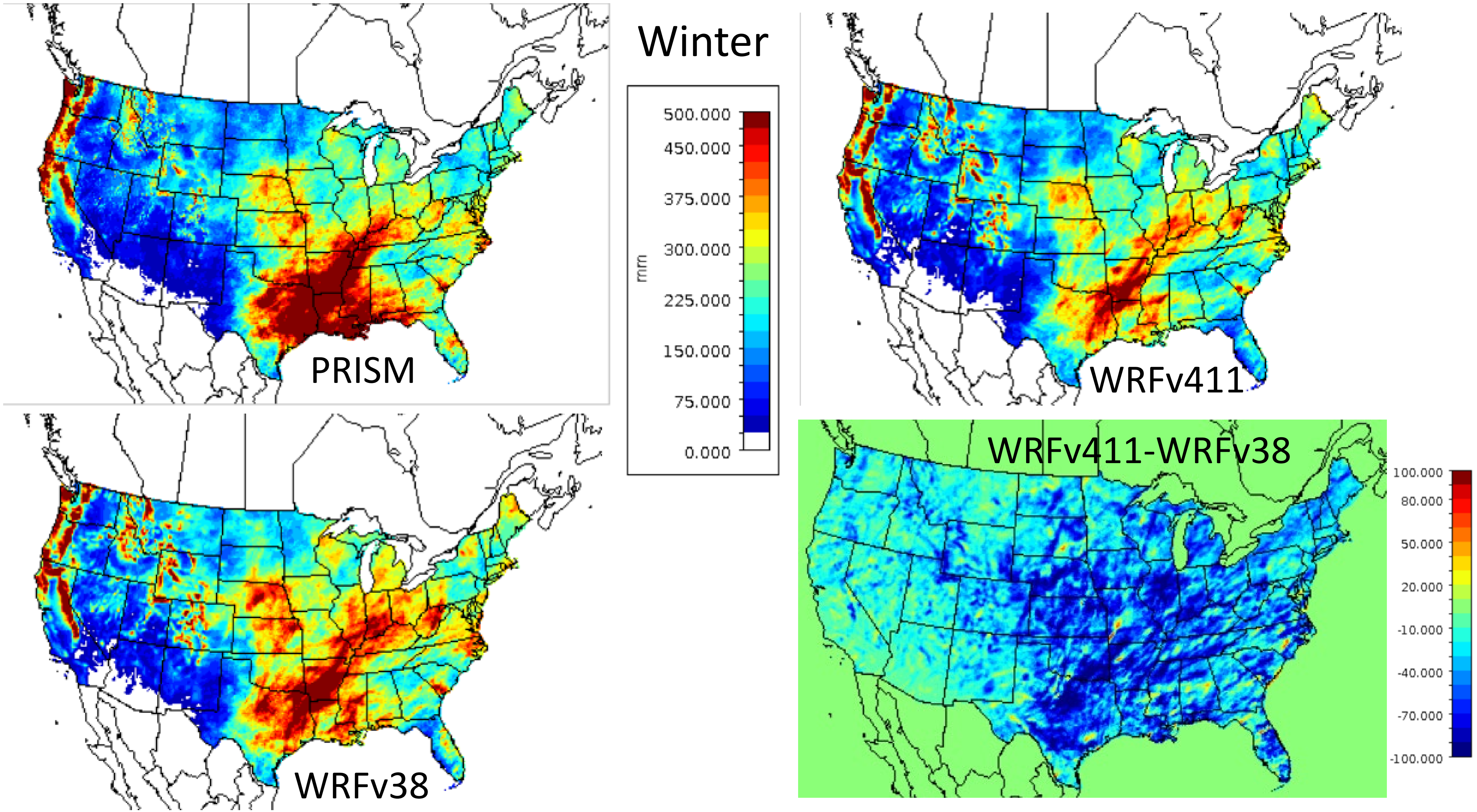

Figure S63. Observed and WRF simulated precipitation for winter 2006 in mm. Observed precipitation from PRISM (upper left), WRFv411 simulated precipitation (upper right), WRFv38 simulated precipitation (lower left), and the difference between WRFv411 and WRFv38 (WRFv411 – WRFv38) precipitation (lower right).

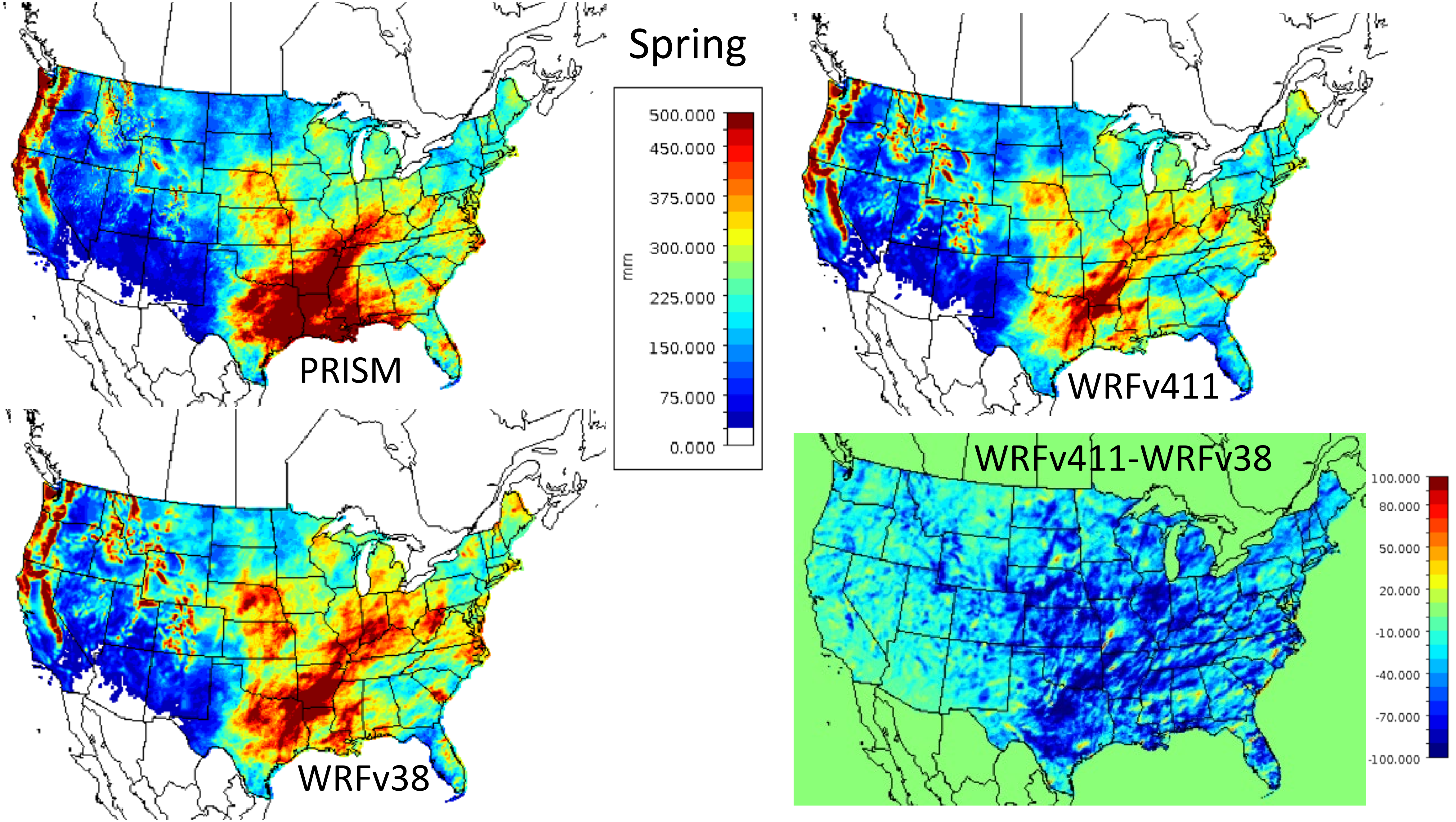

Figure S64. Observed and WRF simulated precipitation for spring 2006 in mm. Observed precipitation from PRISM (upper left), WRFv411 simulated precipitation (upper right), WRFv38 simulated precipitation (lower left), and the difference between WRFv411 and WRFv38 (WRFv411 – WRFv38) precipitation (lower right).

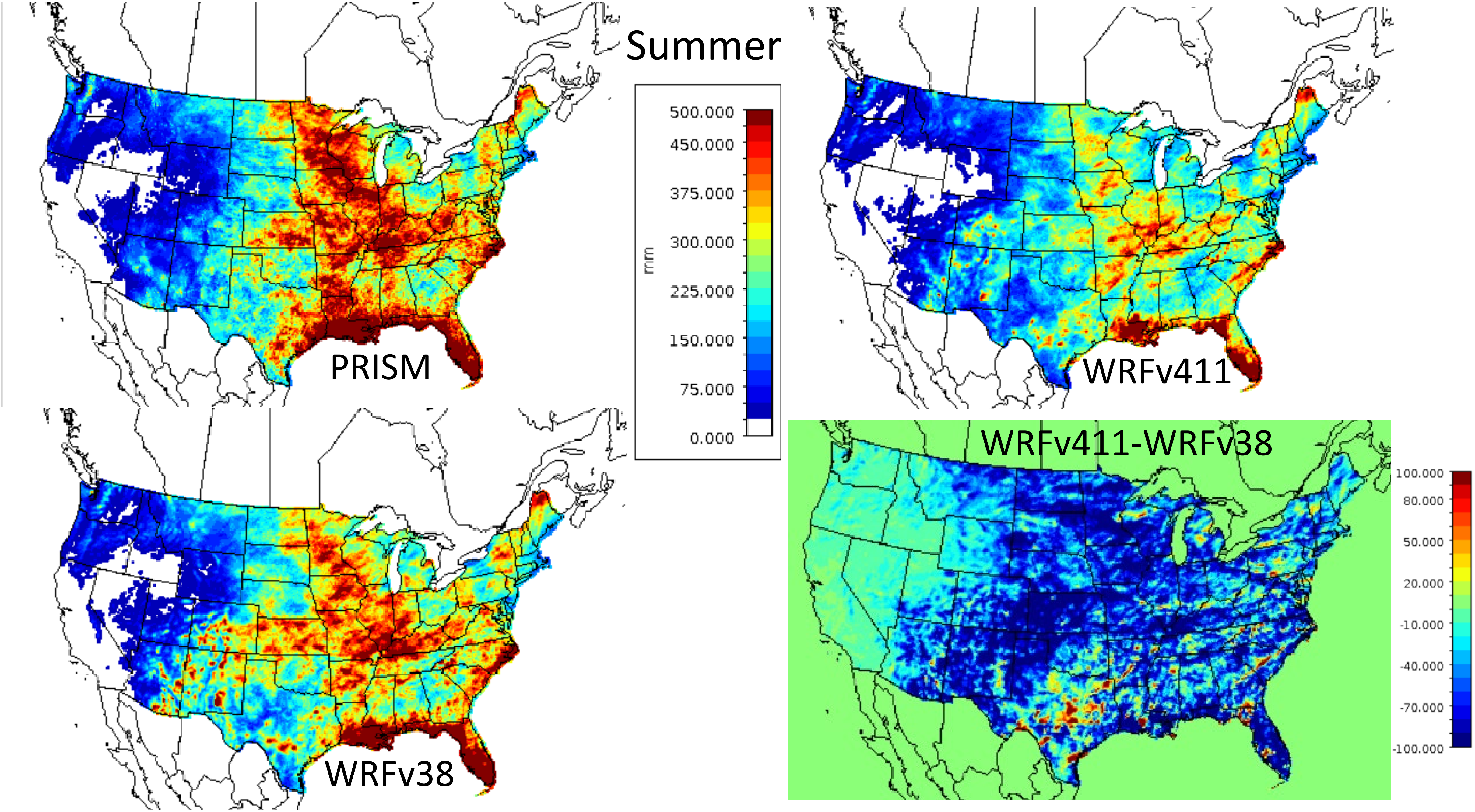

Figure S65. Observed and WRF simulated precipitation for summer 2006 in mm. Observed precipitation from PRISM (upper left), WRFv411 simulated precipitation (upper right), WRFv38 simulated precipitation (lower left), and the difference between WRFv411 and WRFv38 (WRFv411 – WRFv38) precipitation (lower right).

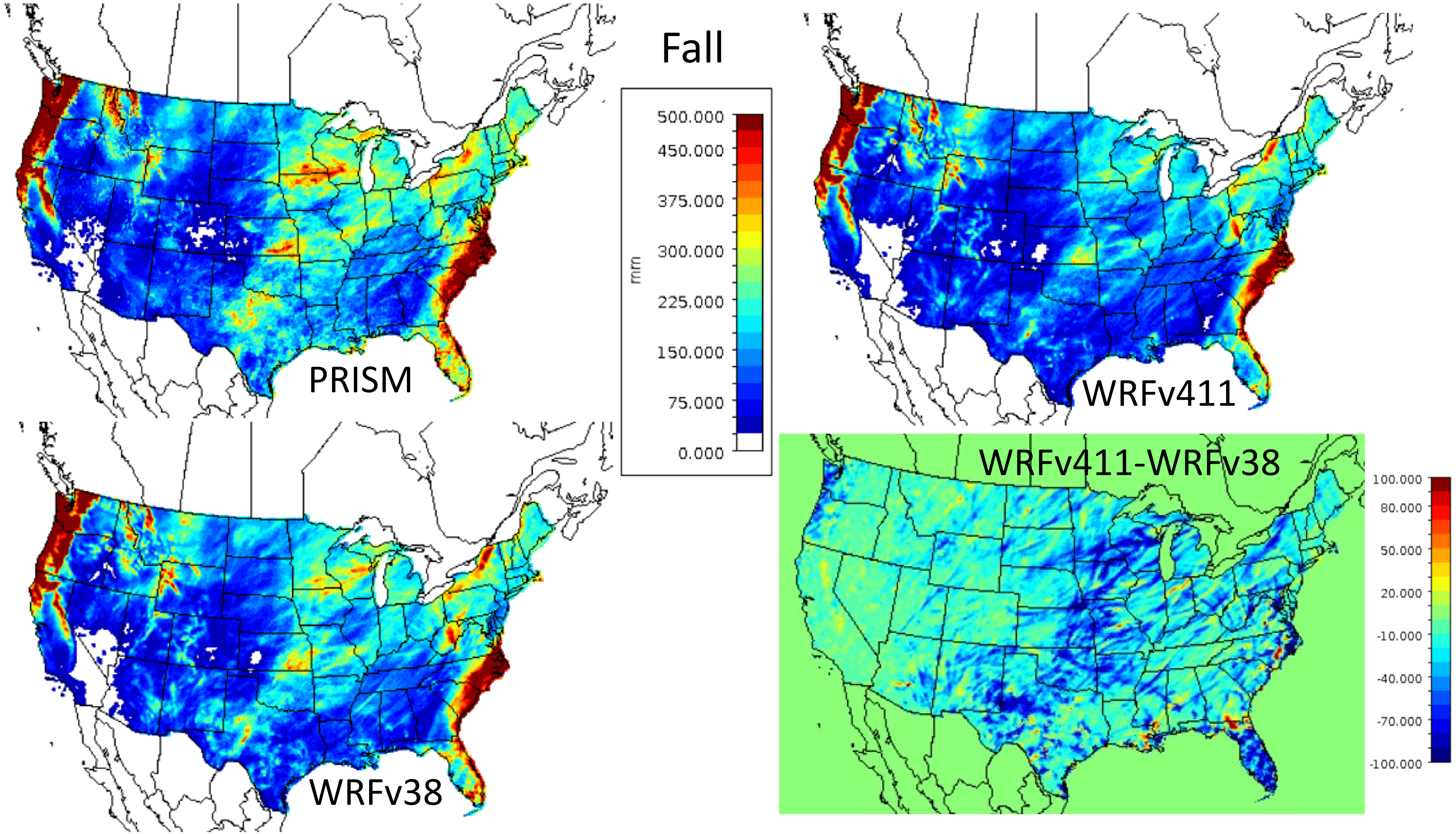

Figure S66. Observed and WRF simulated precipitation for fall 2006 in mm. Observed precipitation from PRISM (upper left), WRFv411 simulated precipitation (upper right), WRFv38 simulated precipitation (lower left), and the difference between WRFv411 and WRFv38 (WRFv411 – WRFv38) precipitation (lower right).